Petrology of sedimentery rocks

G421P13, summer semester, 2/1 hours weekly, 3rd – 4th year

Karel Martínek
Institute of Geology and Palaeontology

syllabus

Lectures

1. Siliciclastic sediments
   – granulometric analysis, provenance and geotectonic position → modal composition, heavy minerals
   – classification – see 1st year course Introduction to petrology of sedimentary rocks
   – sedimentary environments and facies - see course Sedimentary geology (2nd year)
   – diagenesis: compaction, porosity, authigenesis, cement types, diagenetic environments
2. Carbonates I.
   – mineralogy, specific sedimentary structures, grain types (Folk 1962), structural classification (Dunham 1962), sedimentary environments
3. Carbonates II.
   – dolomitization, dedolomitization, porosity changes, early vs. late diagenesis, cement types, diagenetic environments

4. Evaporites, cherts, ferolites, black shales, coal, oil, glauconite, phosphates
5. Cyclicity in sedimentary record, Milankovič orbital cycles, palaeoclimatology
6. Paleosols (humid, semiarid, arid; calcretes, silcretes, dolocretes); Geochemistry of sedimentary rocks (stable isotopes, trace elements, chemostratigraphy, eventstratigraphy, paleoenvironmental changes; cathode luminiscence .....)

practicals

- fieldwork – facies analysis (measured section of carbonate or siliciclastic section), ½ day
- microscopy lab of samples from studied section, 2x ½ day

course work

- facies analysis (2-3 pages report) of studied section

---

requirements to pass the course: oral presentation of scientific paper, fieldwork + microscopy protocols + course work report

exam: test – quiz (30 mins) + essay (1-2 hours)

1. Siliciclastics

primary structures and composition

- grainsize and granulometry, sorting, skewness - quantitative methods, image analysis, sediment dispersal pathways
- classification – see 1st year introductory course; arenite, ortho- , paraconglomerate
- sedimentary structures – see 1st year introductory course and course Sedimentary geology 2nd year

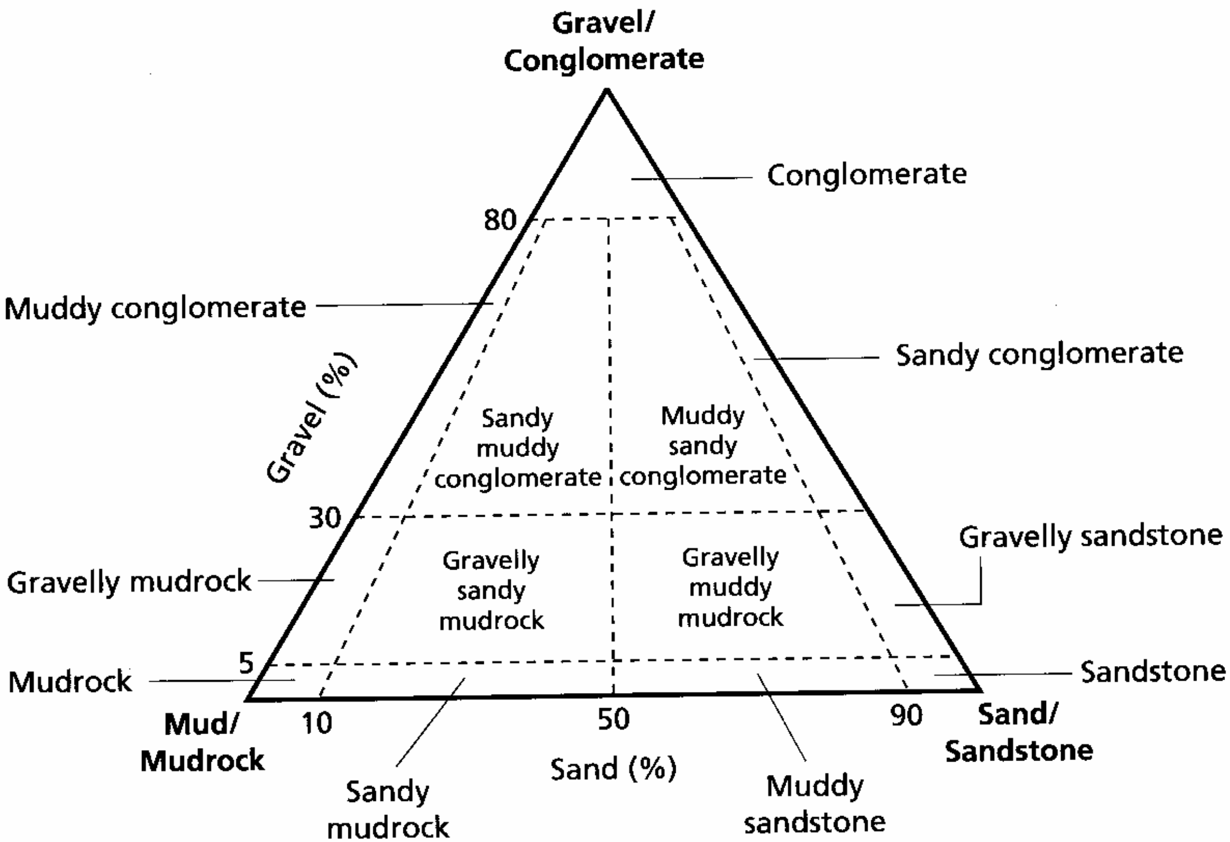

Fig. 2.1 Scheme for classifying sand–gravel–mud mixtures and the terms for sediment and rock (after Udden–Wentworth and Blair & McPherson, 1999).

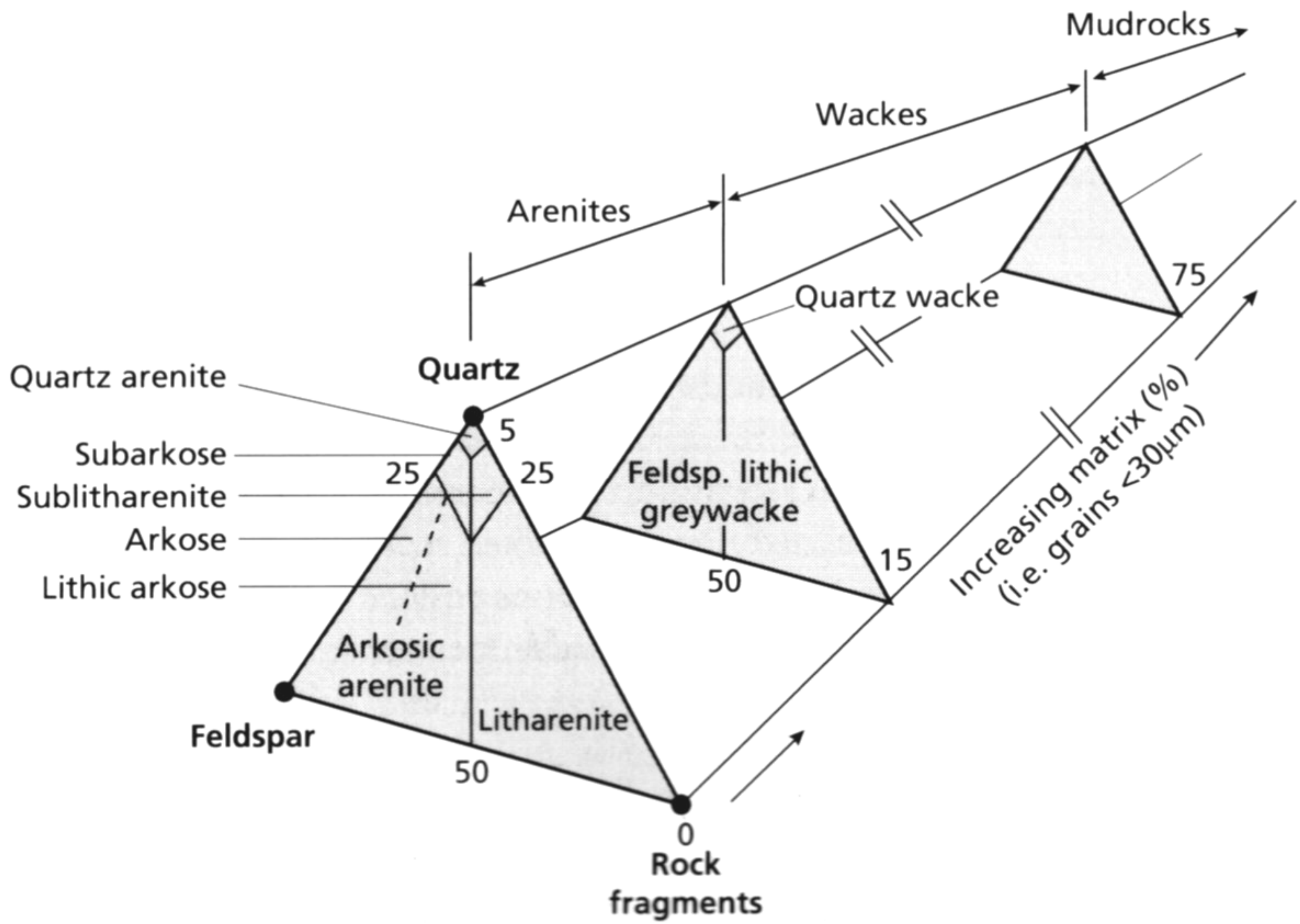
Mudrocks
Wackes
Arenites
Quartz wacke
75
Quartz arenite
Quartz
5
Subarkose
25
25
Sublitharenite
Arkose
Lithic arkose
Feldsp. lithic
greywacke
15
50
Increasing matrix (%)
(i.e. grains <30μm)
Arkosic
arenite
Litharenite
Feldspar
50
0
Rock
fragments

Class	Freq.	Freq. %	Cum. freq.
4–5	40	8	100
3–4	220	44	92
2–3	160	32	48
1–2	60	12	16
0–1	20	4	4

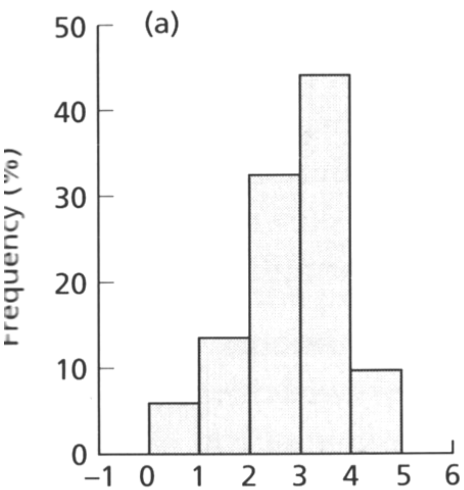

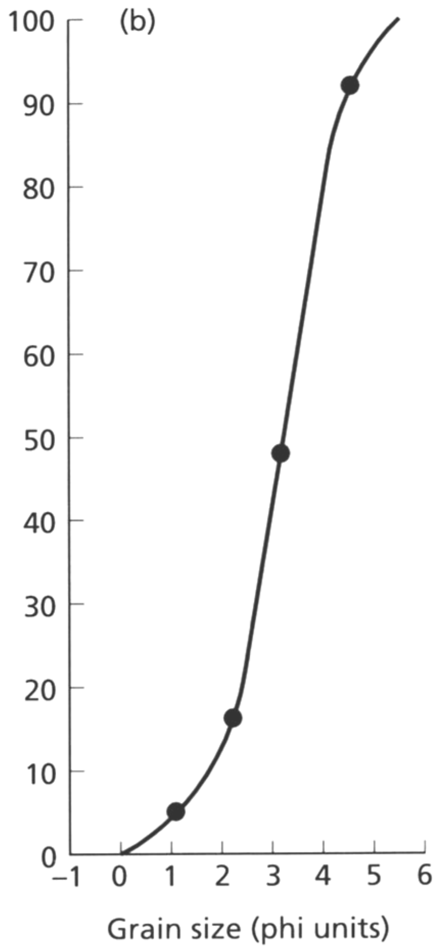

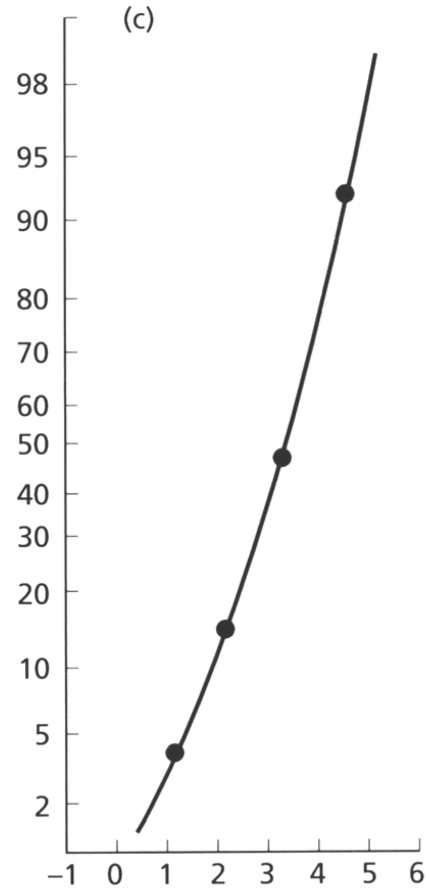

Grain size parameters derived graphically, Folk and Ward formulae

median	3.05ϕ
mean	2.95ϕ
sorting	0.92 (moderately sorted)
skewness	–0.21 (coarse skew)
kurtosis	0.96

$$\text{phi} = -\log_2 D$$

phi:	D [mm]:
0.25	2
0.5	1
1	0.5
2	0.25
3	0.125
4	0.067

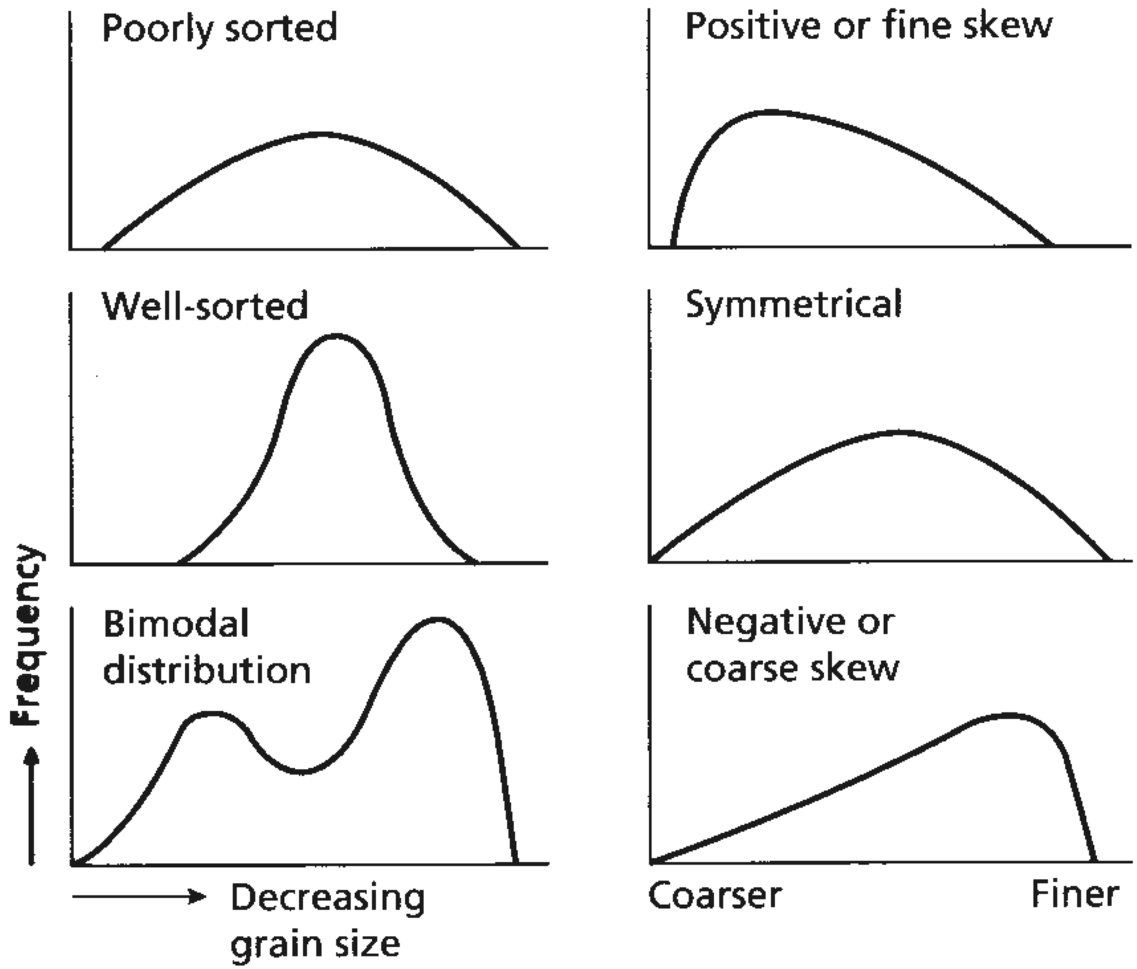

Fig. 2.2 Smoothed frequency distribution curves showing types of sorting and skewness.

Table 2.2 Formulae for the calculation of grain-size parameters from a graphic presentation of the data in a cumulative frequency plot. With the Trask formulae, the percentile measure Pn is the grain size in millimetres at the nth percentage frequency, and with the Folk & Ward formulae, the percentile measure ϕ_n is the grain size in phi units at the nth percentage frequency

Parameter	Trask formula	Folk & Ward formula
Median	$Md = P_{50}$	$Md = \phi_{50}$
Mean	$M = \dfrac{P_{25} + P_{75}}{2}$	$M = \dfrac{\phi_{16} + \phi_{50} + \phi_{84}}{3}$
Sorting	$So = \dfrac{P_{75}}{P_{25}}$	$\sigma\phi = \dfrac{\phi_{84} - \phi_{16}}{4} + \dfrac{\phi_{95} - \phi_{5}}{6.6}$
Skewness	$Sk = \dfrac{P_{25}P_{75}}{Md^2}$	$Sk = \dfrac{\phi_{16} + \phi_{84} - 2\phi_{50}}{2(\phi_{84} - \phi_{16})} + \dfrac{\phi_{5} + \phi_{95} - 2\phi_{50}}{2(\phi_{95} - \phi_{5})}$

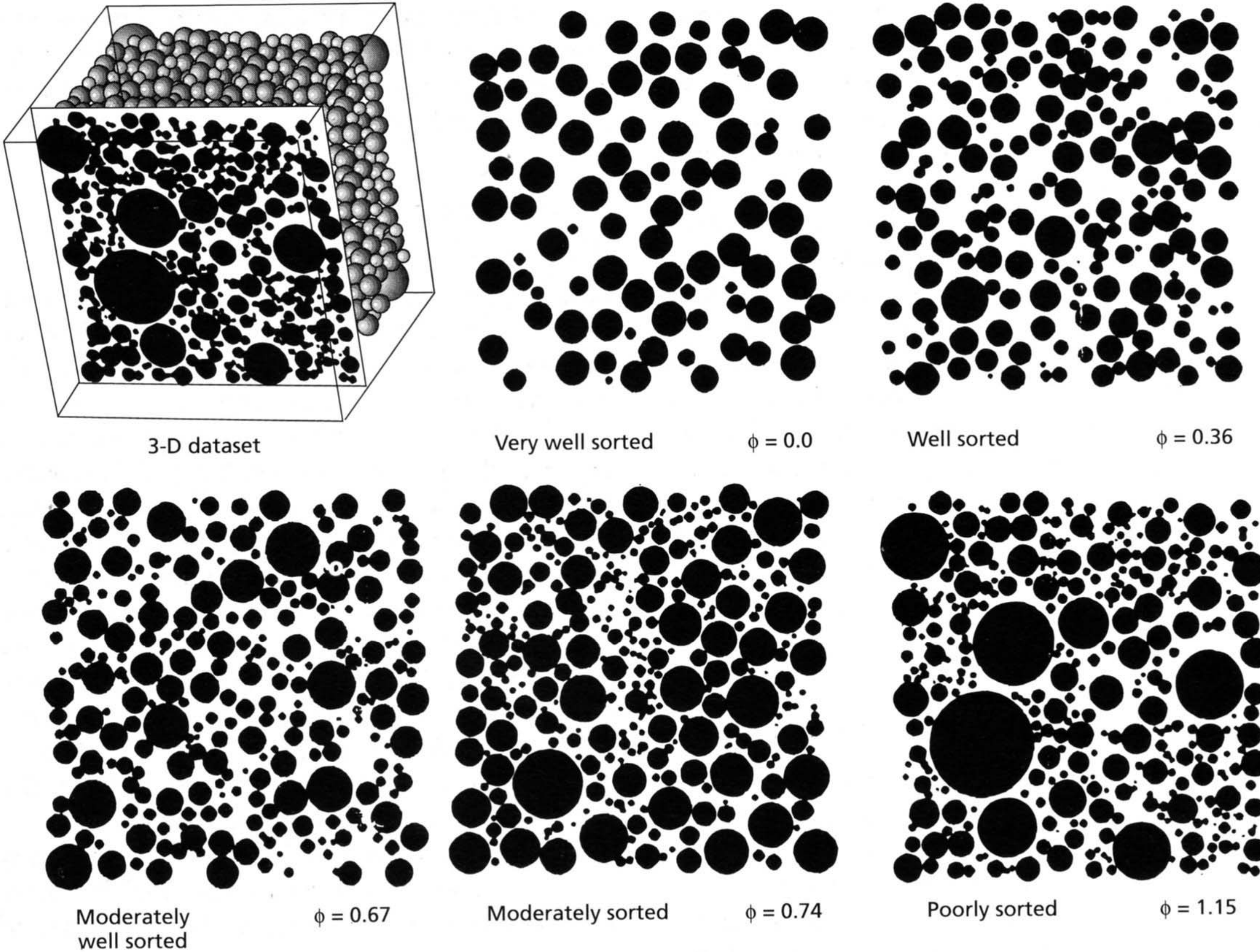

3-D dataset
Very well sorted
ϕ = 0.0
Well sorted
ϕ = 0.36
Moderately well sorted
ϕ = 0.67
Moderately sorted
ϕ = 0.74
Poorly sorted
ϕ = 1.15

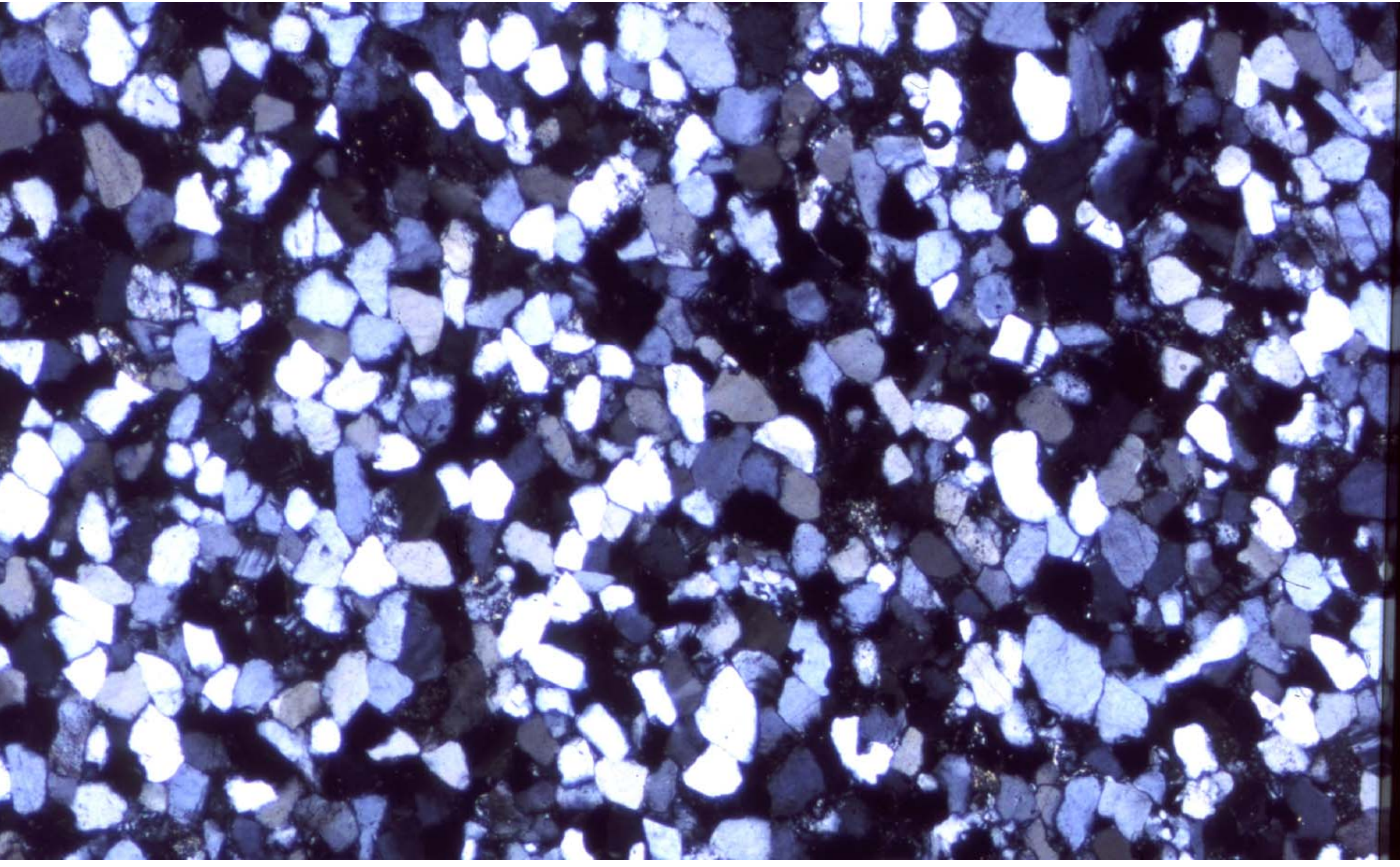

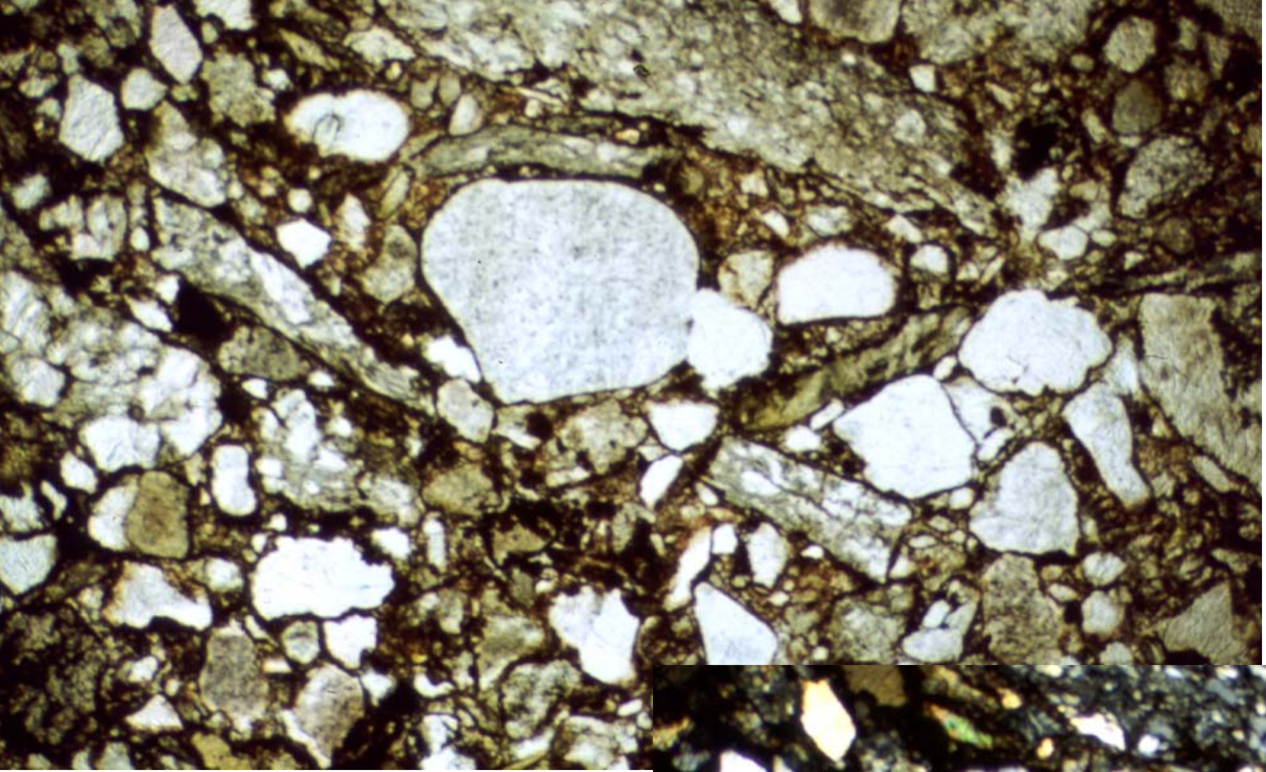

grain size sorting
vs.
mineralogical sorting
(mineralogical maturity)

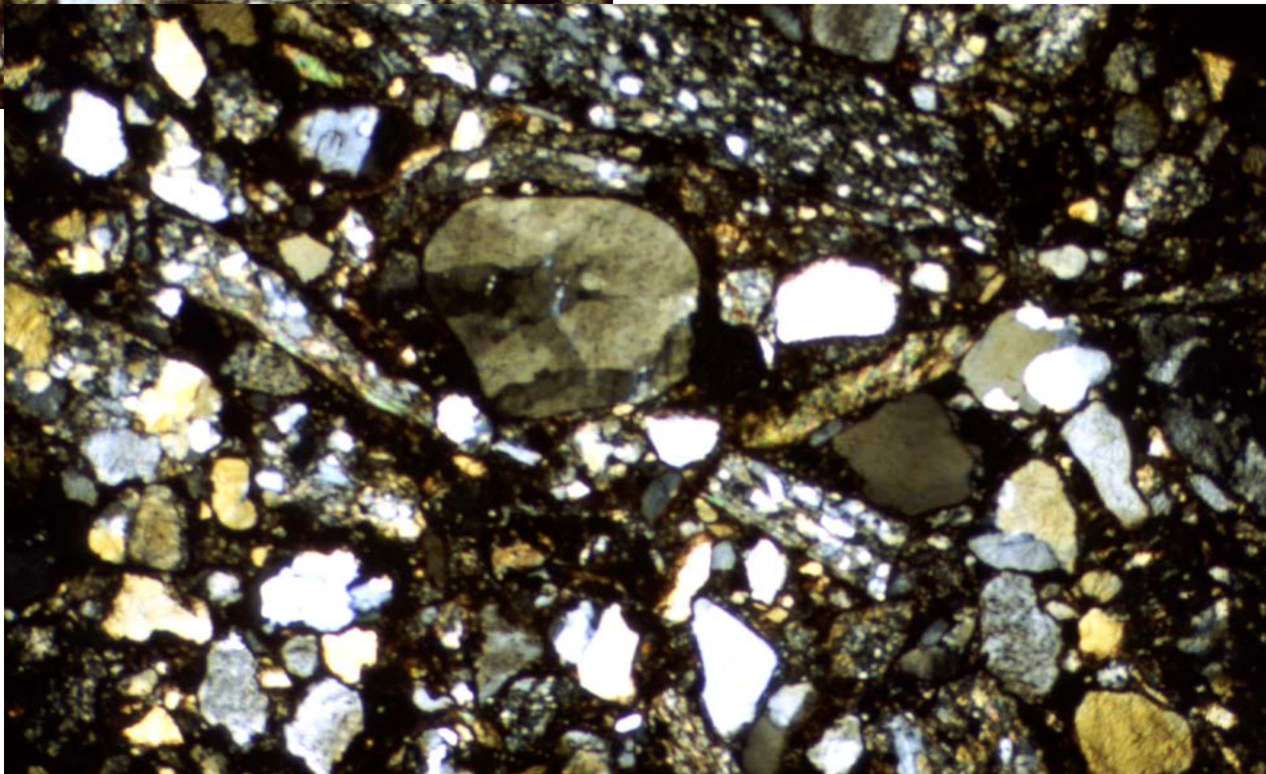

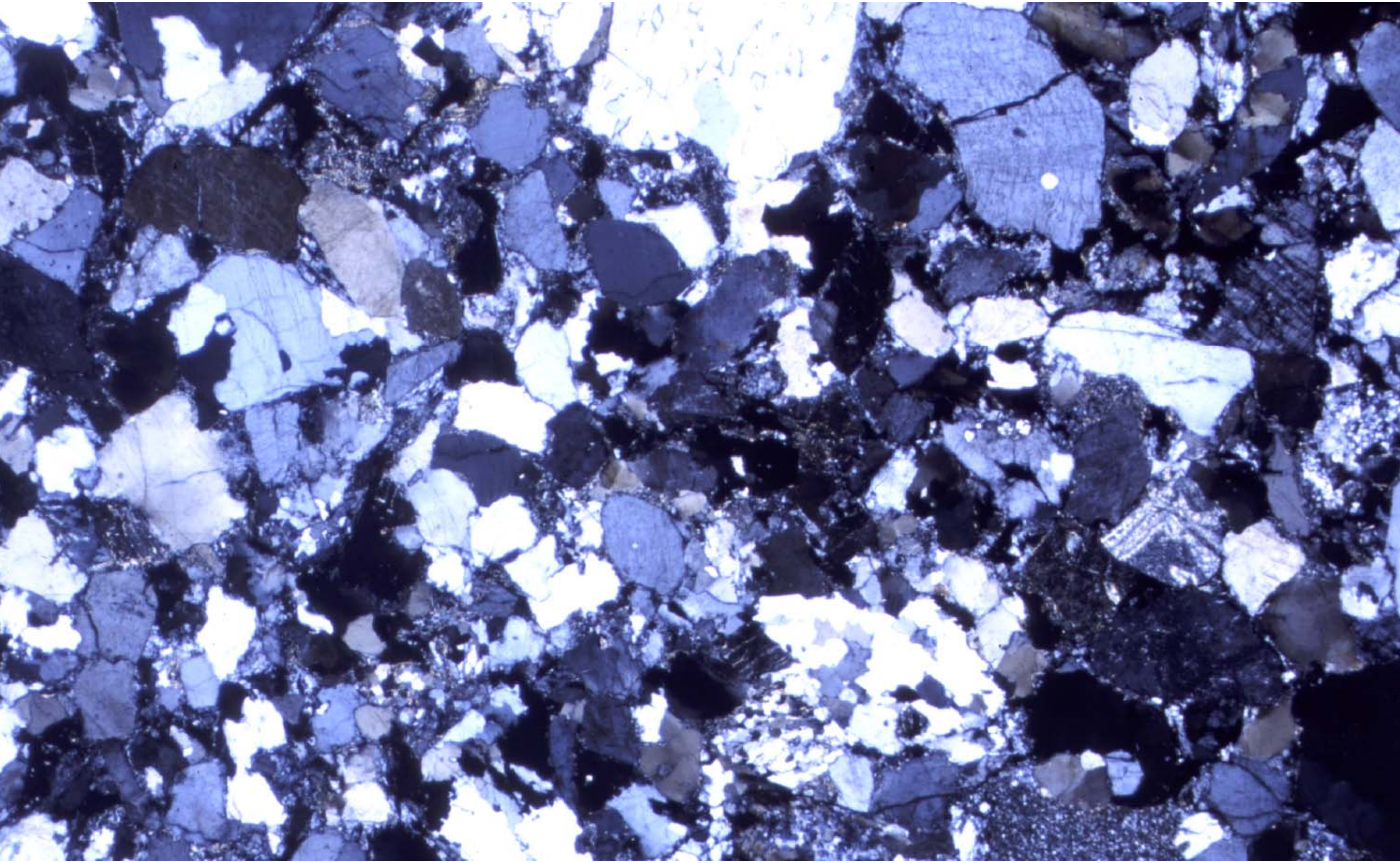

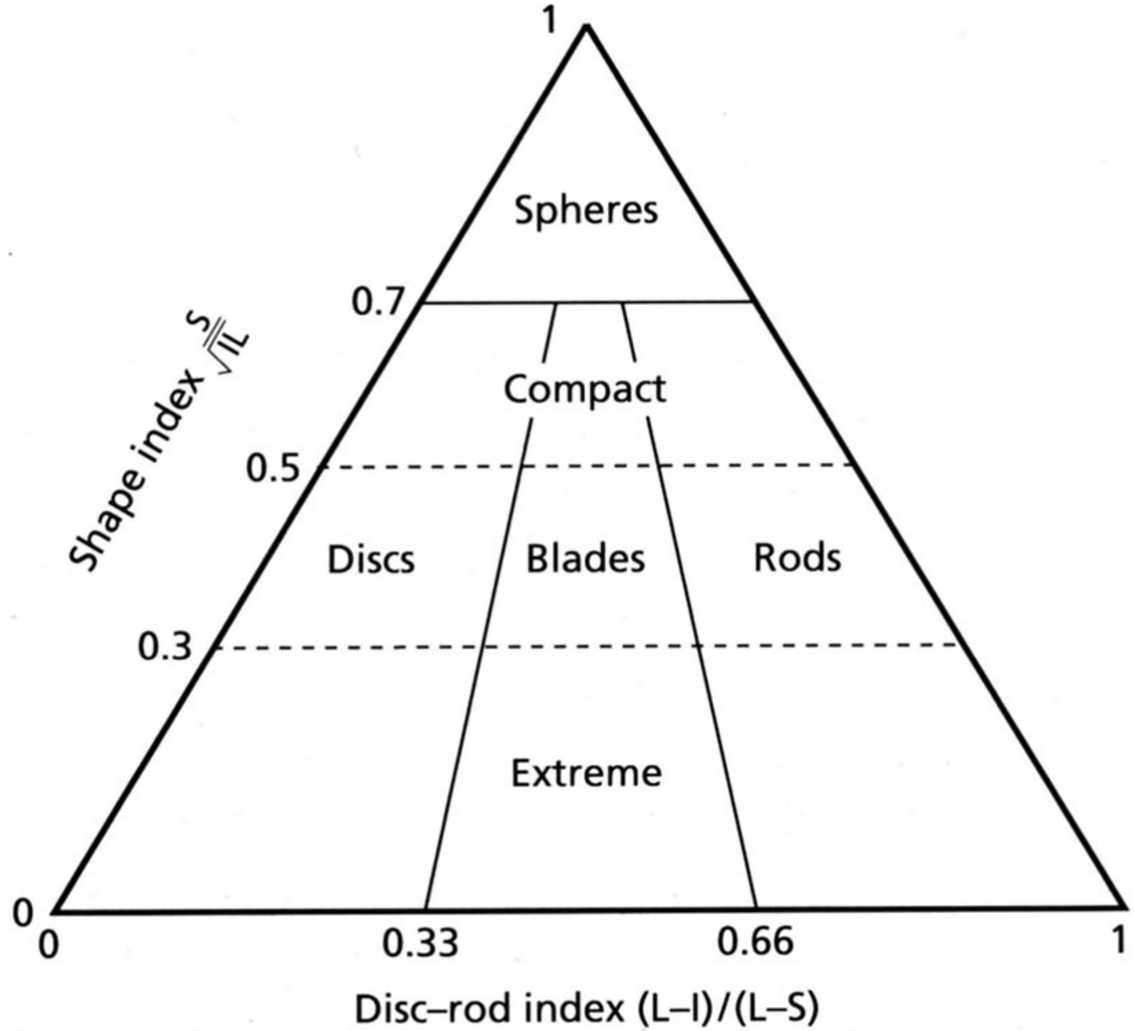

Fig. 2.5 The four classes of grain shape: spheres, discs, rods and blades, based on the shape index (a measure of the sphericity) and the disc–rod index. L, I and S represent the long, intermediate short axes of the grains, respectively (after Illenberger, 1991).

grain shapes

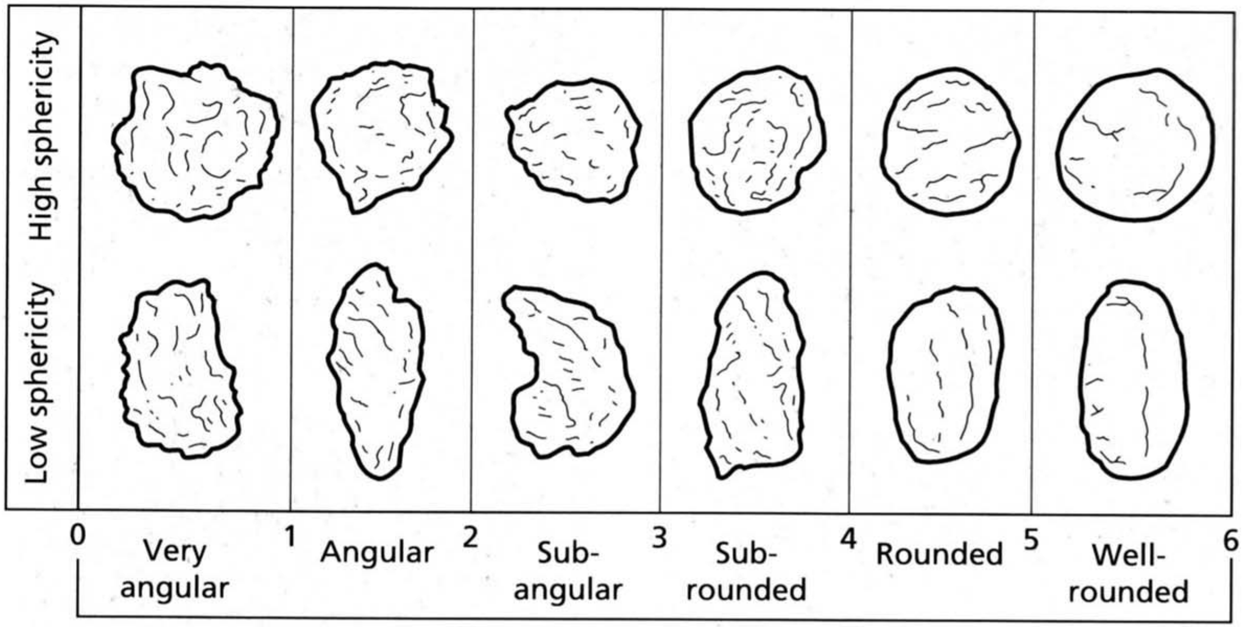

Fig. 2.6 Categories of roundness for sediment grains. For each category a grain of low and high sphericity is shown. After Pettijohn *et al*. (1987).

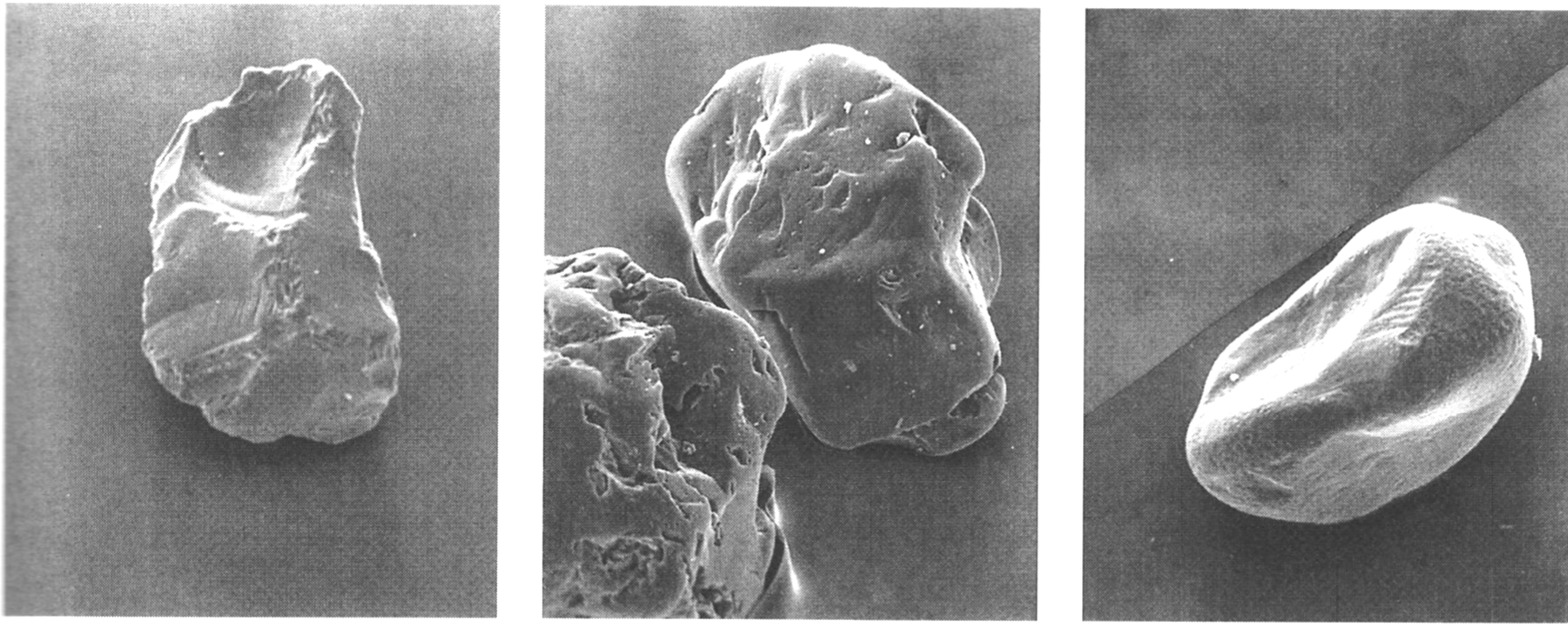

Fig. 2.7 Scanning electron micrographs of quartz sand grains from three modern environments. (a) Grain from glacial outwash deposit, Ottawa, Canada, showing conchoidal fractures and angular shape. (b) Grain from high-energy beach, Sierra Leone, West Africa, showing rounded shape and smooth surface with small v-shaped percussion marks. (c) Grain from desert sand sea, Saudi Arabia, showing frosted, pock-marked surface (as a result of upturned plates, which are visible at higher magnifications) and conchoidal fractures resulting from mechanical chipping.

microstructures

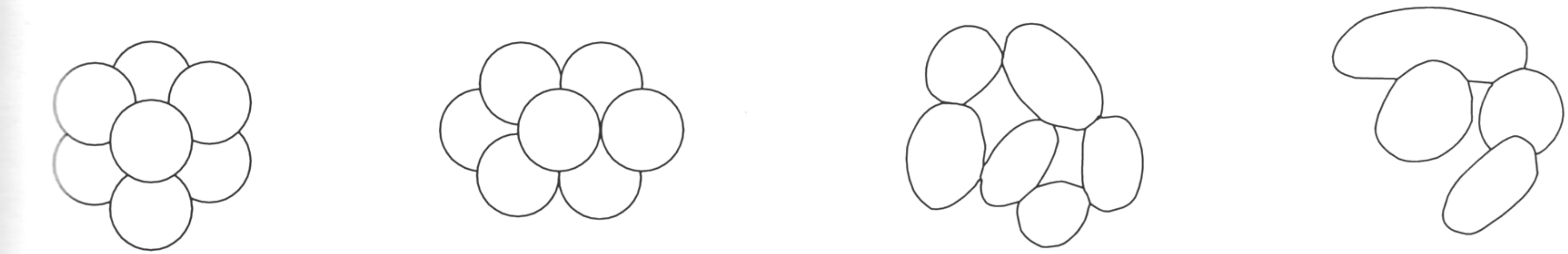

(a) Cubic packing (48% porosity)

(b) Rhombohedral packing (26% porosity)

(c) Point contacts

(d) Concavo-convex contacts

(e) Sutured contacts

(f) Preferred orientation of grains

(g) Grain-supported fabric

(h) Matrix-supported fabric

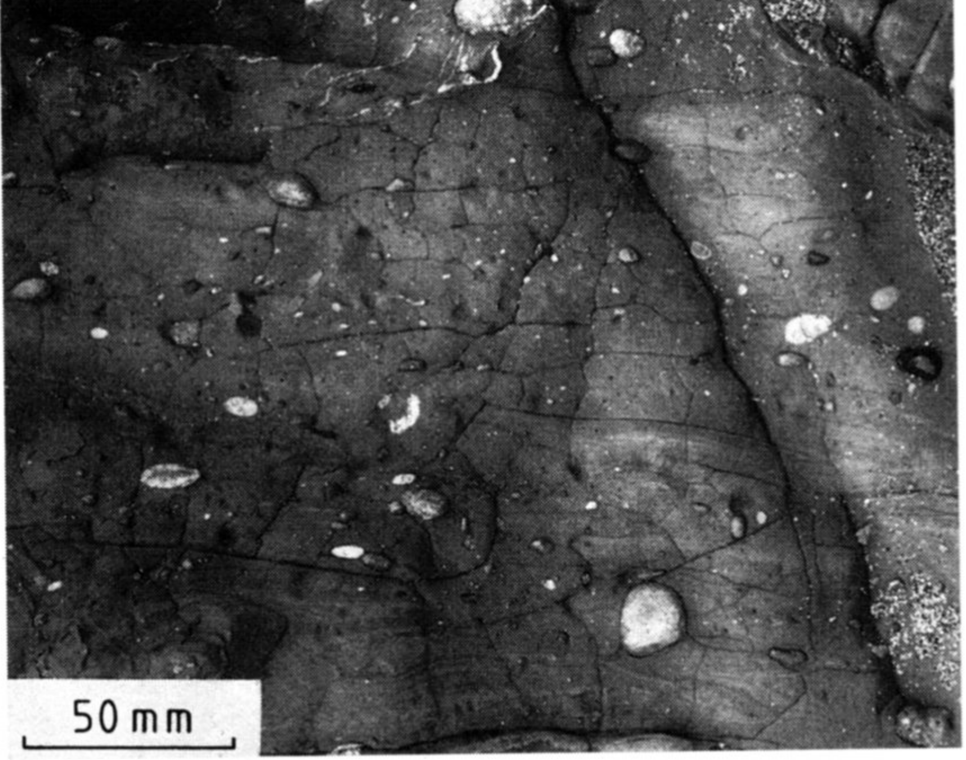

Fig. 2.9 Matrix-support fabric: pebbles 'float' in matrix. Notice also subtle synsedimentary folds. Tertiary deep-water pebbly mudstone of debris-flow origin. California, USA.

Fig. 2.10 Clast-support fabric; pebbles, mainly quartzite, are in contact and were deposited on a fan delta. Late Precambrian, Southern Norway.

provenance analysis

modal composition - climate, geotectonic position, unroofing history; heavy mineral association vs. accesoric minerals of source rocks: influence of climate, hydrodynamics and associated processes

methods:

- detailed mineralogy/chemistry of heavy minerals (garnets, turmalines, pyroxens)
- zircon geochronology, apatite fission-track analysis – thermal/tectonosedimentary history
- claystone provenance – trace minerals, geochronology

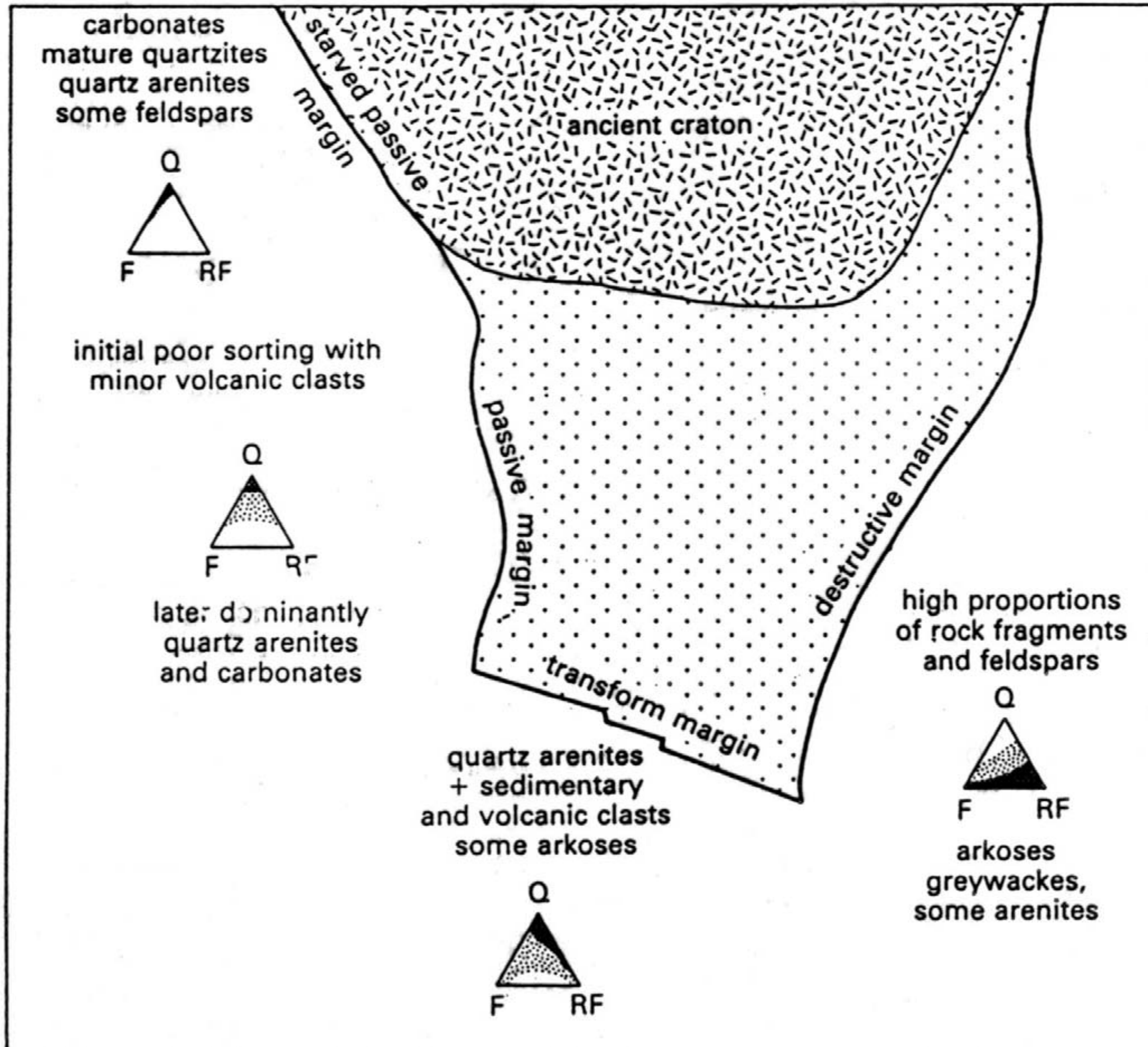

Fig. 5.10. Average modal compositions of groups of sandstones from different tectonic environments. This technique is only valid where many different sandstone modal compositions are available and cannot be used for single sandstone samples (modified from Folk, 1974b). Component details are documented in Table 5.5.

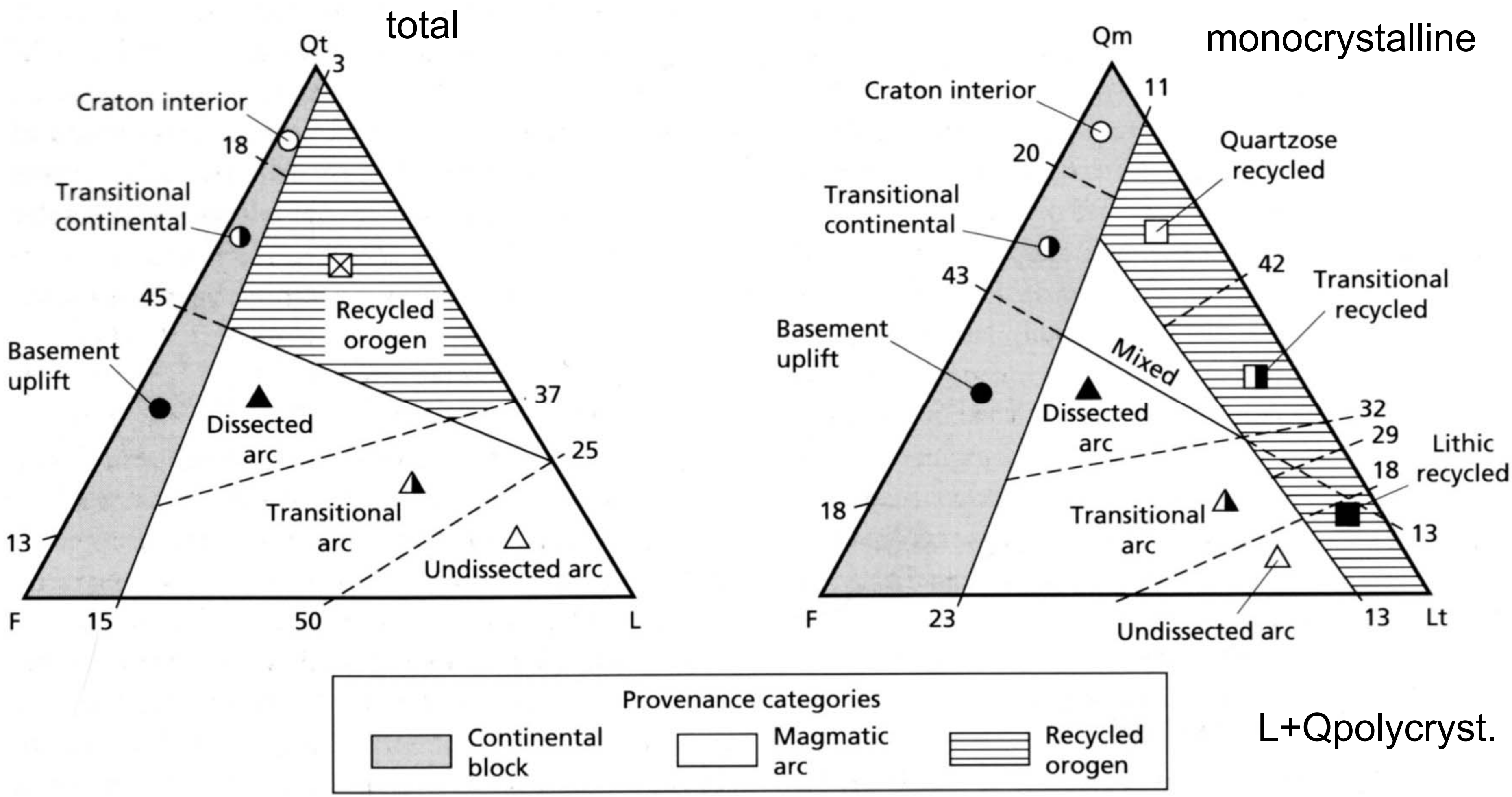

total
Qt
3
Craton interior
18
Transitional continental
45
Recycled orogen
Basement uplift
Dissected arc
37
25
Transitional arc
Undissected arc
13
F
15
50
L
monocrystalline
Qm
11
Craton interior
Quartzose recycled
20
Transitional continental
42
43
Transitional recycled
Basement uplift
Mixed
Dissected arc
32
29
Lithic recycled
18
18
Transitional arc
13
Undissected arc
F
23
13
Lt
Provenance categories
Continental block
Magmatic arc
Recycled orogen
L+Qpolycryst.

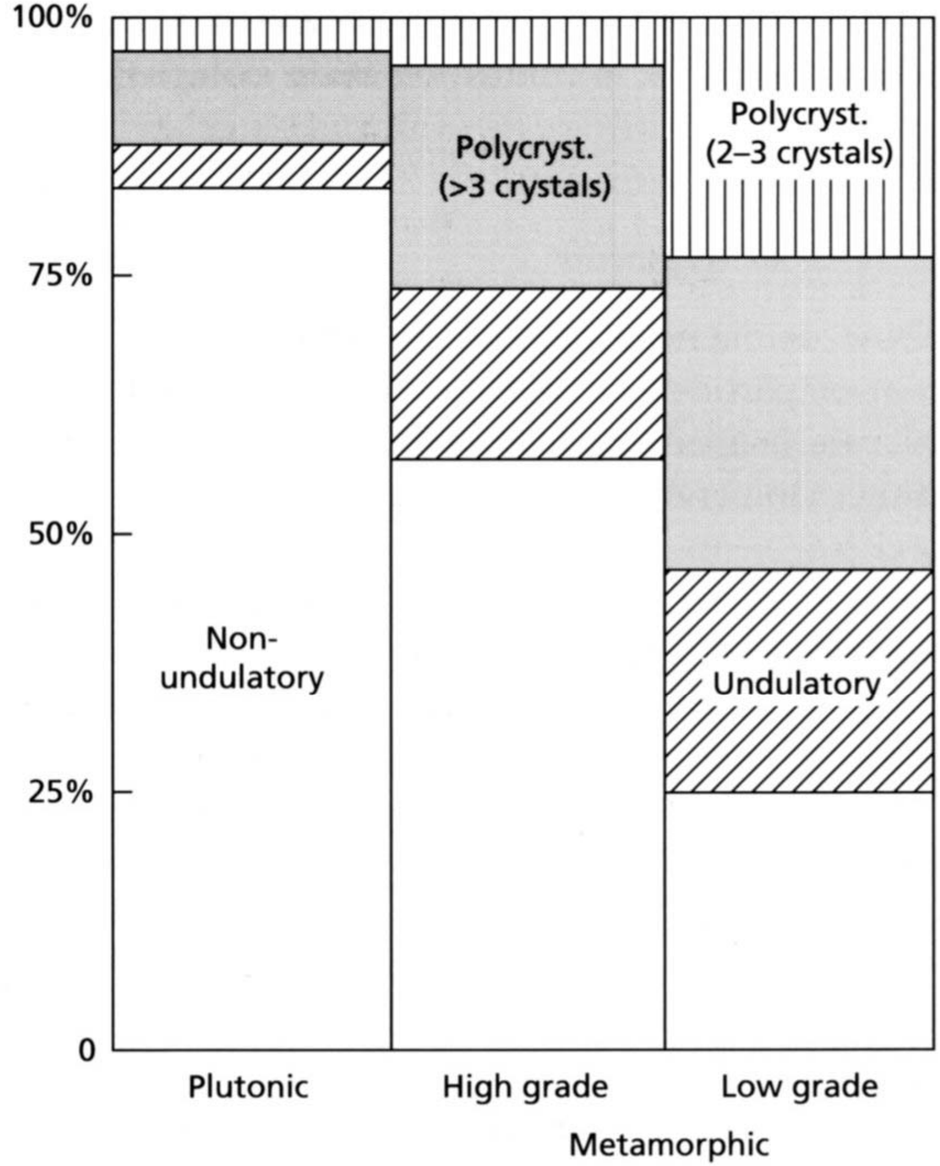

Fig. 2.48 Relative abundance of detrital monocrystalline and polycrystalline quartz grains in Holocene sands derived from known plutonic and metamorphic sources. After Basu *et al.* (1975).

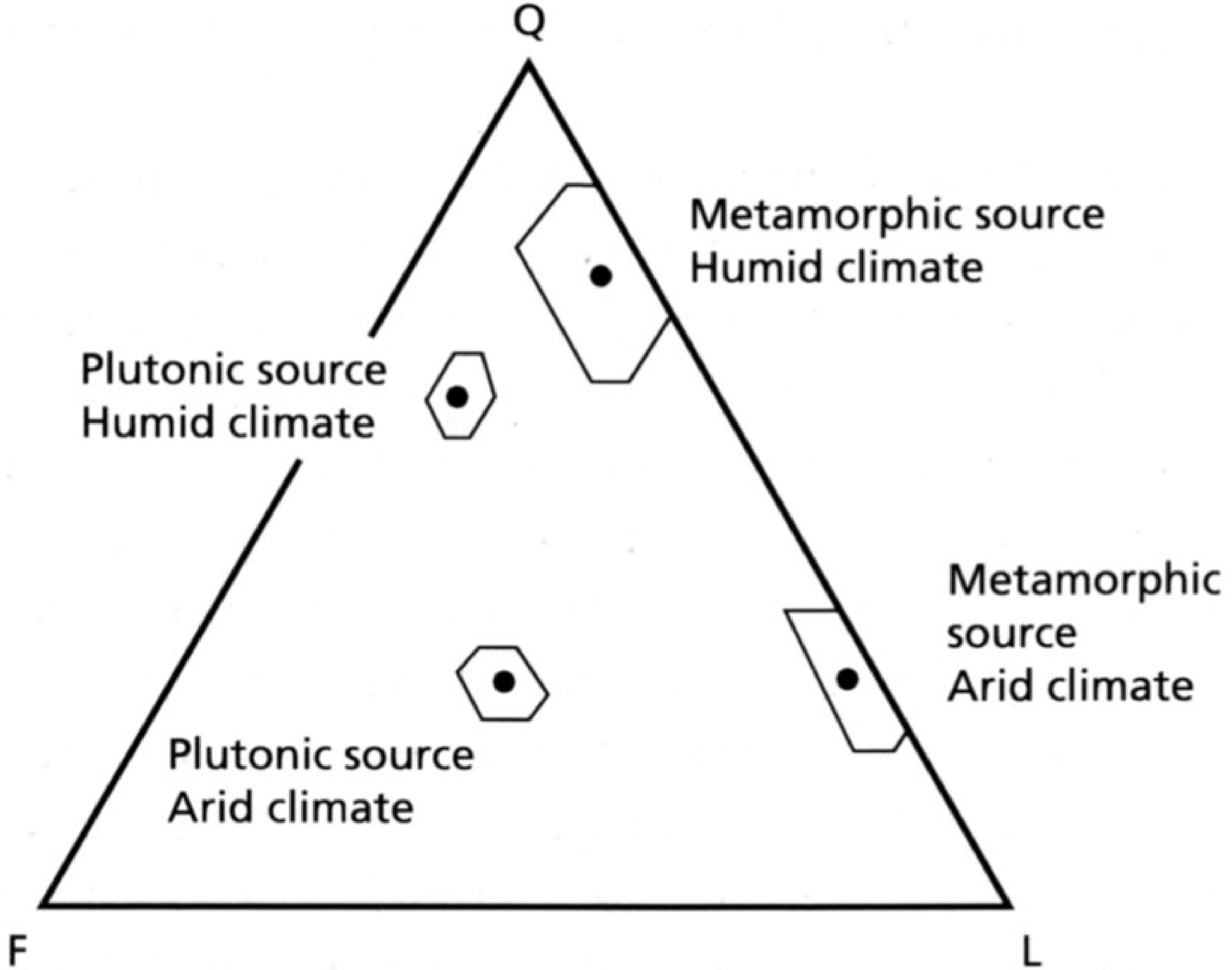

Fig. 2.46 Average compositions of medium sand-size fraction of first-cycle stream sediment derived from plutonic igneous and metamorphic sources under different climatic conditions. Q, quartz; F, feldspar; L, lithics.

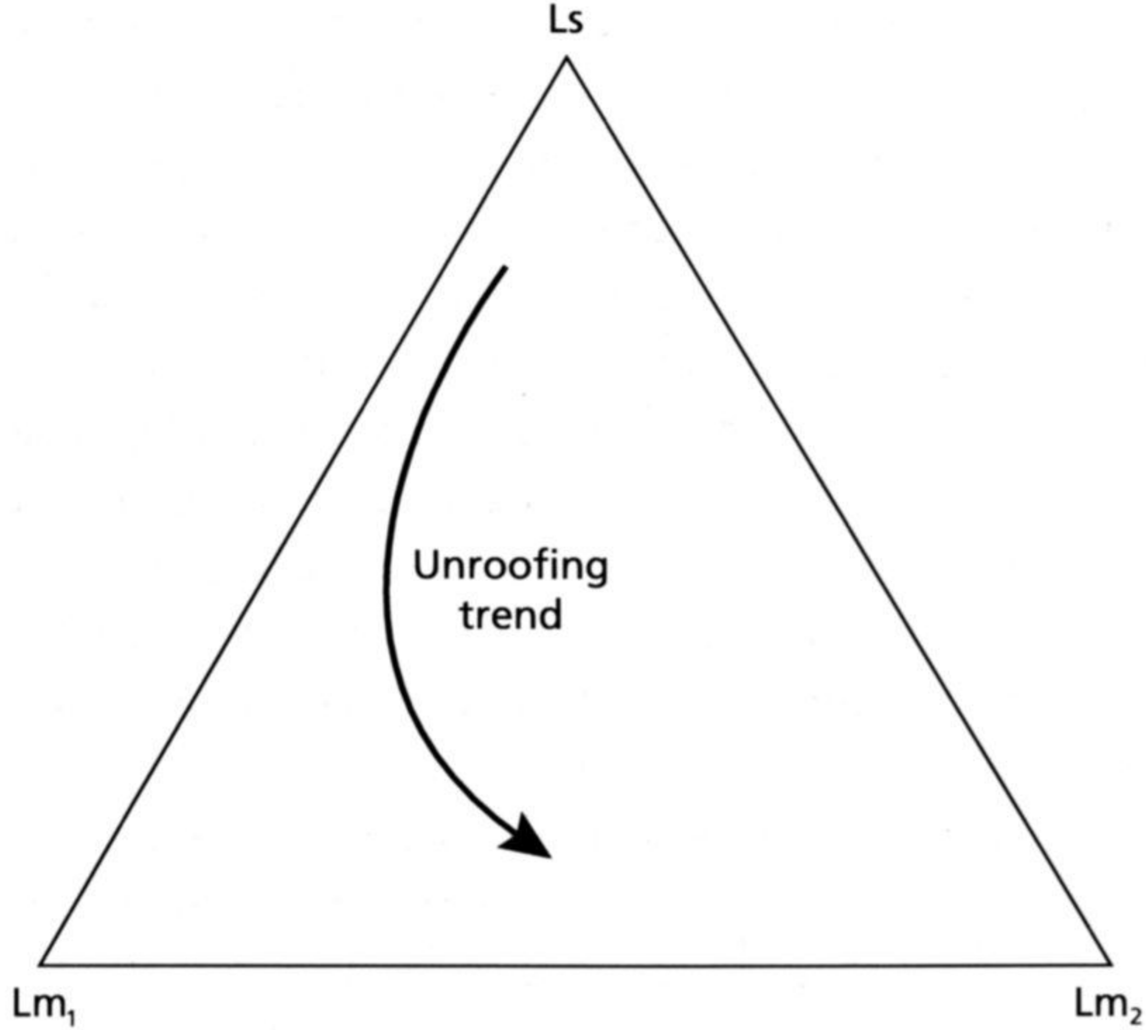

Fig. 2.47 The trend in lithic grains (Ls, sedimentary; Lm_1, low-grade metamorphic; Lm_2, medium-grade metamorphic) in sandstones derived from the unroofing of a sedimentary–metasedimentary complex of an arc–continent collision belt.

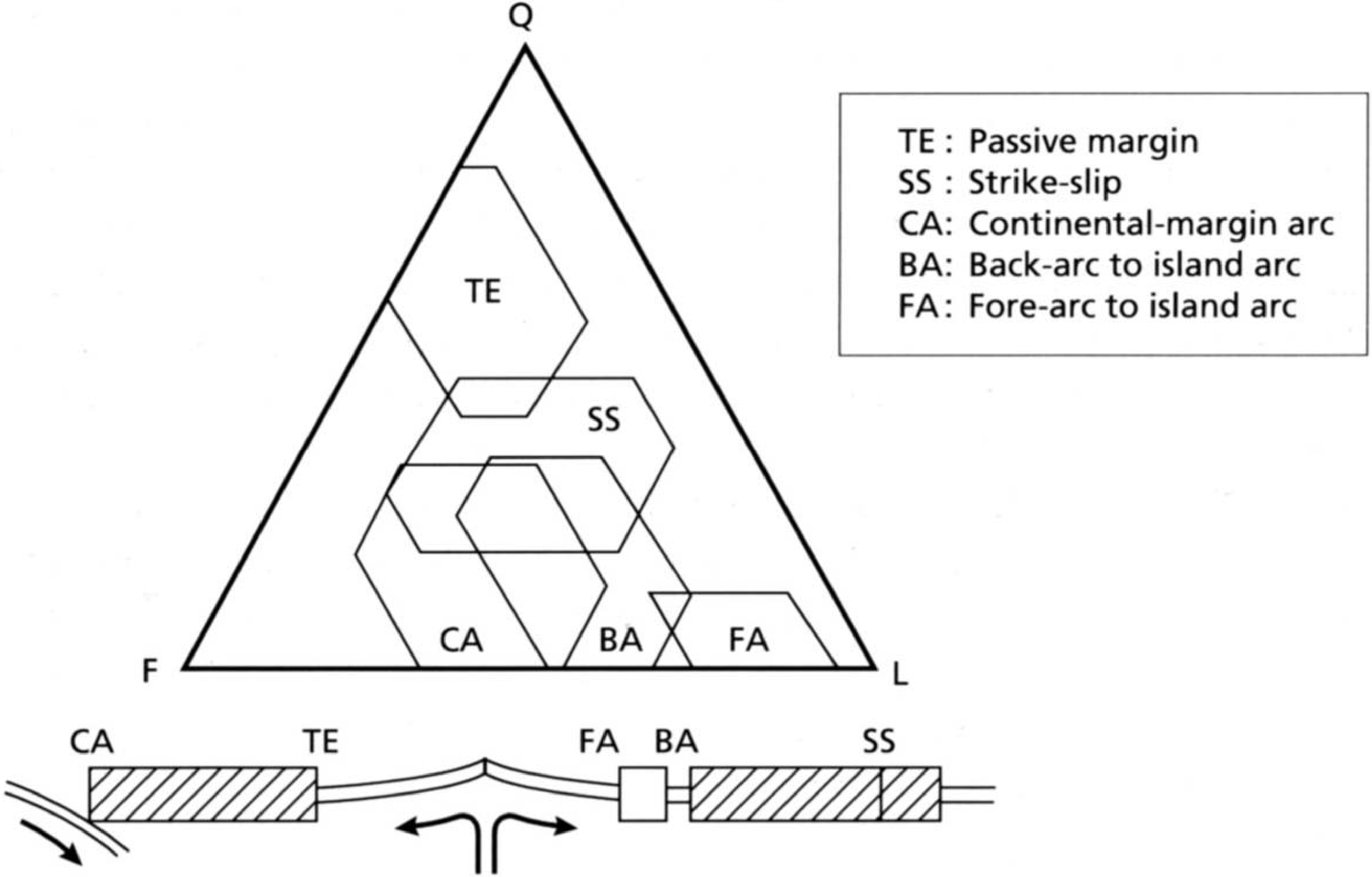
Q
F
L
TE
SS
CA
BA
FA
TE : Passive margin
SS : Strike-slip
CA: Continental-margin arc
BA: Back-arc to island arc
FA: Fore-arc to island arc
CA
TE
FA
BA
SS

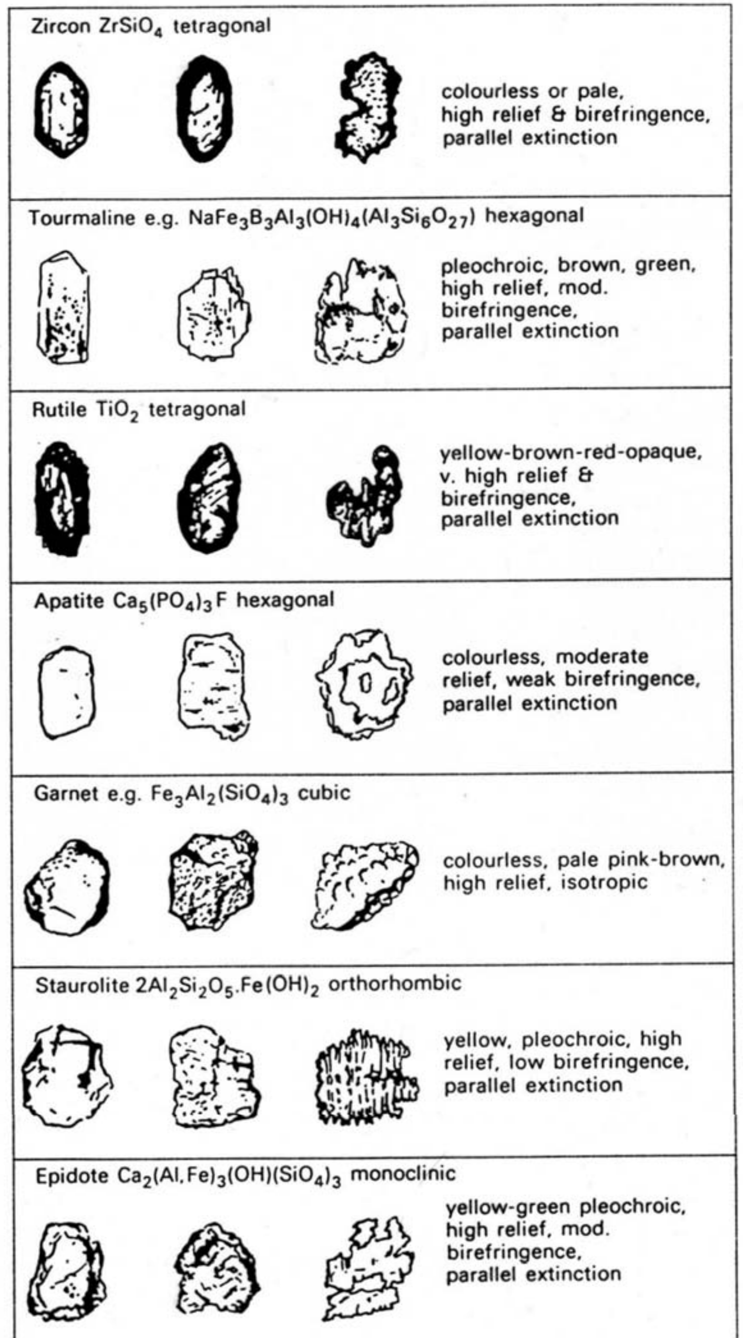

Fig. 2.55 Sketches of the seven most common heavy minerals (with the degree of weathering and or dissolution increasing to the right) together with their optical properties. After Füchtbauer (1974).

Table 4-2
Common Accessory Minerals in Sandstones and Types of Crystalline Rocks in Which They Usually Originate

Igneous rocks	Metamorphic rocks	Indeterminate[a]
Aegerine	Actinolite	Enstatite
Augite	Andalusite	Hornblende
Chromite	Chloritoid	Hypersthene
Ilmenite	Cordierite	Magnetite
Olivine	Diopside	Sphene
Topaz	Epidote	Tourmaline
	Garnet	Zircon
	Glaucophane	
	Kyanite	
	Jadeite	
	Rutile	
	Sillimanite	
	Staurolite	
	Tremolite	
	Wollastonite	

[a] Common in both igneous and metamorphic rocks.

Table 8-2. *Heavy mineral associations and provenance (modified from Feo-Codecido, 1956, p. 997)*

Association	*Source*
Apatite, biotite, brookite, hornblende, monazite, muscovite, rutile, titanite, tourmaline (pink variety), zircon	Acid igneous rocks
Cassiterite, dumortierite, fluorite, garnet, monazite, muscovite, topaz, tourmaline (blue variety), wolframite, xenotime	Granite pegmatites
Augite, chromite, diopside, hypersthene, ilmenite, magnetite, olivine, picotite, pleonaste	Basic igneous rocks
Andalusite, chondrodite, corundum, garnet, phlogopite, staurolite, topaz, vesuvianite, wollastonite, zoisite	Contact metamorphic rocks
Andalusite, chloritoid, epidote, garnet, glaucophane, kyanite, sillimanite, staurolite, titanite, zoisite-clinozoisite	Dynamothermal metamorphic rocks
Barite, iron ores, leucoxene, rutile, tourmaline (rounded grains), zircon (rounded grains)	Reworked sediments

Table 8-3. *Stability of some detrital heavy minerals*

Ultrastable	Rutile, zircon, tourmaline, anatase
Stable	Apatite, garnet (iron-poor), staurolite, monazite, biotite, ilmenite, magnetite
Moderately stable	Epidote, kyanite, garnet (iron-rich), sillimanite, sphene, zoisite
Unstable	Hornblende, actinolite, augite, diopside, hypersthene, andalusite
Very unstable	Olivine

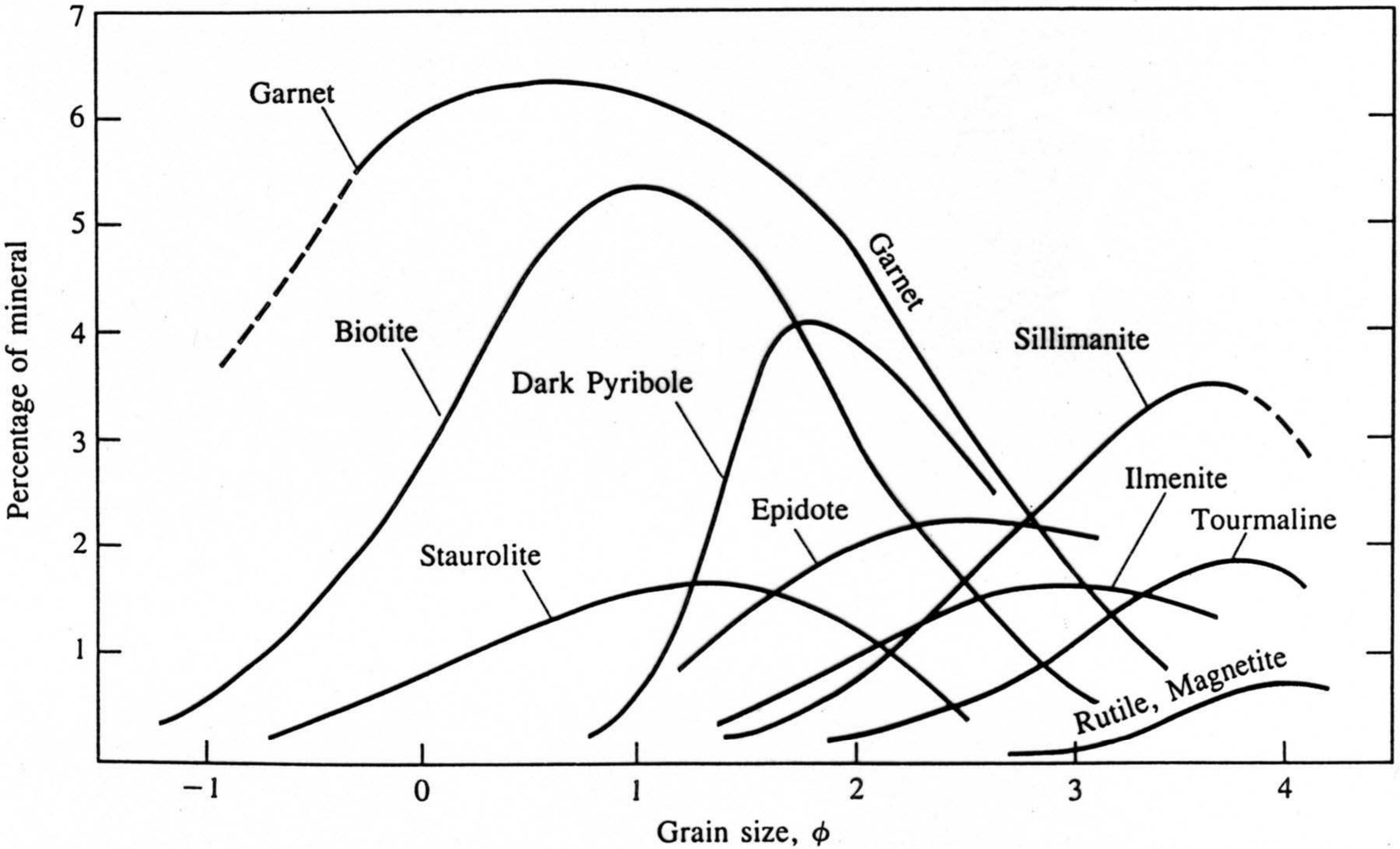

Figure 4-15
Size distributions of heavy minerals in the Kitt Brook delta (Pleistocene), Connecticut. The distributions are the combined effect of the sizes of these minerals in the source terrane and the sorting processes during transport and deposition. [E. R. Force and B. D. Stone, 1990, *U.S. Geol. Surv. Bull., 1874,* 19.]

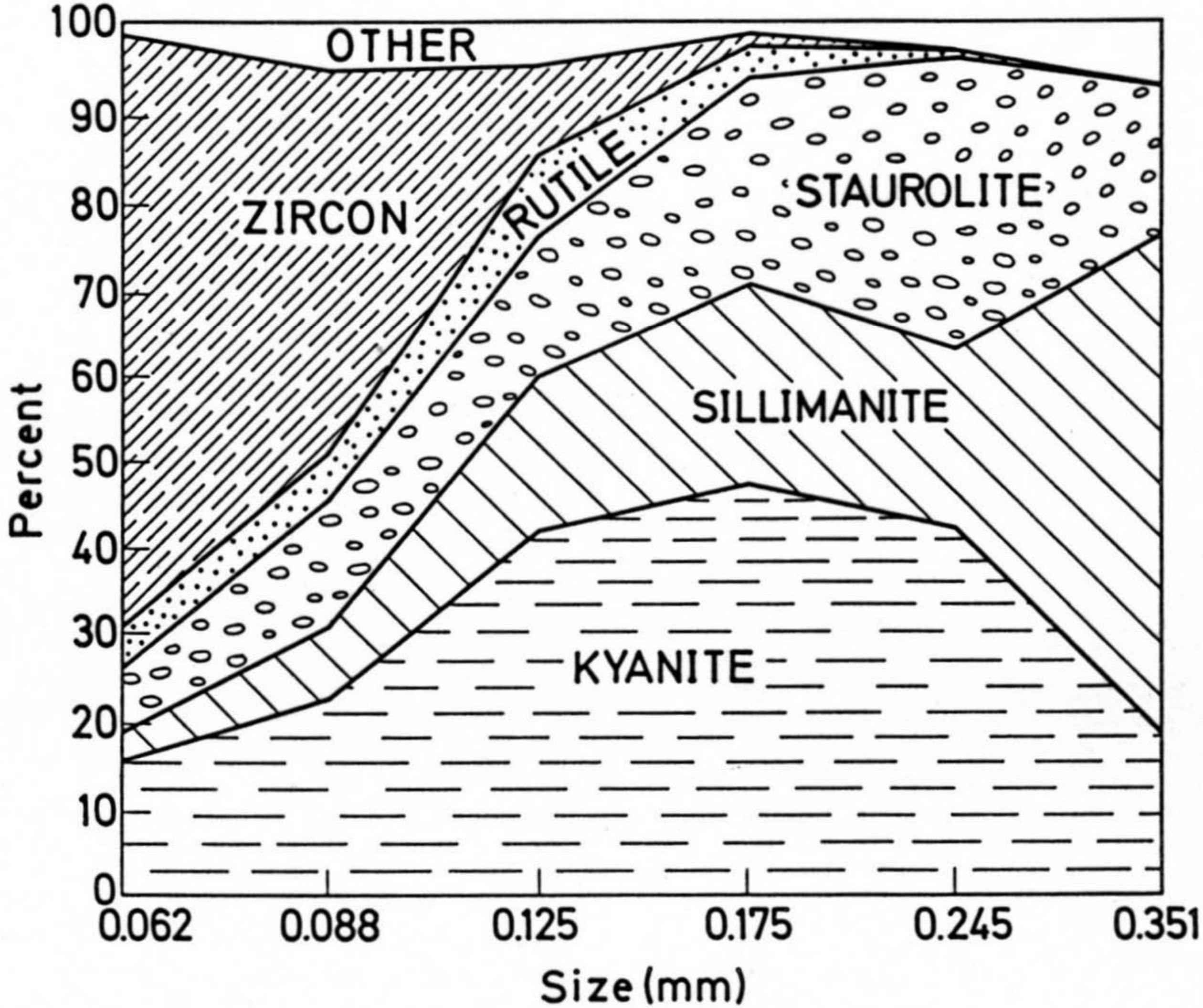

Fig. 8-7. Diagram showing relations between grain size and heavy mineral frequencies. Lafayette sand, western Kentucky (redrawn from Potter, 1955, Fig. 3)

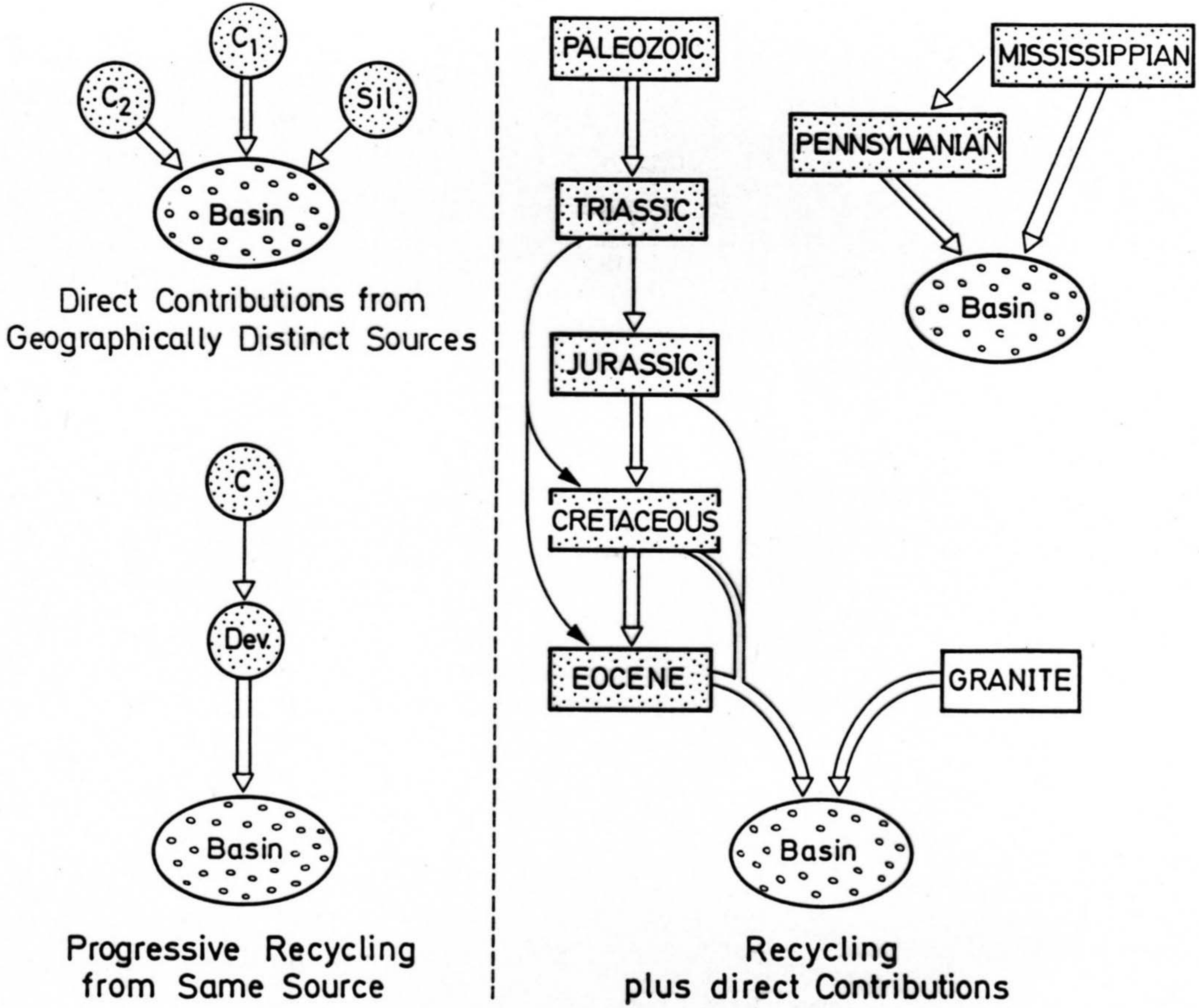

Fig. 8-8. Some common paths of mineral evolution

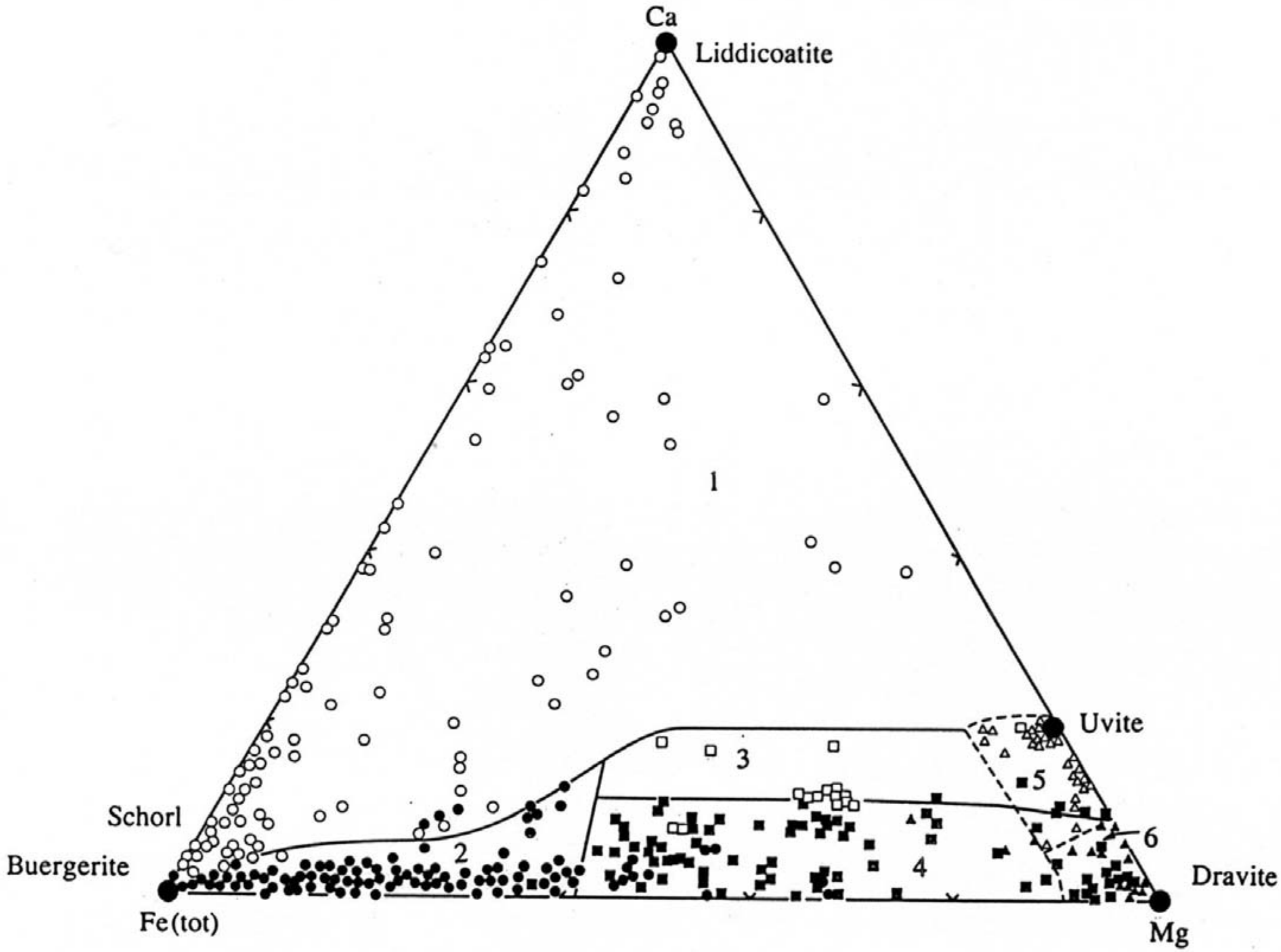

Figure 4-16
Ca–Fe–Mg molecular proportions for tourmaline from various types of crystalline rocks. Several of the common end-members are plotted for reference. The fields are (1) Li-rich granitoid pegmatites and aplites; (2) Li-poor granitoids and associated pegmatites and aplites; (3) Ca-rich metapelites, metasandstones, and calcsilicate rocks; (4) Ca-poor metapelites, metasandstones, and quartz-tourmaline rocks; (5) metacarbonates; and (6) meta-ultramafics. [D. J. Henry and C. V. Guidotti, 1985, *Amer. Miner., 70,* 4.]

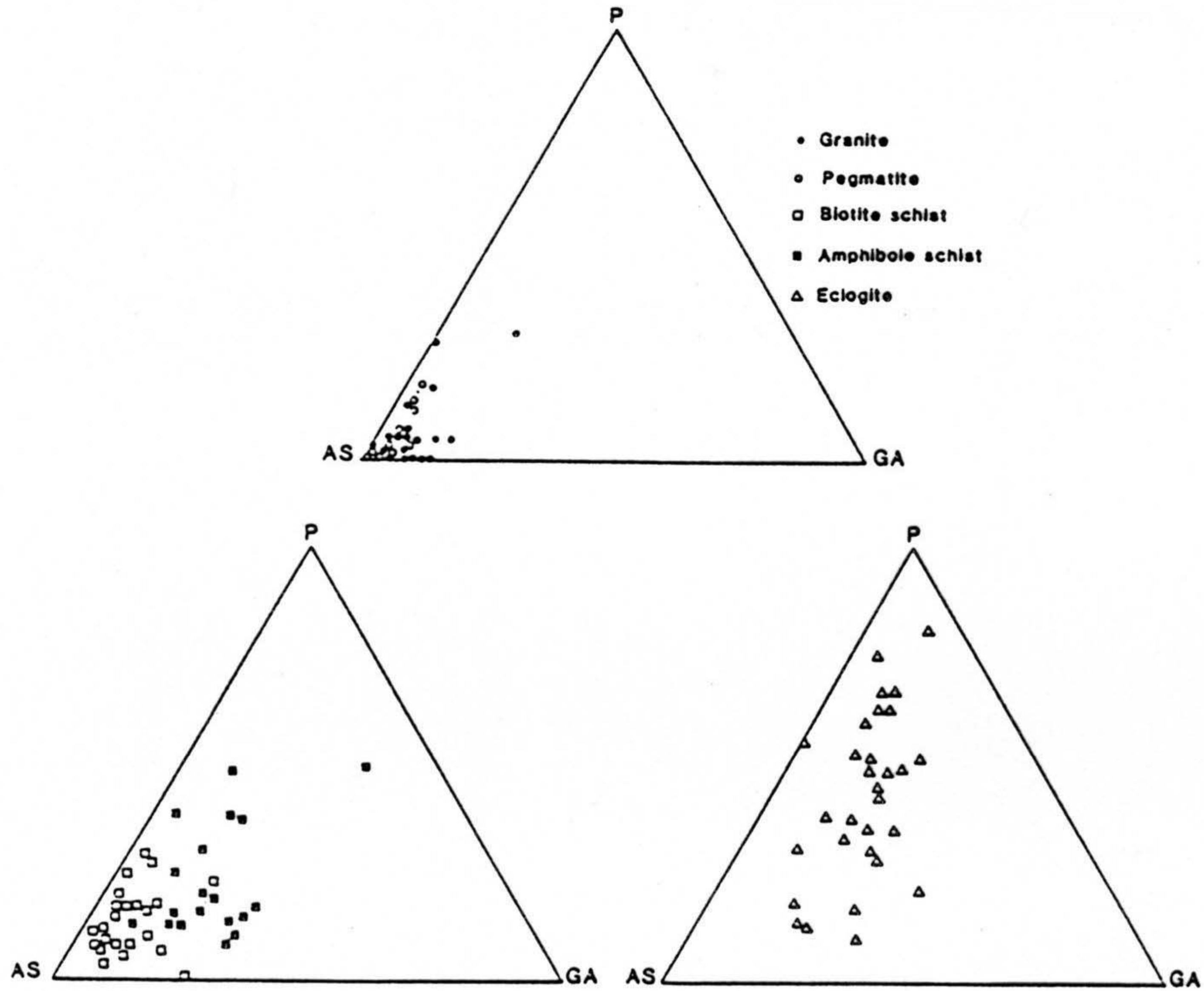

Fig. 11. Variation in composition of garnets from different source lithologies, from Wright (1938). AS, almandine + spessartine; P, pyrope; GA, grossular + andradite.

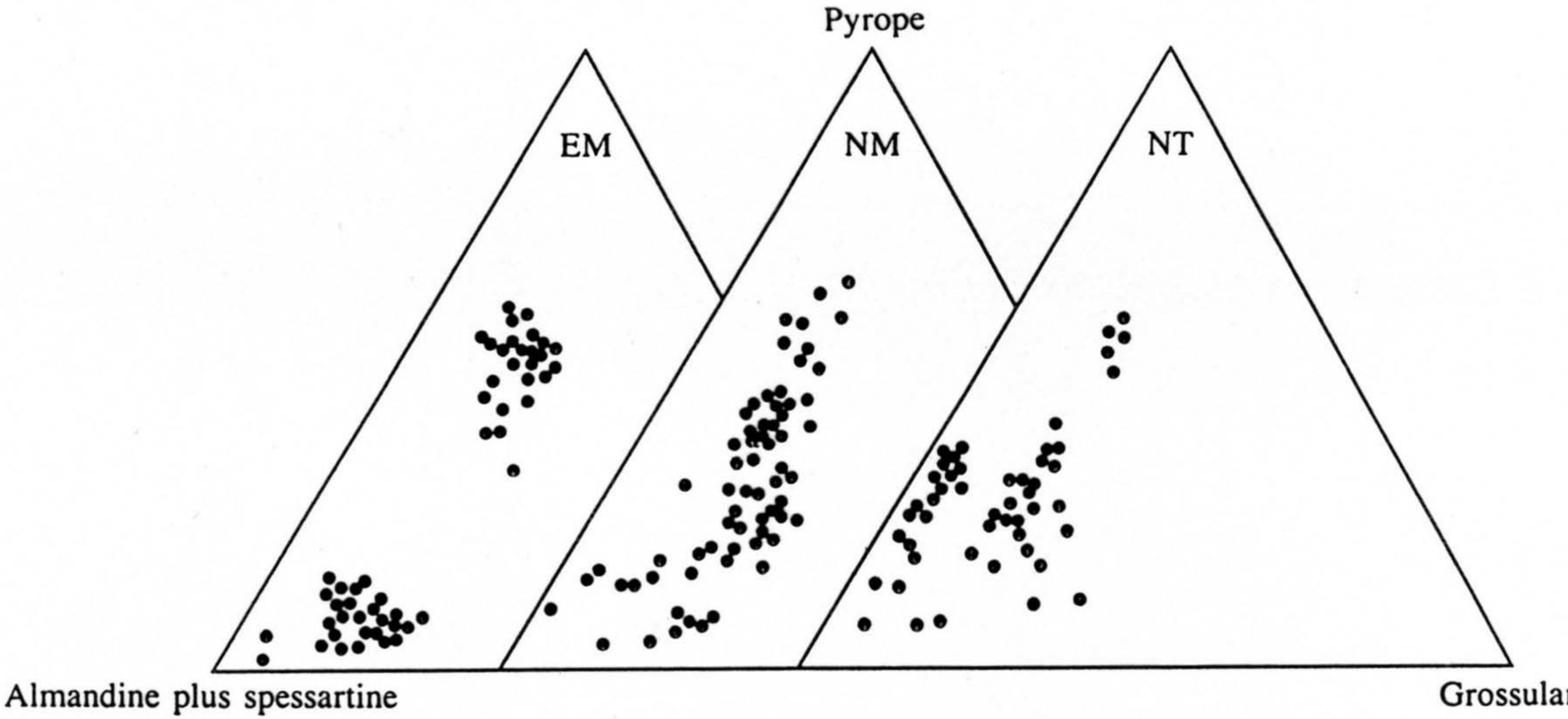

Figure 4-17
Comparison of electron microprobe analyses of garnet grains. Sample EM is from Etive Formation, Murchison Field; NM, from Ness Formation, Murchison Field, NT, from Ness Formation, Tern Field, which is about 50 km from Murchison. The Ness Formation immediately overlies the Etive Formation. [Modified from Morton, 1985a, p. 556.]

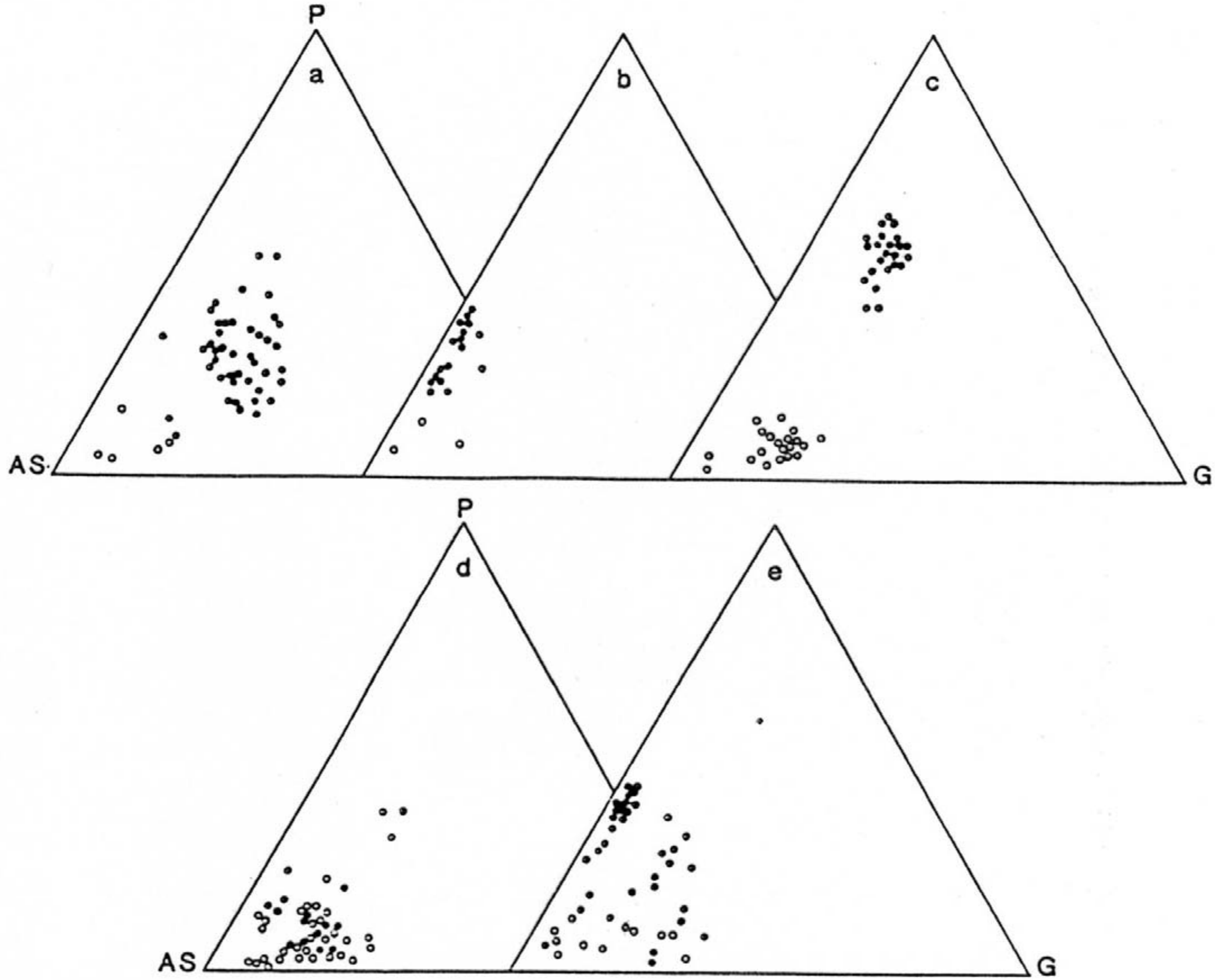

Fig. 10. Illustration of the variety of compositions shown by detrital garnets of North Sea sediments. (a) Oseberg Formation (Middle Jurassic), Oseberg Field (from Hurst & Morton 1988). (b) Broom Formation (Middle Jurassic), Murchison Field (from Morton 1985*b*). (c) Etive Formation (Middle Jurassic), Murchison Field (from Morton 1985*b*). (d) Ness Formation (Middle Jurassic), Oseberg Field (from Hurst & Morton 1988). (e) Forties formation (Palaeocene), Forties Field (from Morton 1987*b*). AS, almandine + spessartine; P, pyrope; g, grossular. Open circles have spessartine > 5%, closed circles have spessartine < 5%.

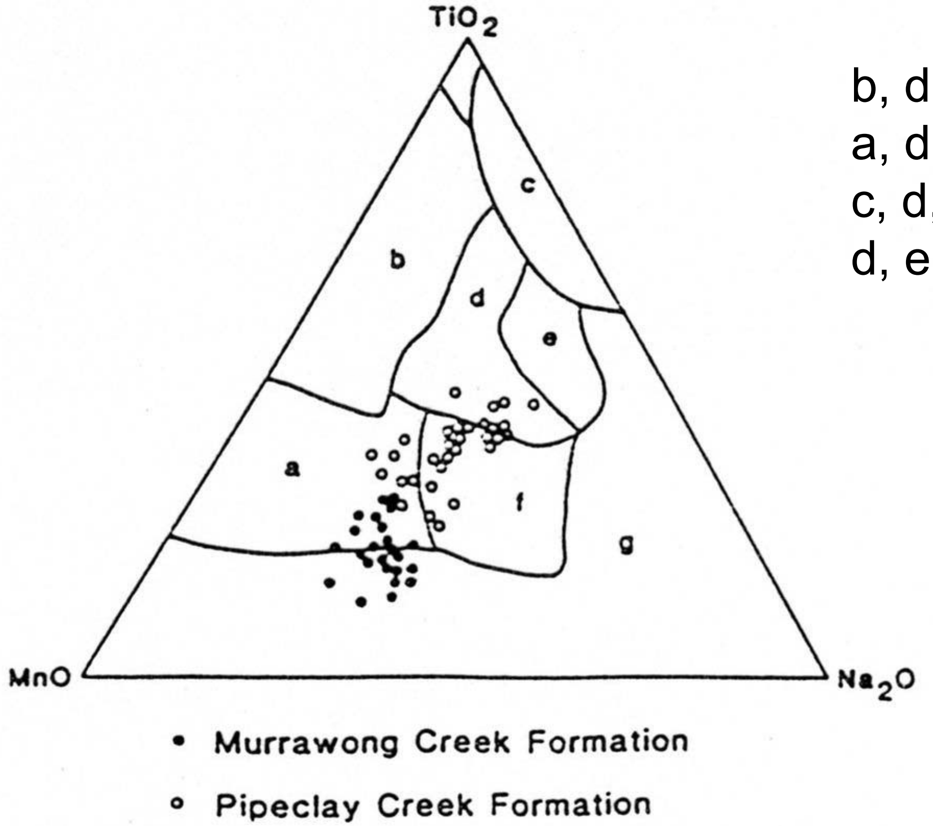

Fig. 4. Discrimination of provenance of detrital pyroxenes from two formations belonging to a Palaeozoic clastic sequence in eastern Australia, using the plot described by Nisbet & Pearce (1977). Ocean floor basalts plot in fields b and d. Volcanic arc basalts plot in fields a, d, e and f. Within-plate alkalic basalts plot in fields c, d, f and g. Within-plate tholeiites plot in fields d and e.

b, d – oc. basalt
a, d, e, f – volc. arc basalt
c, d, f, g – within-plate alkali basalts
d, e – within-plate tholeiites

authigenic minerals : abundant
allogenic minerals : stable to ultrastable
proportion of allogenic heavy minerals : small (locally nil)

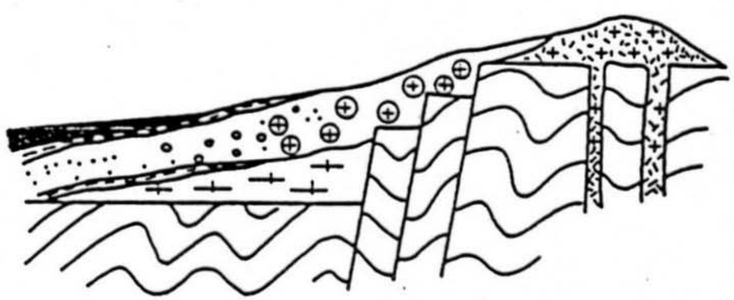

pyroclastic fan
(e.g. Stockheim)

authigenic minerals : common
allogenic minerals : labile to ultrastable
proportion of allogenic heavy minerals : large

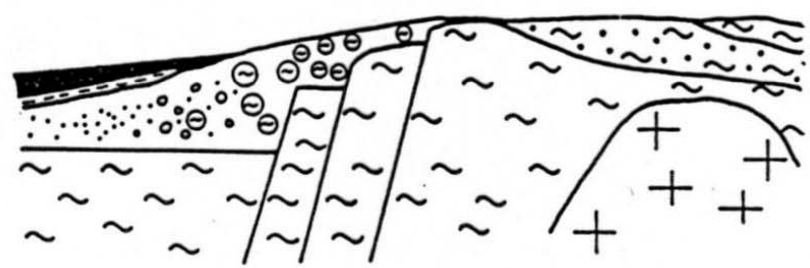

mixed fan
alluvial > pyroclastic
(e.g. Erbendorf)

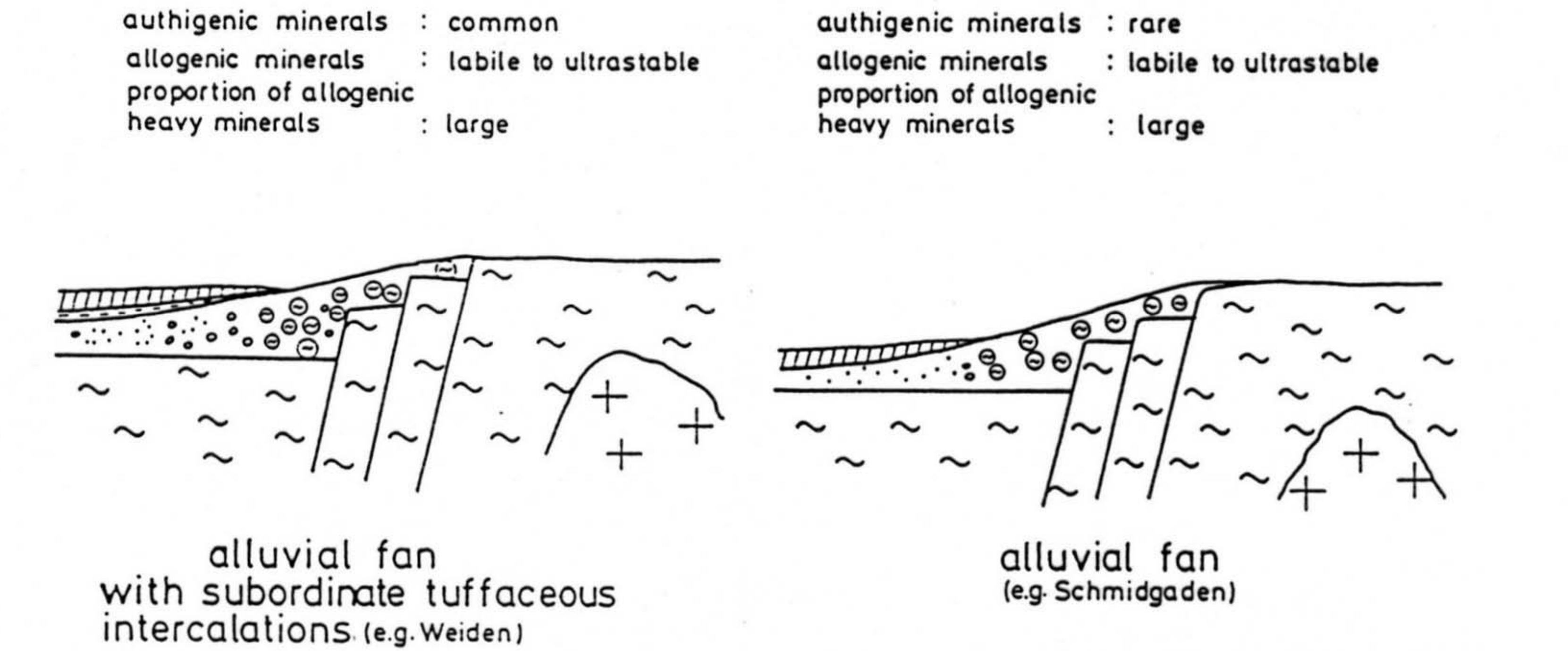

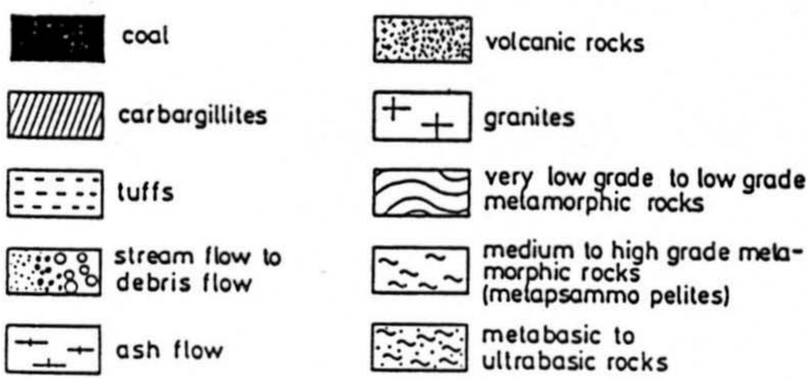

Fig. 5. Cartoon to illustrate the various types of fans as well as the sort and amount of heavy minerals present in these clastic and volcaniclastic rocks.

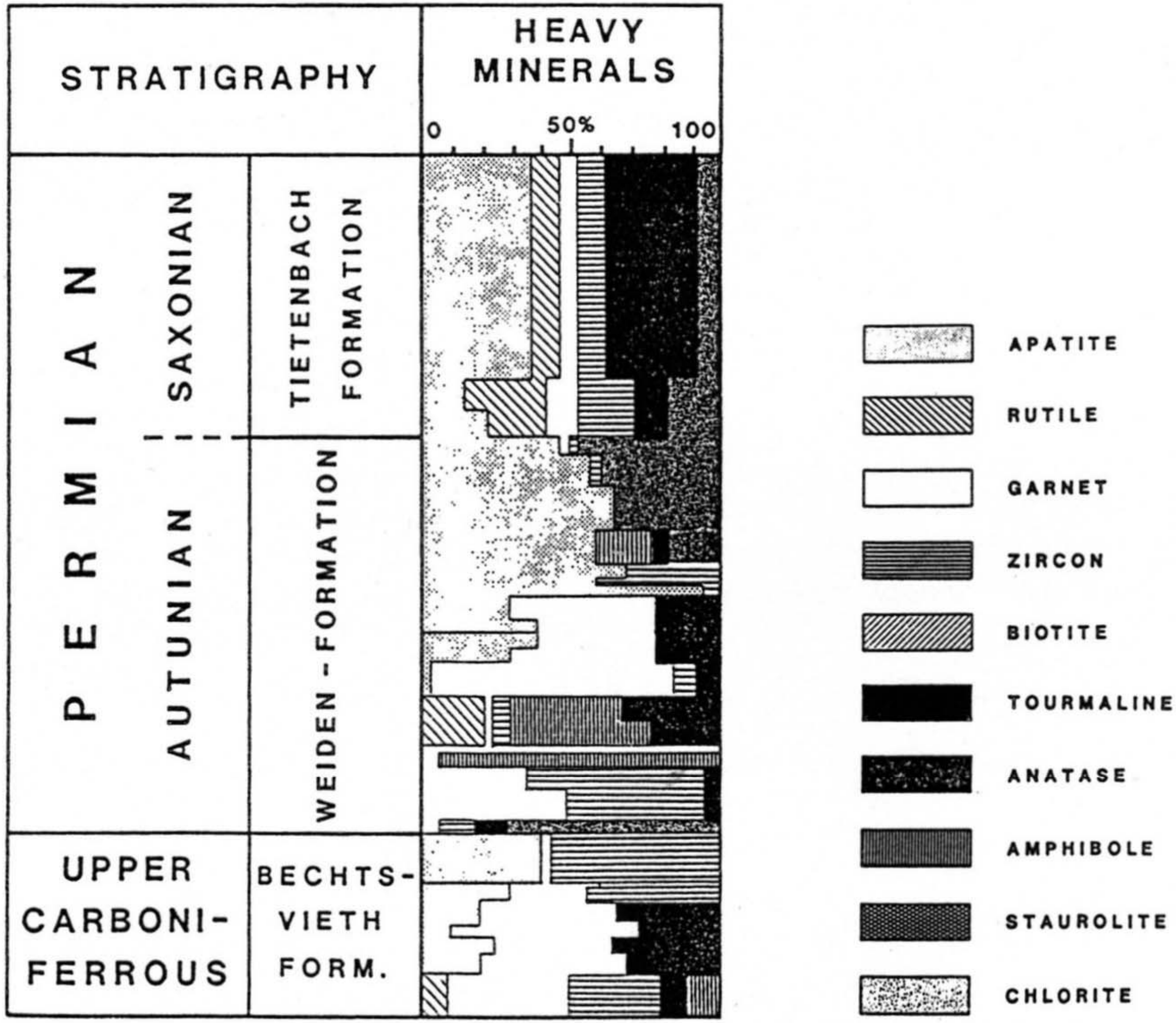

Fig. 6. The heavy mineral log of Erbendorf basin (mixed fan type II) taken as representative for the stratigraphically-controlled

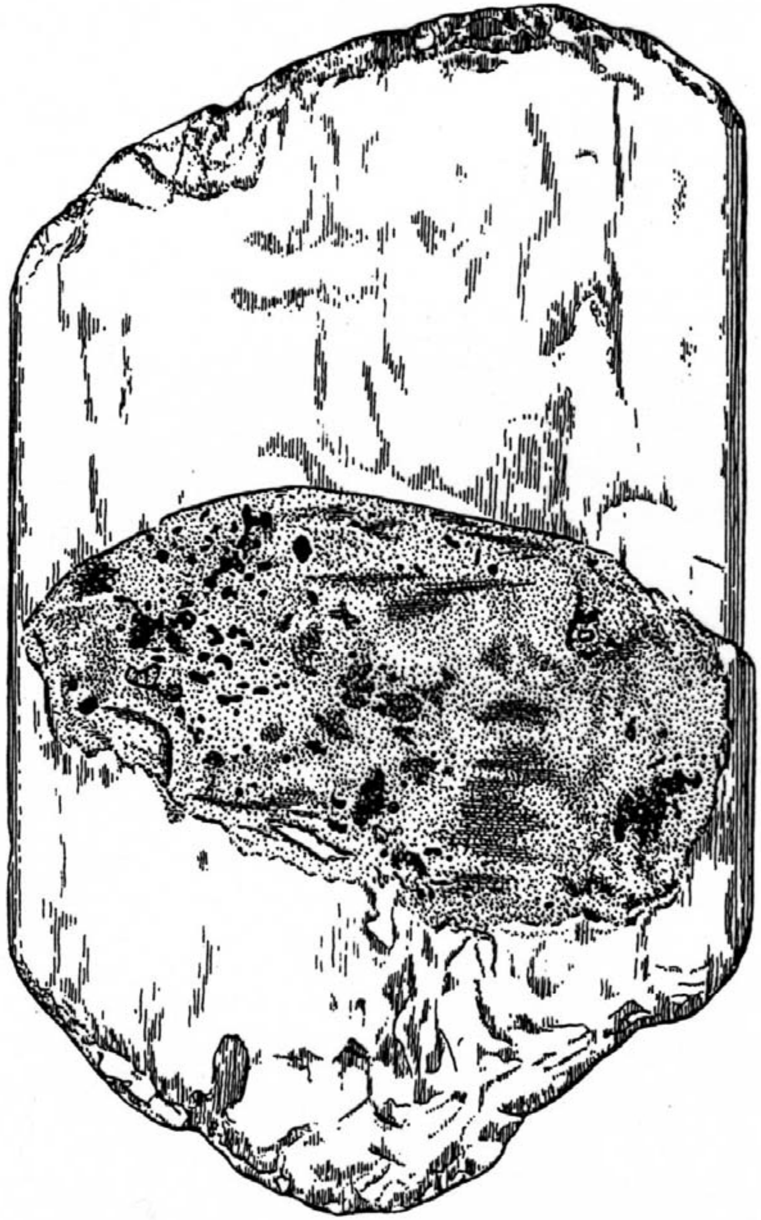

Fig. 8-3. Abraded tourmaline overgrowth on abraded detrital core, Cretaceous McNairy Sand, Henry County, Tennessee, U.S.A. (Redrawn from Potter and Pryor, 1961, Plate 2)

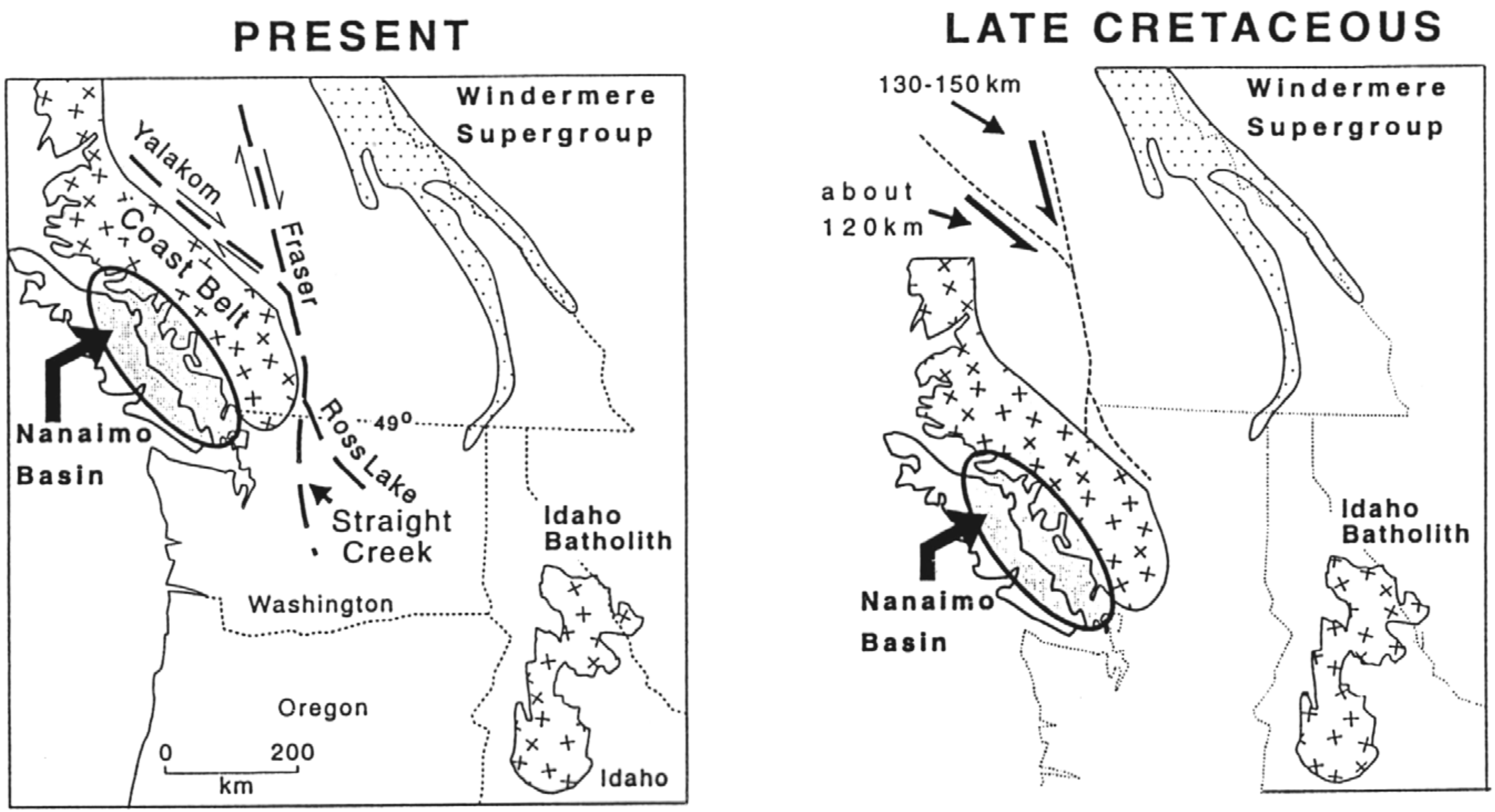

FIG. 5.—Schematic diagrams showing position of Nanaimo Basin and Coast Belt at present (left) and approximate position during latest Cretaceous (right) with about 250 of dextral strike-slip movement restored on Fraser-Straight Creek and Yalakom-Ross Lake fault systems. This minimum estimate of offset does not include offset on the several other early Tertiary strike-slip faults in northwest Washington and southern B. C. or any estimate of the amount of early Tertiary extension.

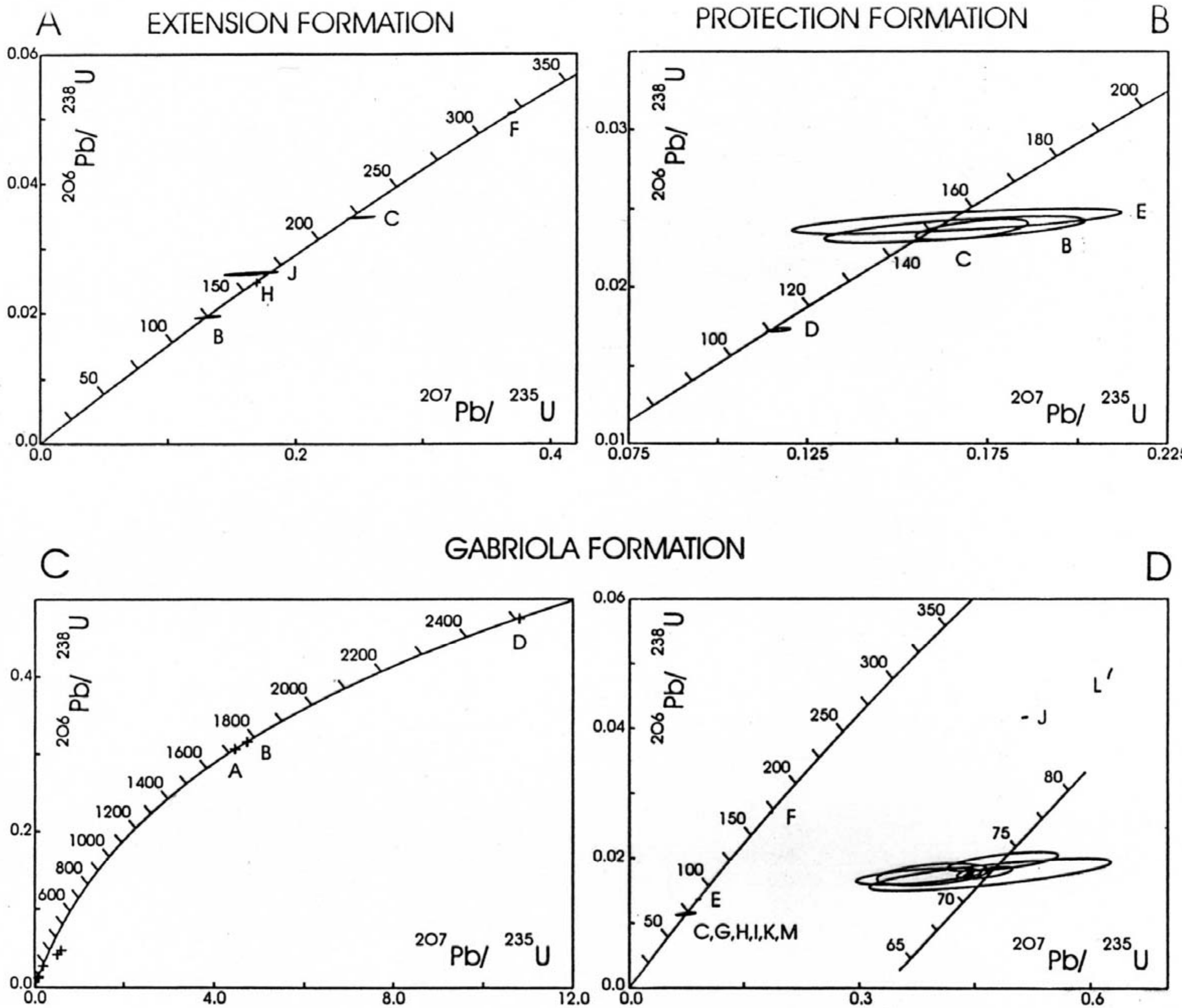

FIG. 4.—U-Pb Concordia plots showing detrital zircon data. (A) Extension Formation; (B) Protection Formation; (C) Gabriola Formation (all data); (D) Gabriola Formation, expanded scale plot of post Pre-Cambrian data.

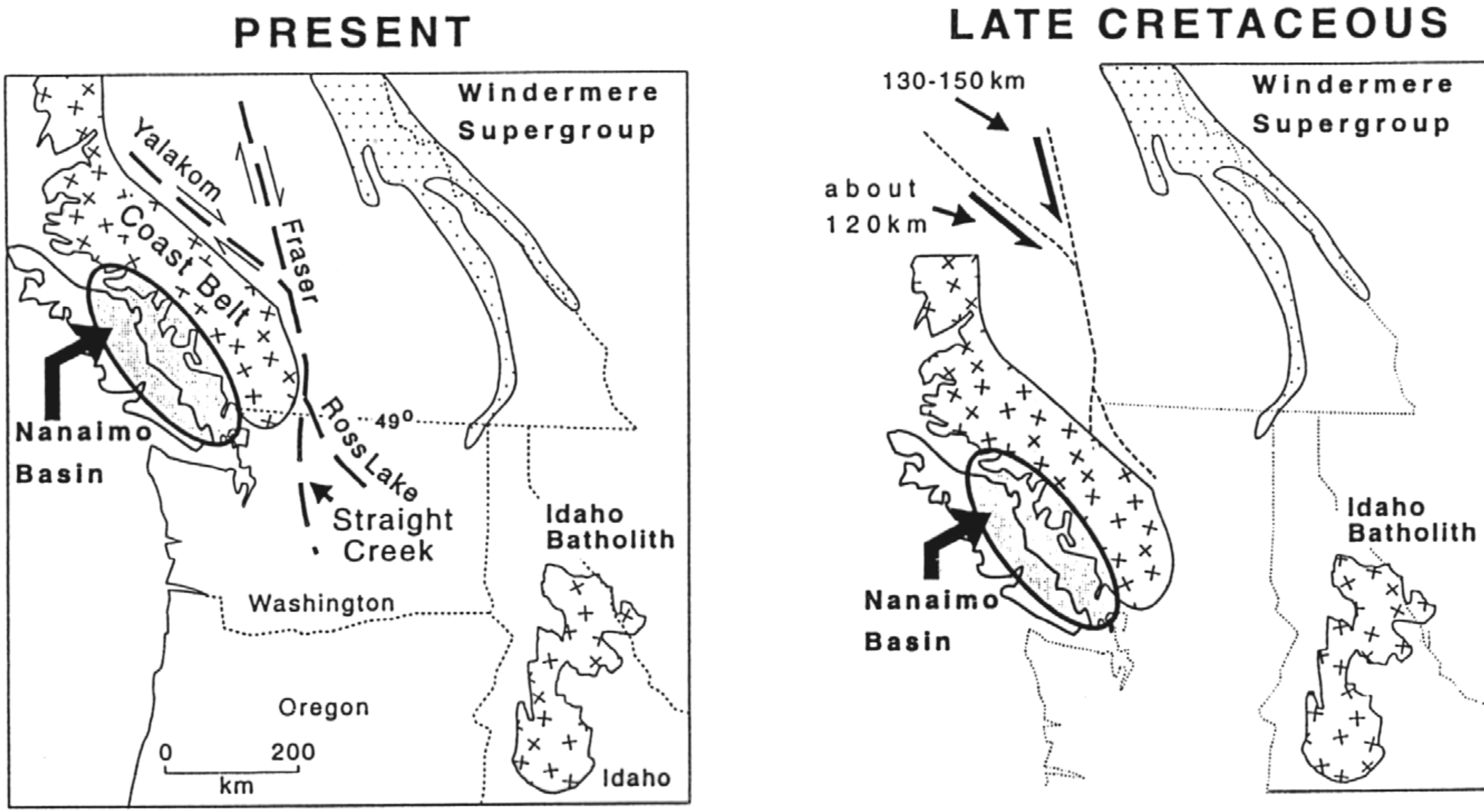

FIG. 5.—Schematic diagrams showing position of Nanaimo Basin and Coast Belt at present (left) and approximate position during latest Cretaceous (right) with about 250 of dextral strike-slip movement restored on Fraser-Straight Creek and Yalakom-Ross Lake fault systems. This minimum estimate of offset does not include offset on the several other early Tertiary strike-slip faults in northwest Washington and southern B. C. or any estimate of the amount of early Tertiary extension.

diagenesis

- geothermal gradient, thermal models
- porosity, permeability
- pressure solution, secondary porosity
- compaction
- cements - quartz (syntaxial overgrowths, ..), carbonate, authigenic feldspars (overgrowths), clay minerals, zeolites, haematite, barite
- diagenetic environments
- clay mineral crystalinity

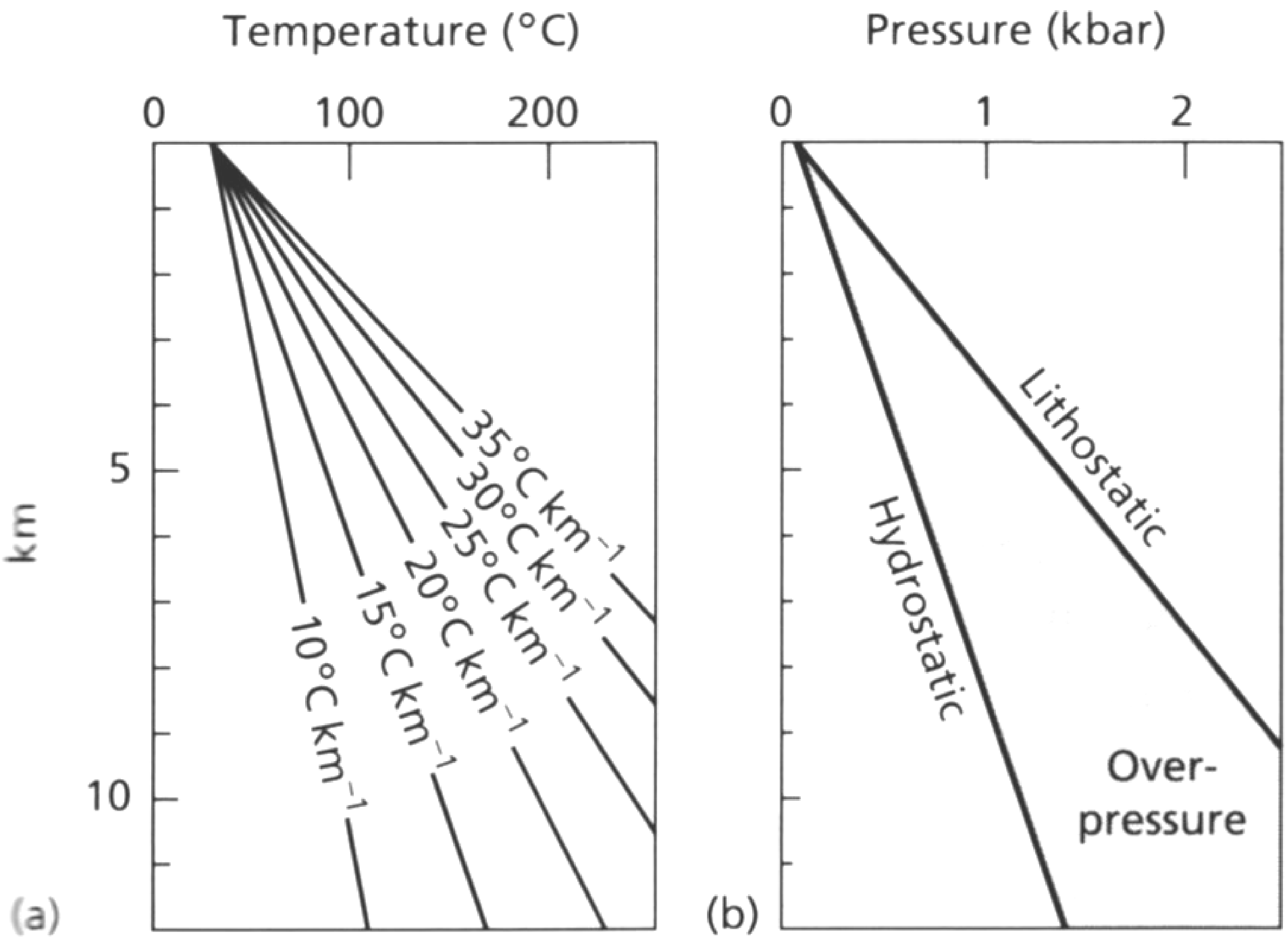

Fig. 2.53 (a) Increase in temperature with increasing depth for different geothermal gradients. (b) Increase in hydrostatic and lithostatic (overburden) pressure with increasing depth.

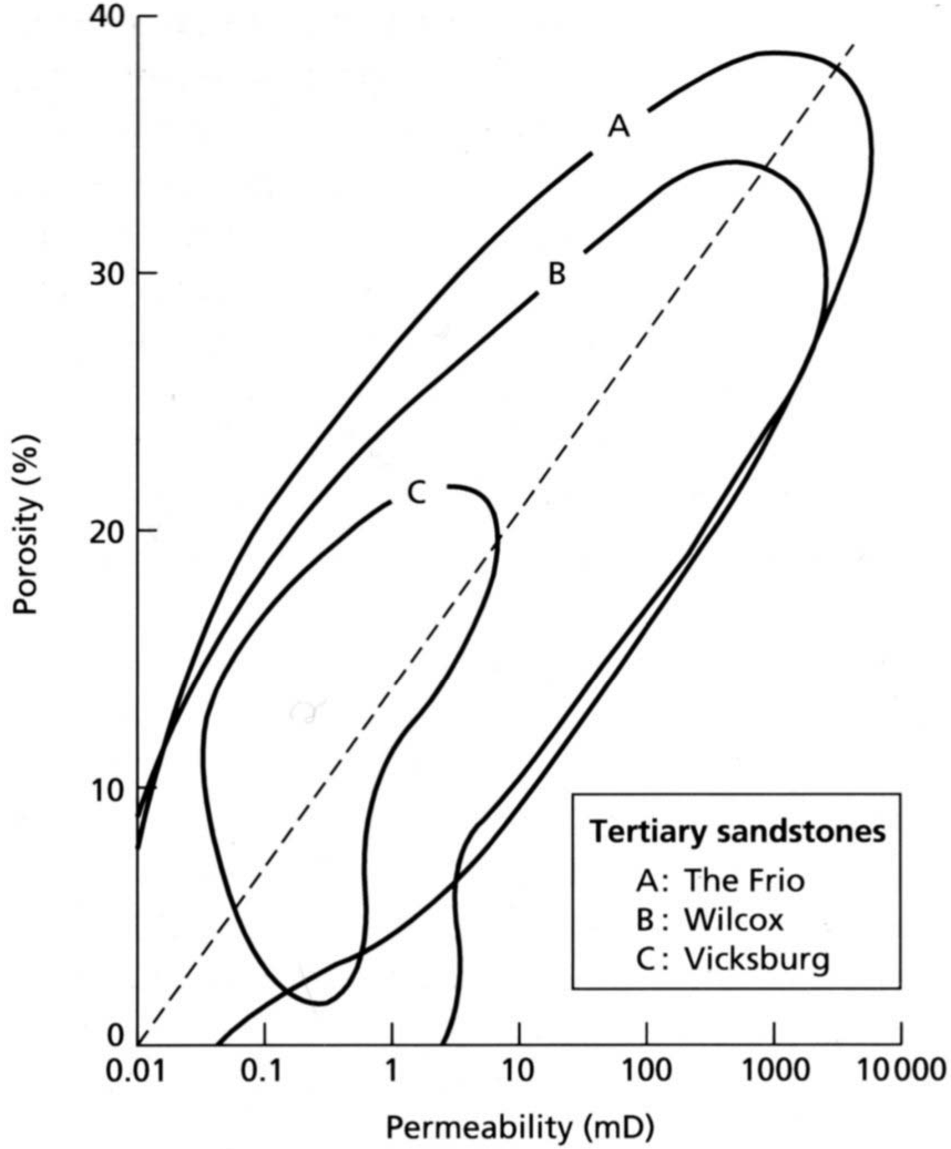

Fig. 2.59 Porosity–permeability plot for three Tertiary sandstones of the Gulf Coast subsurface, the Frio (a), Wilcox (b) and Vicksburg (c), showing the general increase in permeability with increasing porosity. After Loucks *et al*. (1984).

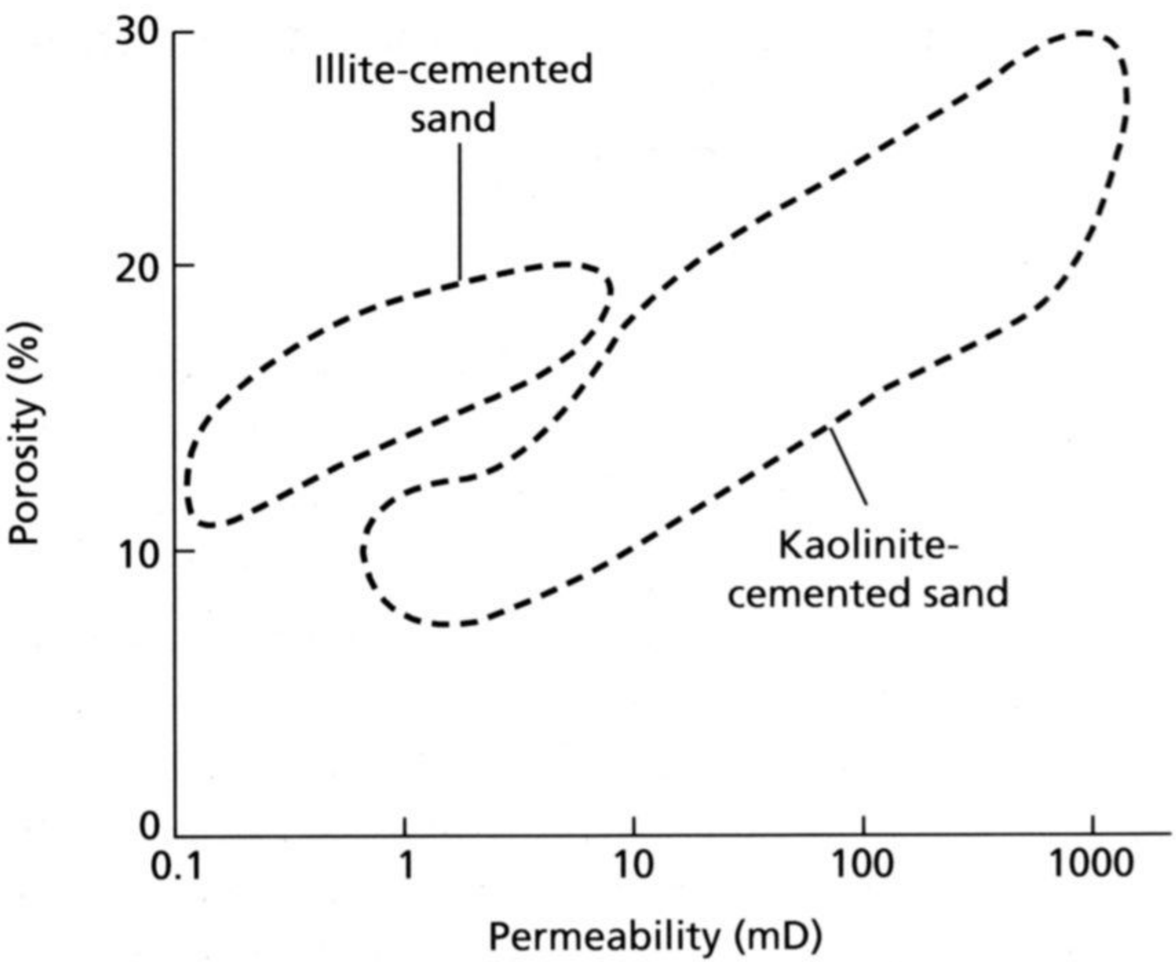

Fig. 2.56 Porosity–permeability plot for kaolinite- and illite-cemented aeolian sandstones in the Permian Rotliegendes. Southern North Sea. After Stalder (1973).

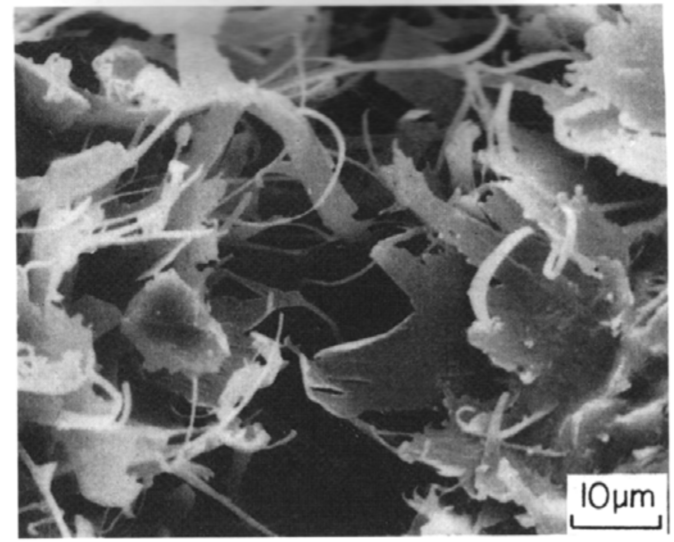

Fig. 2.54 Scanning electron micrograph of authigenic illite in the form of radially arranged flakes and whiskers growing into pore space between two sand grains (left and right of picture). Rotliegend desert sandstone, Lower Permian. Northern Germany.

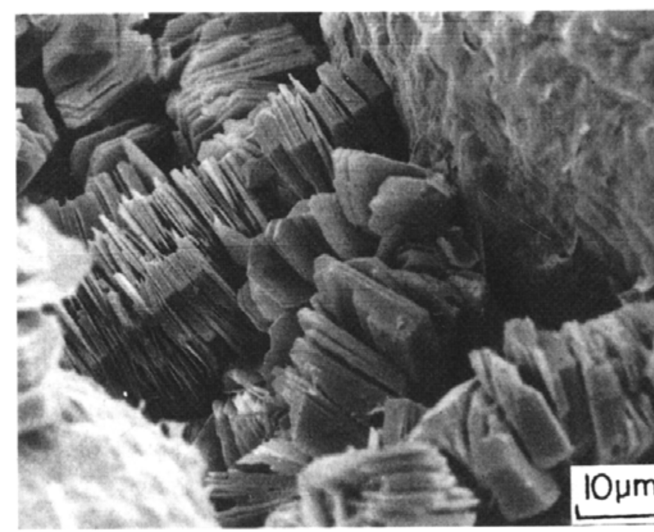

Fig. 2.55 Scanning electron micrograph of authigenic kaolinite, consisting of stacked pseudohexagonal platy crystals, between rounded sand grains. Rotliegend desert sandstone. Lower Permian. Northern Germany.

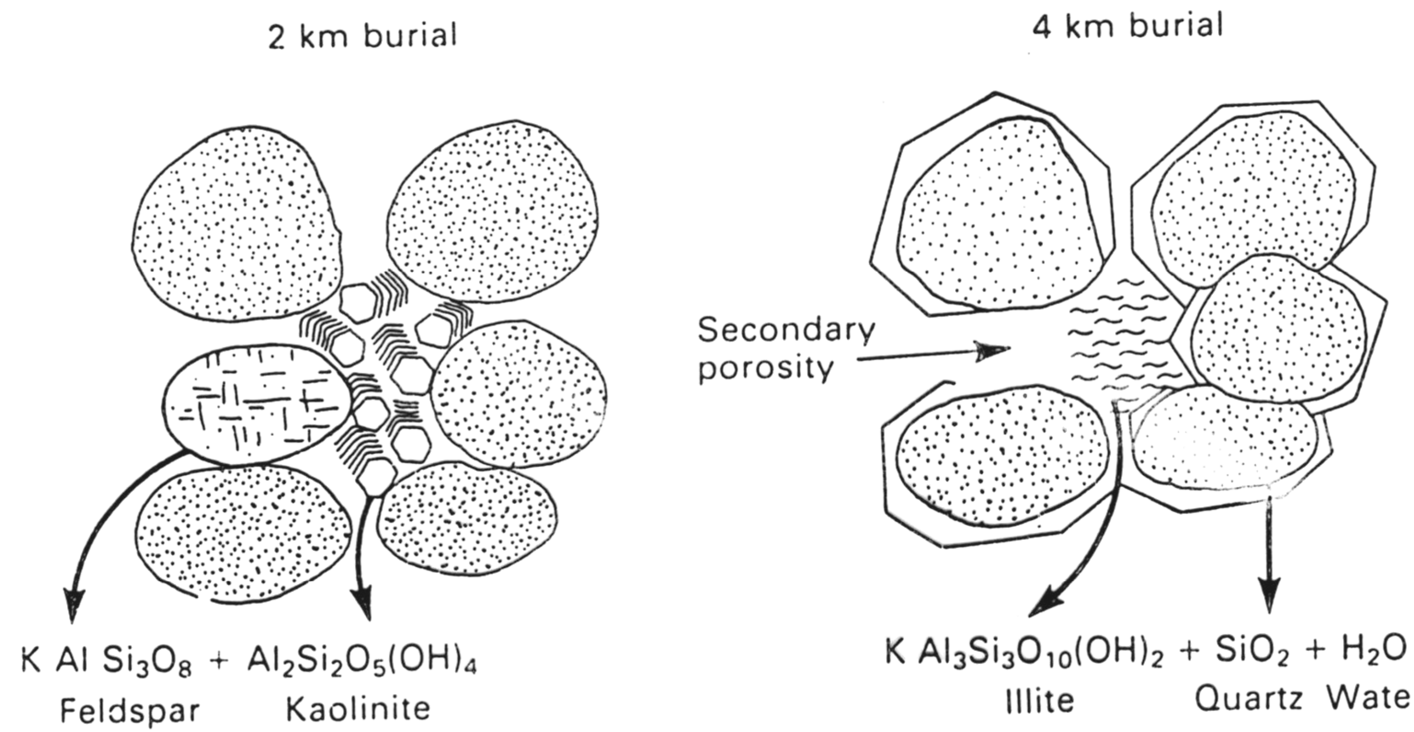

Fig. 5.28. Chemical reactions between feldspar and kaolinite are triggered by continued burial to produce illite, quartz overgrowth cements plus secondary porosity (from Bjørlykke, 1983).

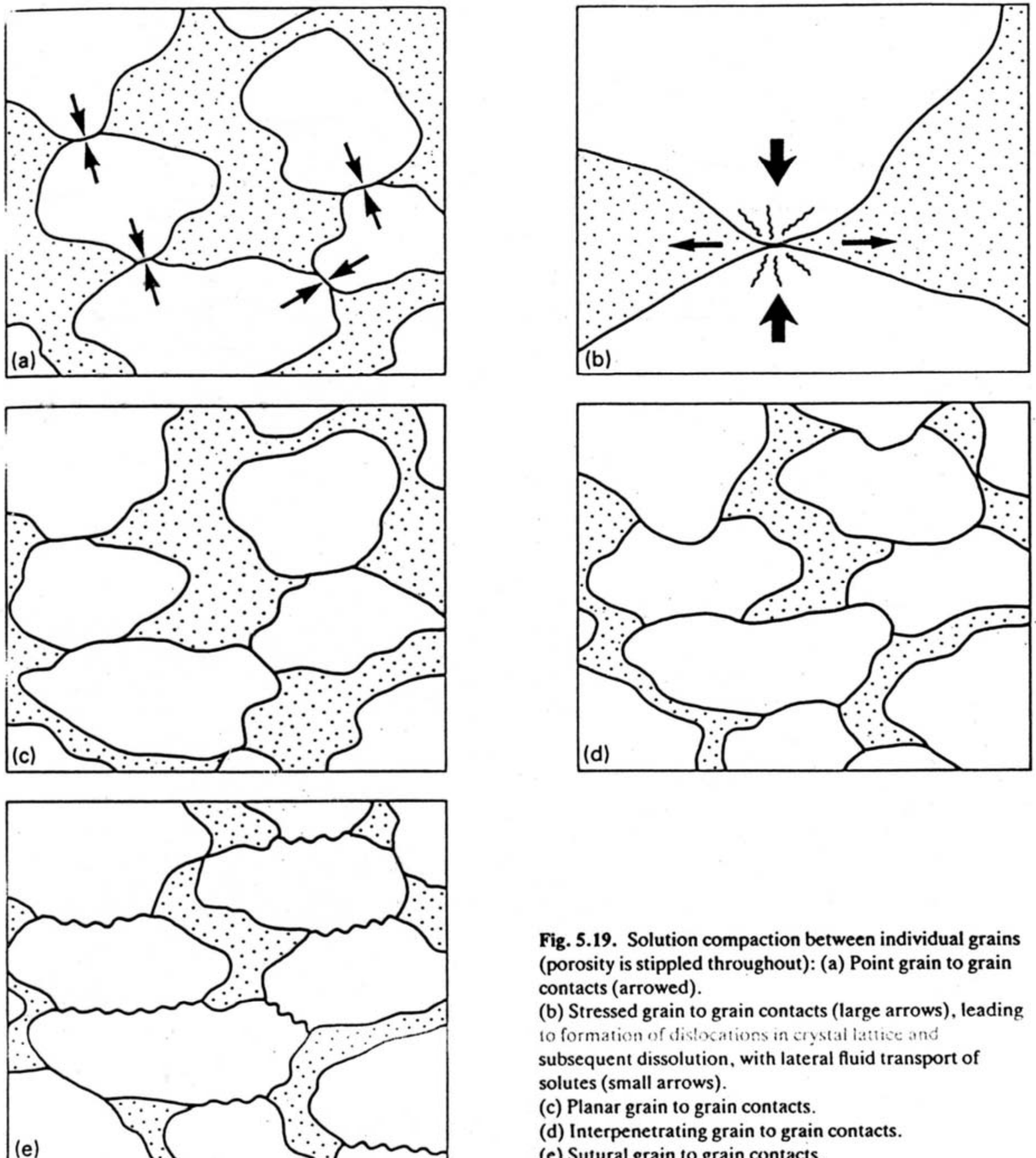

Fig. 5.19. Solution compaction between individual grains (porosity is stippled throughout): (a) Point grain to grain contacts (arrowed).
(b) Stressed grain to grain contacts (large arrows), leading to formation of dislocations in crystal lattice and subsequent dissolution, with lateral fluid transport of solutes (small arrows).
(c) Planar grain to grain contacts.
(d) Interpenetrating grain to grain contacts.
(e) Sutural grain to grain contacts.

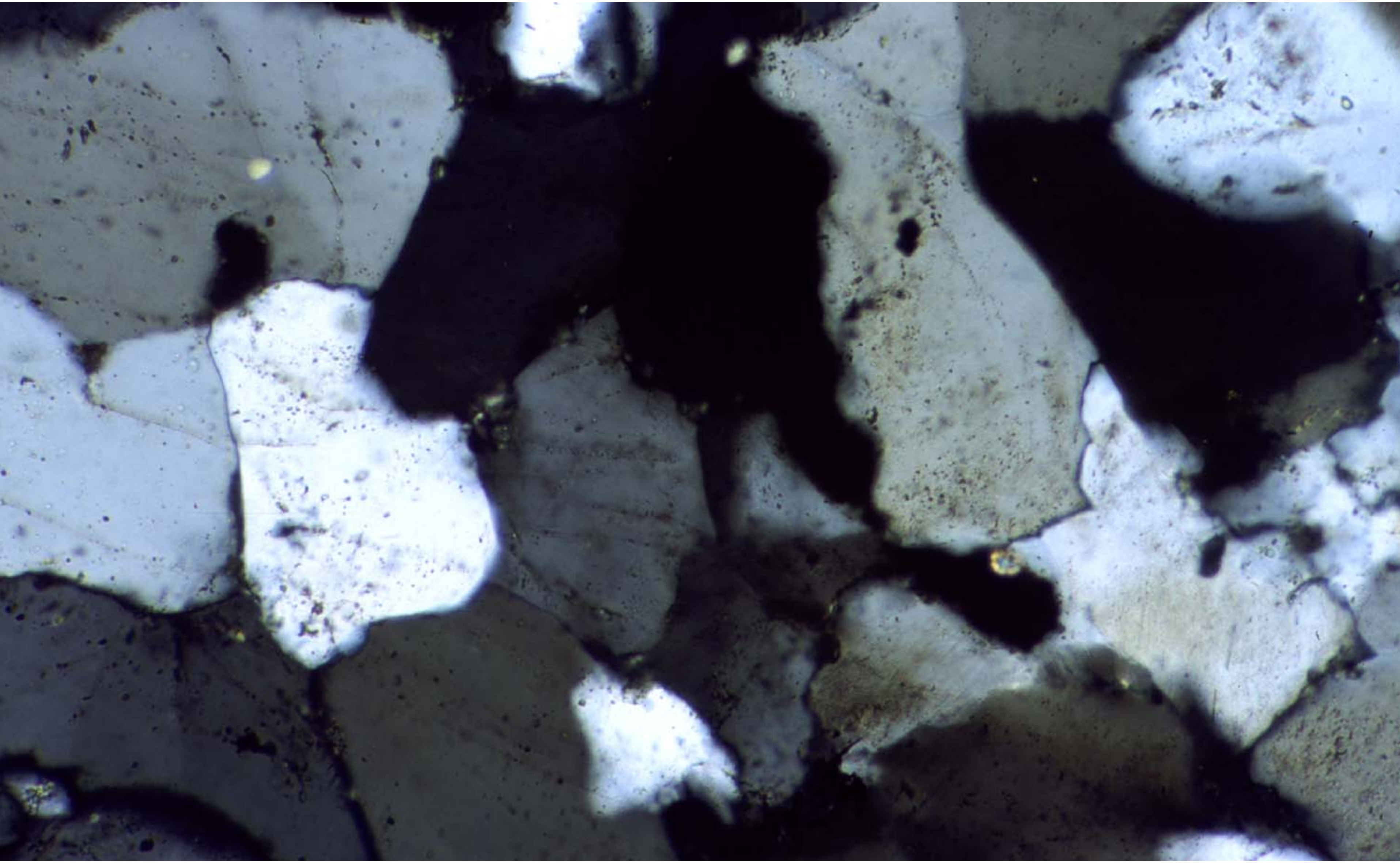

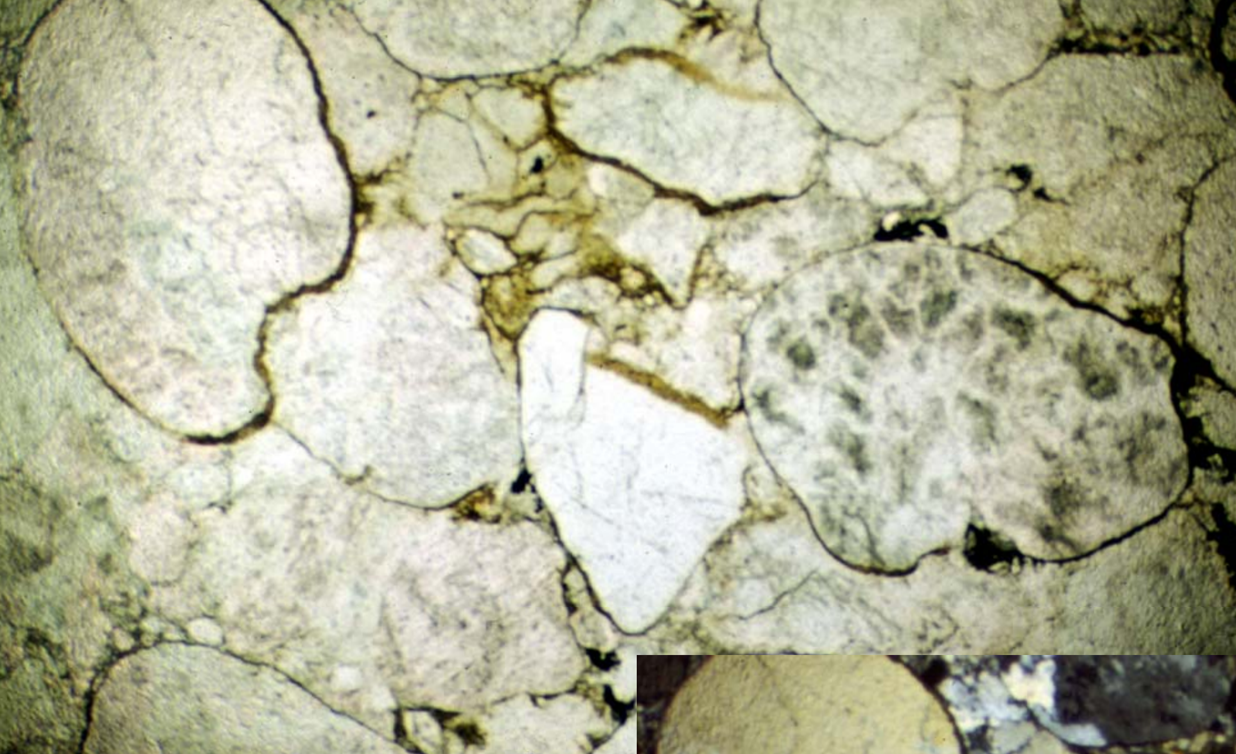

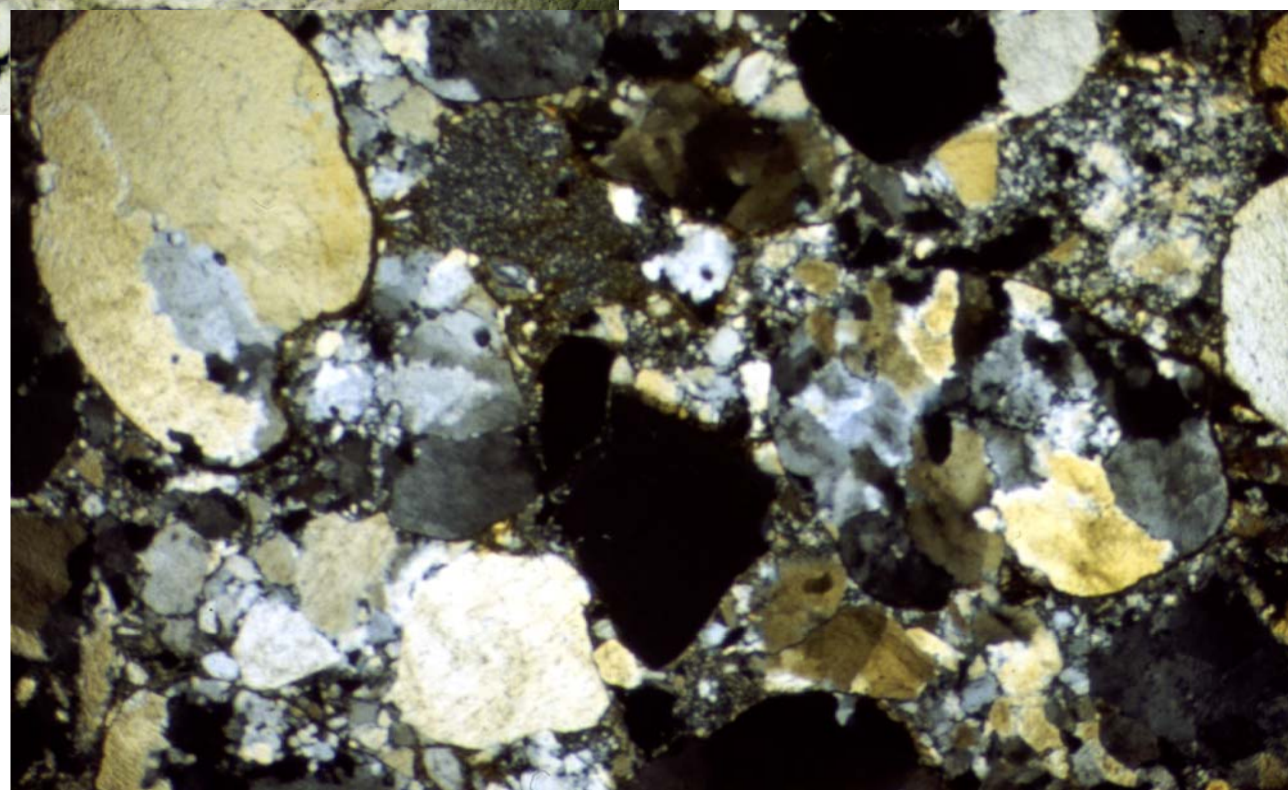

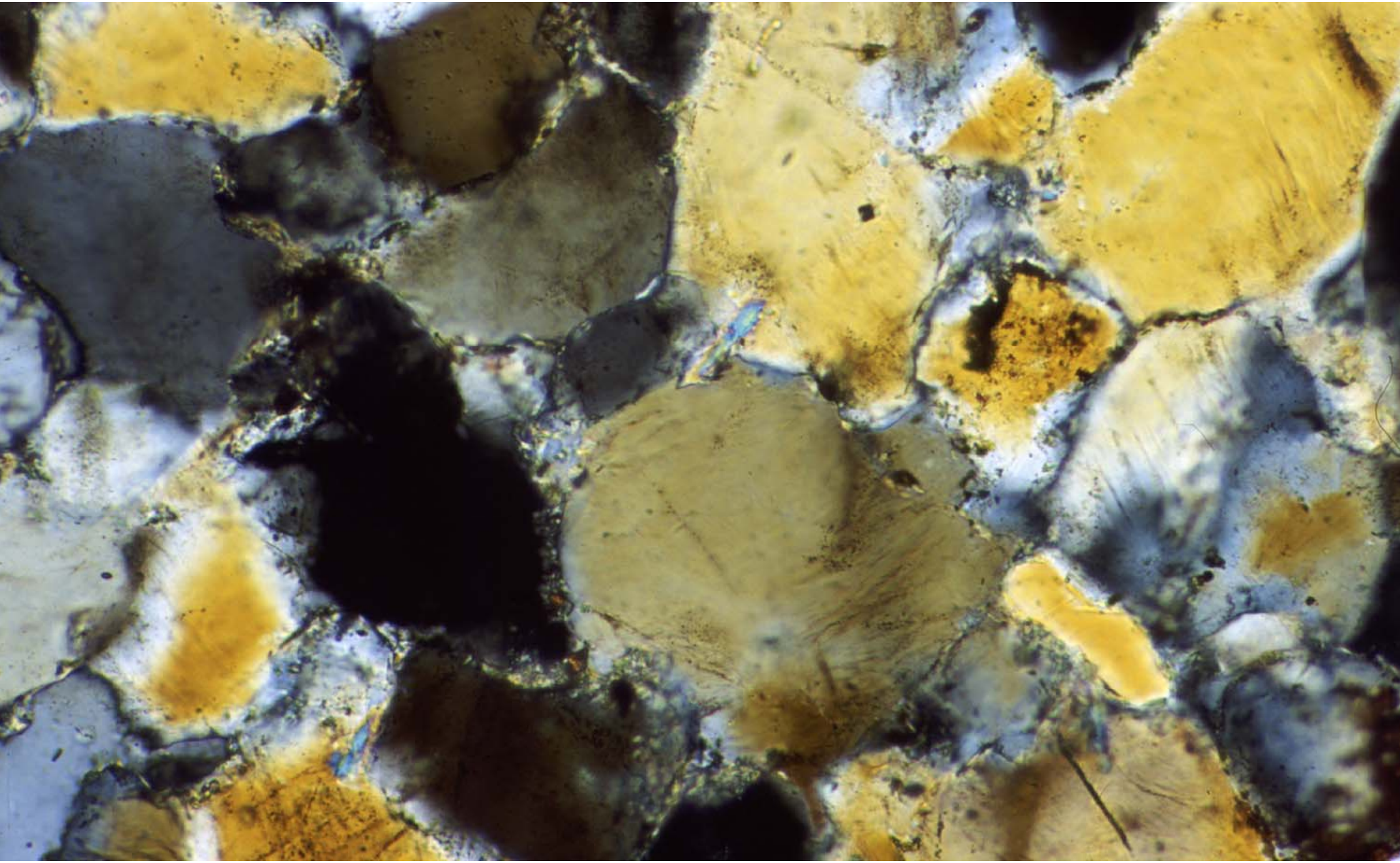

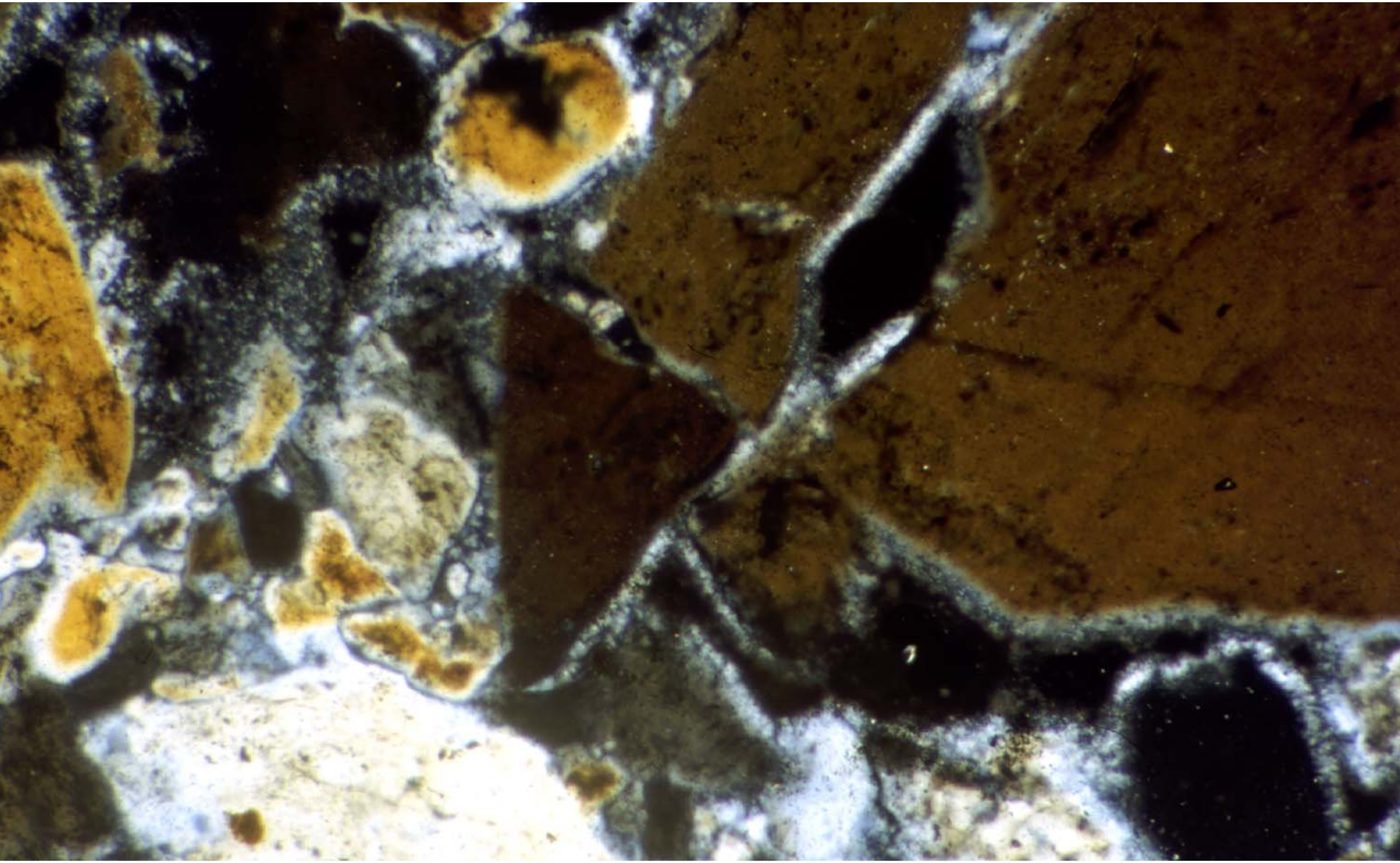

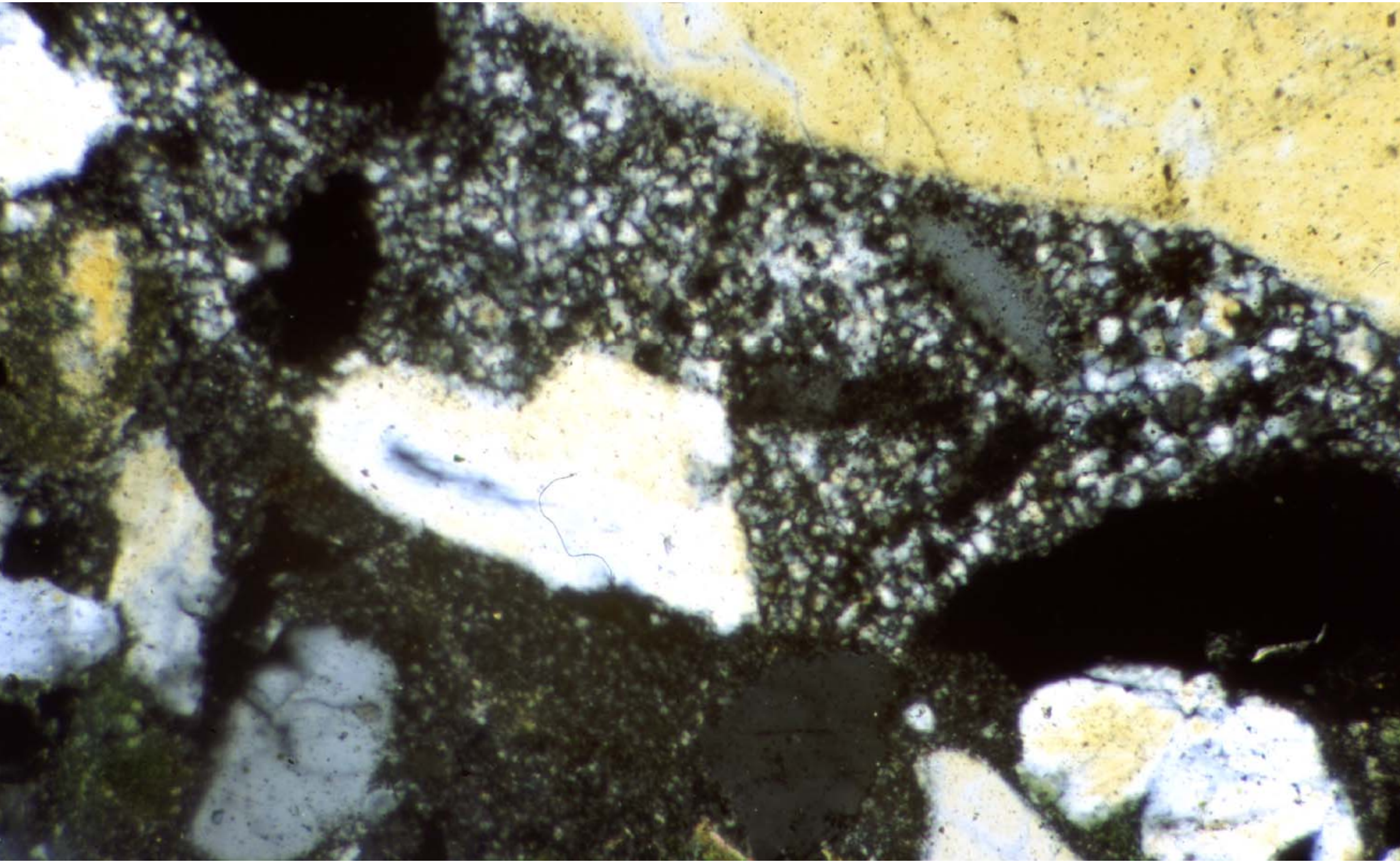

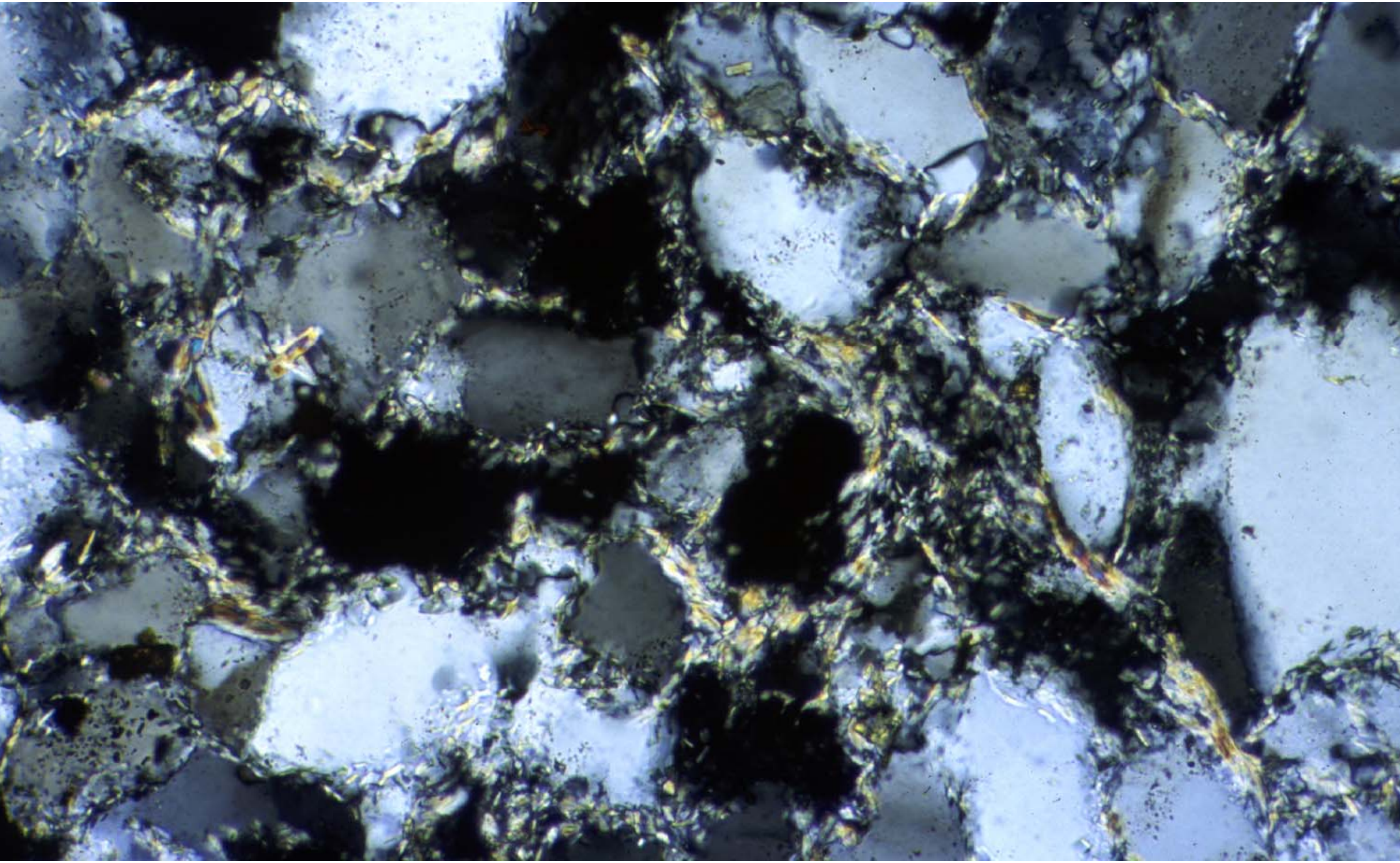

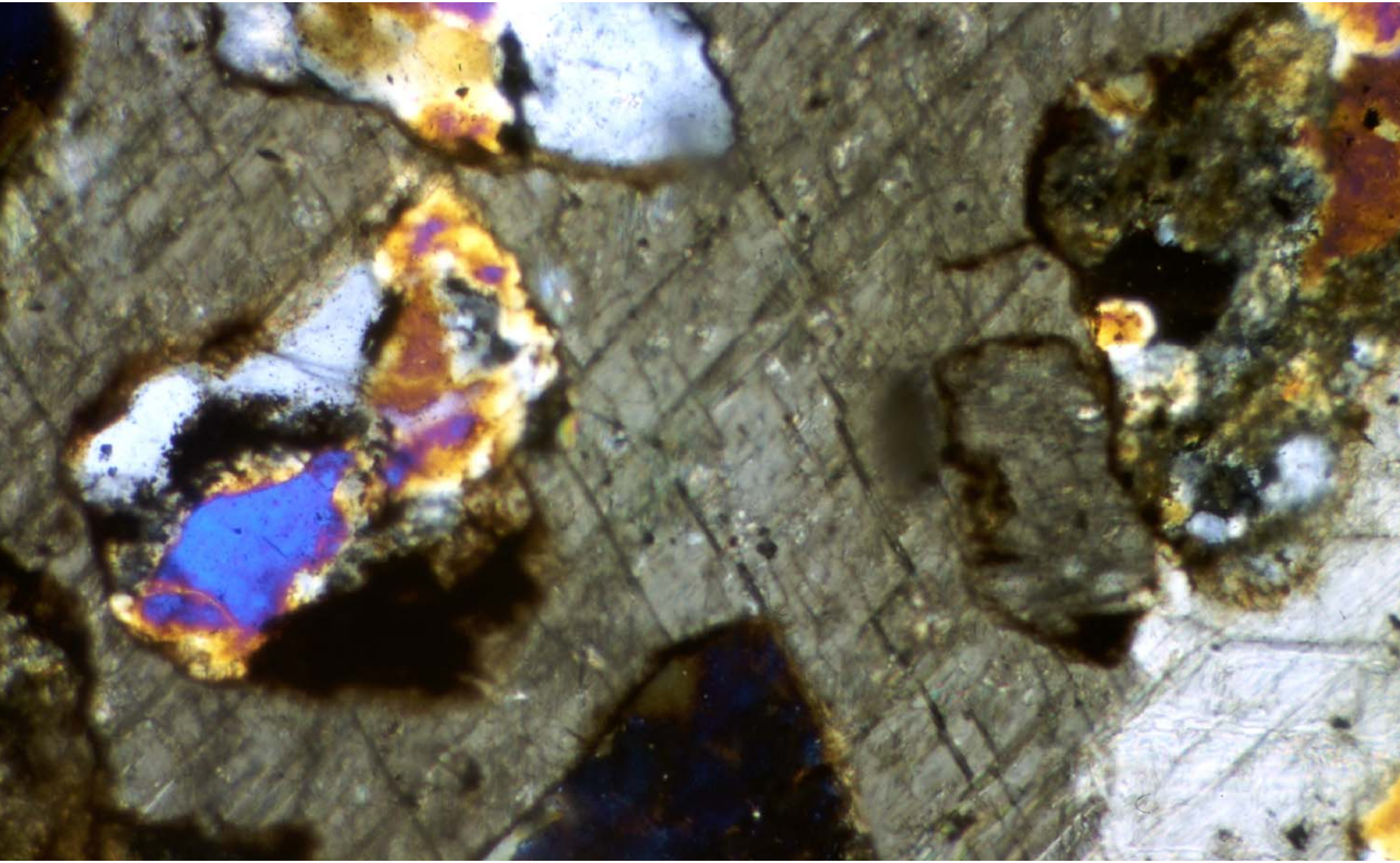

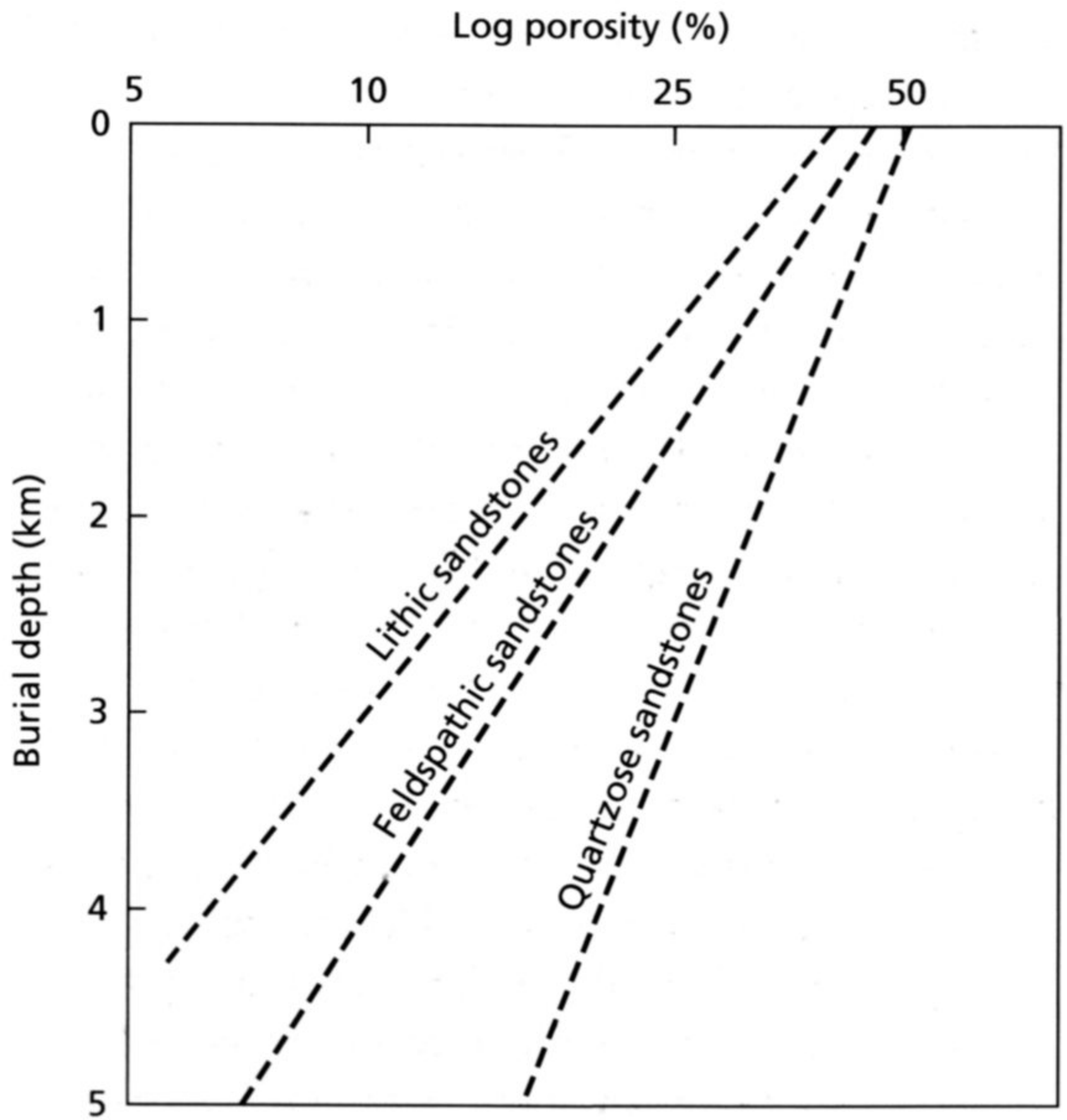

Fig. 2.60 Porosity–depth relationship for sandstones of different composition. After Dickinson (1985), based on several sources.

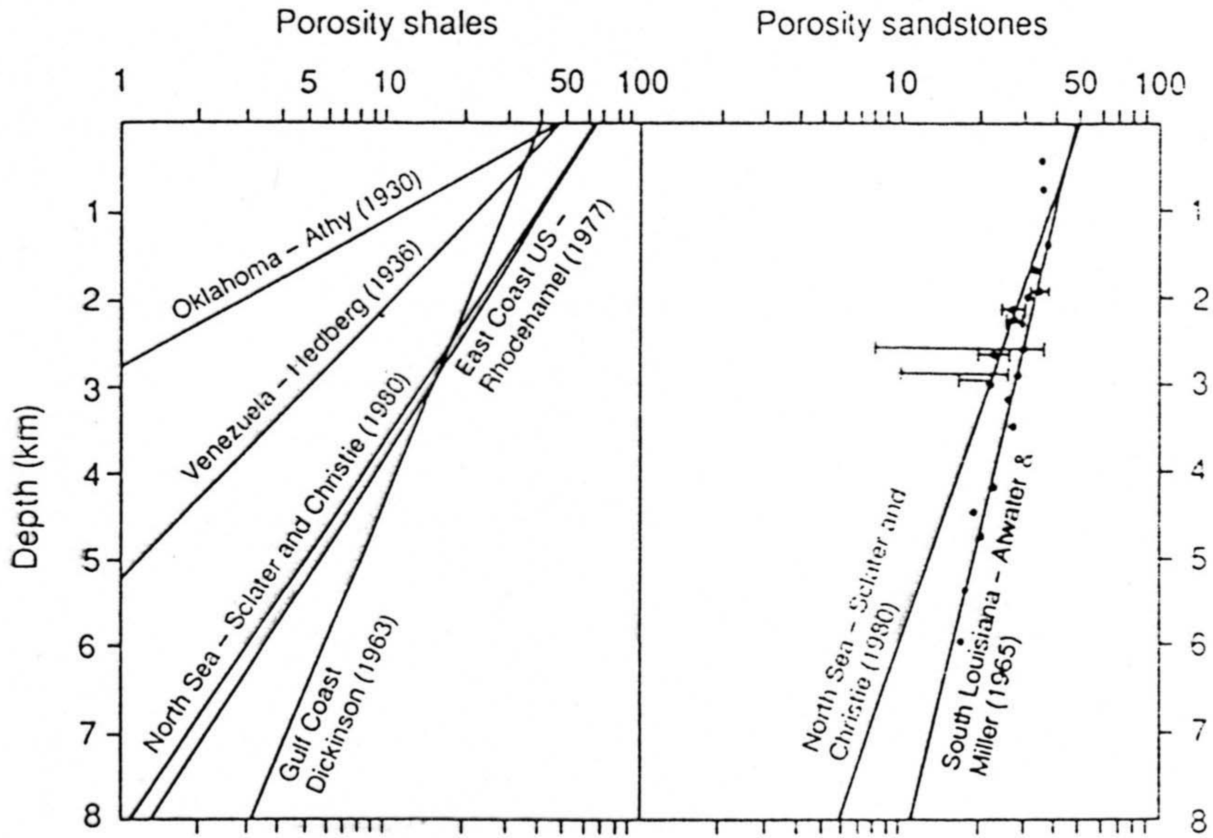

Fig. 8.2. Plots of log porosity against depth for shales and sandstones (after Sclater and Christie 1980). The North Sea shale data are from sonic log values in normally pressured sections, porosities being calculated from the sonic velocity/porosity relation proposed by Magara (1976). The North Sea sandstone data are from the data of Seeley (1978) supplemented by data from sonic logs. The best-fit lines for the North Sea data and for the south Louisiana data of Atwater and Miller (1965) are constrained to pass through the surface porosity values of Pryor (1973).

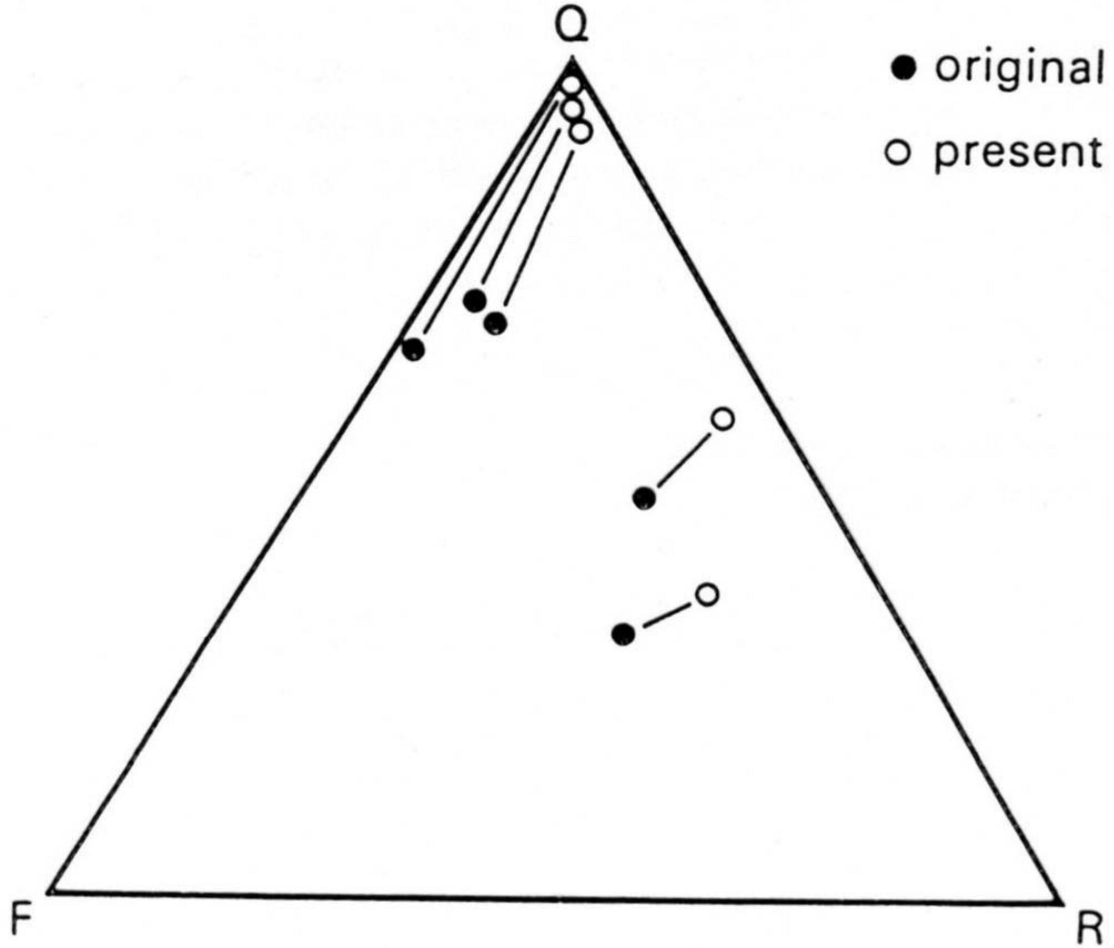

Fig. 5.37. Triangular diagram showing the present composition of five sandstones, after dissolution and alteration, and their reconstructed composition, assuming 15% of the grains which occupied oversized pores were rock fragments and 85% were feldspar (from McBride, 1985).

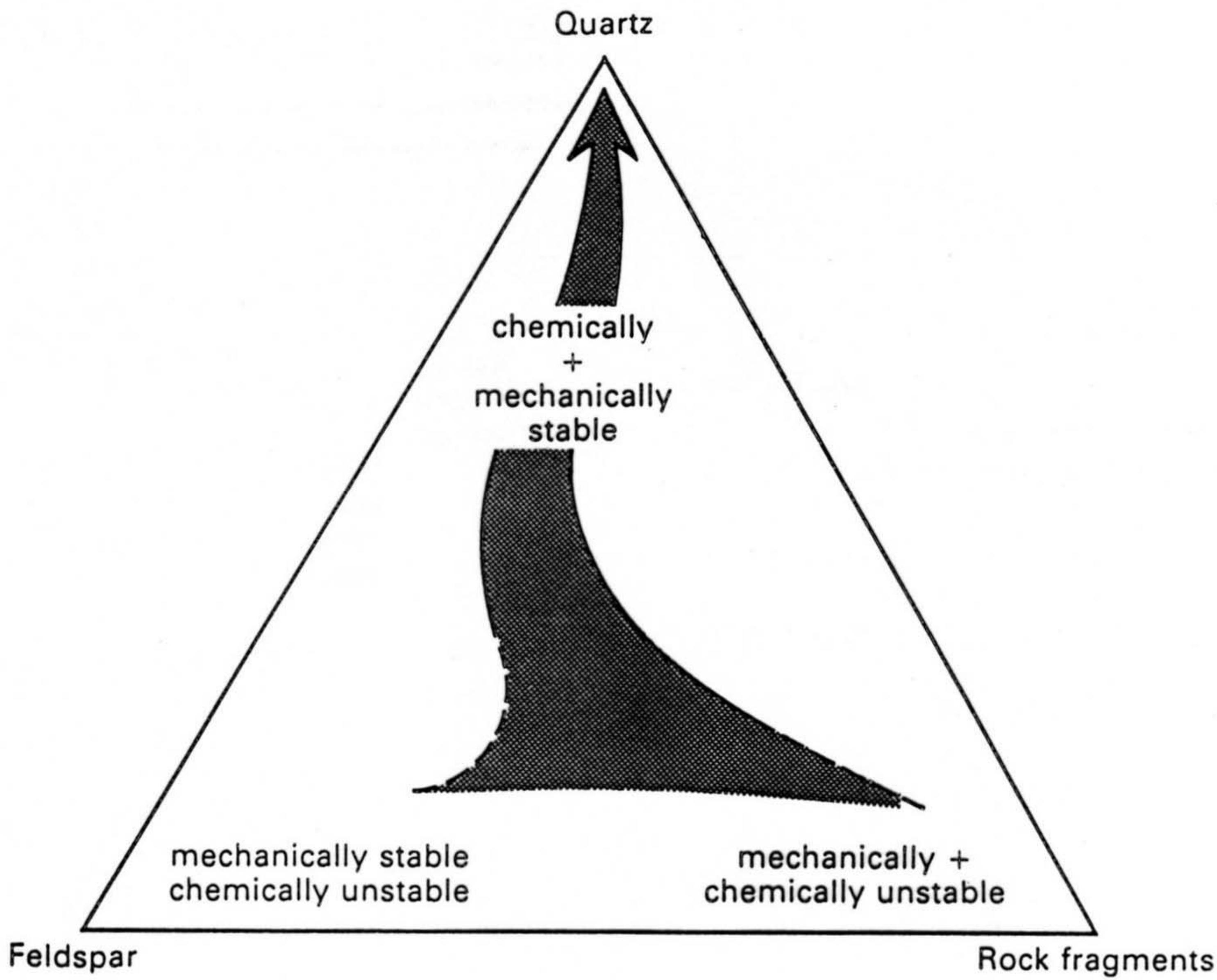
Quartz
chemically
+
mechanically
stable
mechanically stable
chemically unstable
mechanically +
chemically unstable
Feldspar
Rock fragments

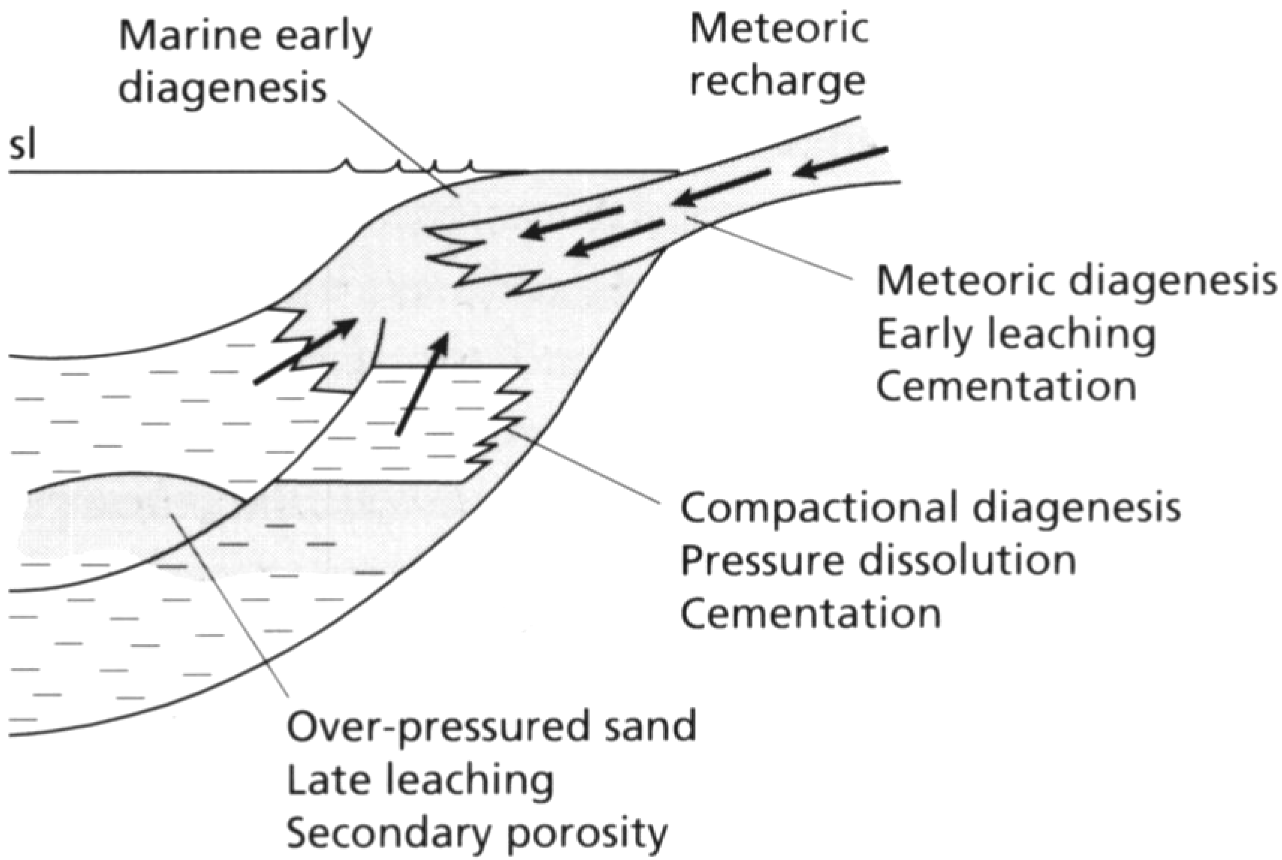

Fig. 2.57 Sketch illustrating main siliciclastic diagenetic environments. After Bjørlykke (1988).

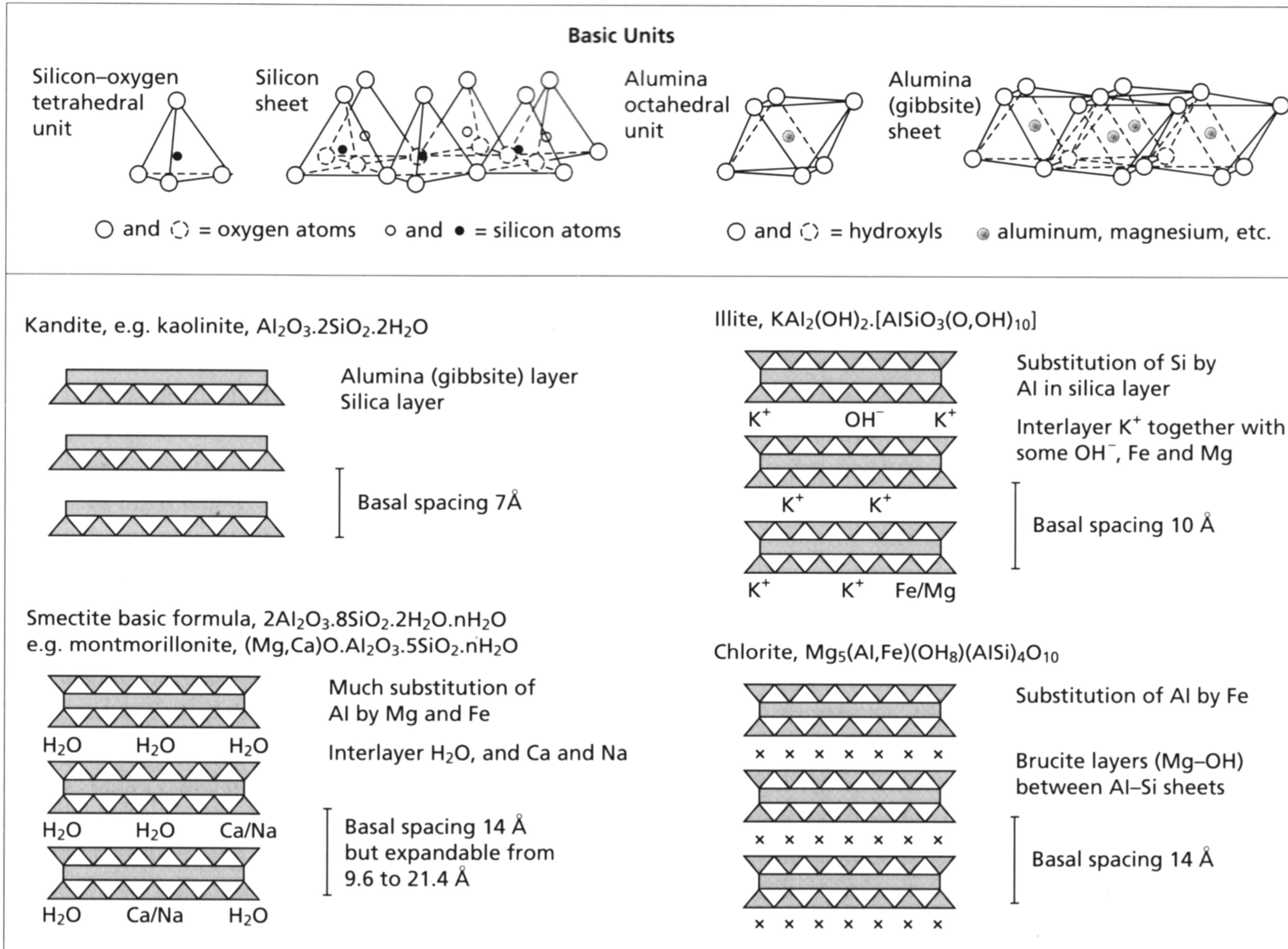
Basic Units
Silicon–oxygen tetrahedral unit
Silicon sheet
Alumina octahedral unit
Alumina (gibbsite) sheet
○ and ◌ = oxygen atoms
○ and ● = silicon atoms
○ and ◌ = hydroxyls
aluminum, magnesium, etc.
Kandite, e.g. kaolinite, $Al_2O_3.2SiO_2.2H_2O$
Alumina (gibbsite) layer
Silica layer
Basal spacing 7Å
Illite, $KAl_2(OH)_2.[AlSiO_3(O,OH)_{10}]$
Substitution of Si by Al in silica layer
K^+
OH^-
K^+
Interlayer K^+ together with some OH^-, Fe and Mg
K^+
K^+
Basal spacing 10 Å
K^+
K^+
Fe/Mg
Smectite basic formula, $2Al_2O_3.8SiO_2.2H_2O.nH_2O$
e.g. montmorillonite, $(Mg,Ca)O.Al_2O_3.5SiO_2.nH_2O$
Much substitution of Al by Mg and Fe
H_2O
H_2O
H_2O
Interlayer H_2O, and Ca and Na
H_2O
H_2O
Ca/Na
Basal spacing 14 Å but expandable from 9.6 to 21.4 Å
H_2O
Ca/Na
H_2O
Chlorite, $Mg_5(Al,Fe)(OH_8)(AlSi)_4O_{10}$
Substitution of Al by Fe
Brucite layers (Mg–OH) between Al–Si sheets
Basal spacing 14 Å

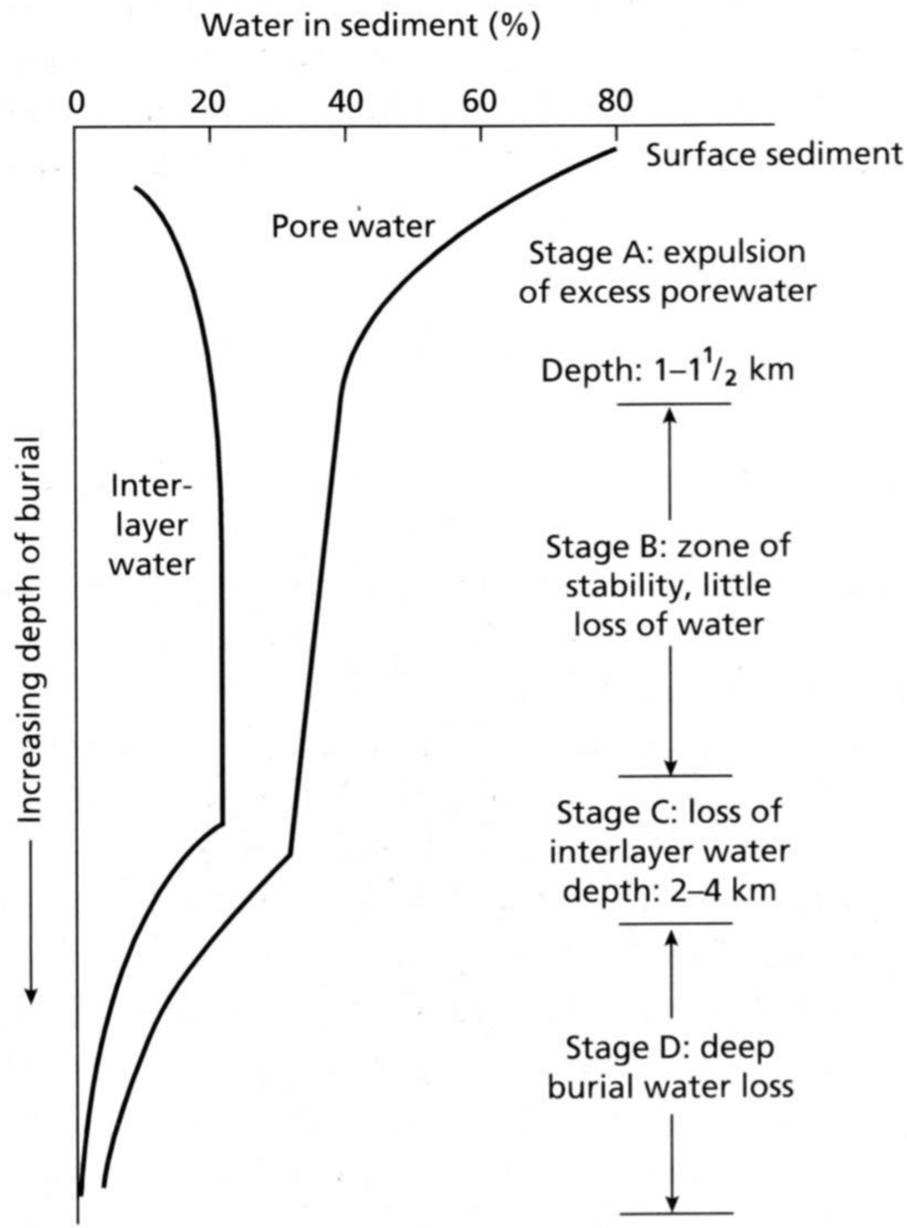

Fig. 3.8 Diagram illustrating the stages of water loss from muddy sediments with increasing depth of burial.

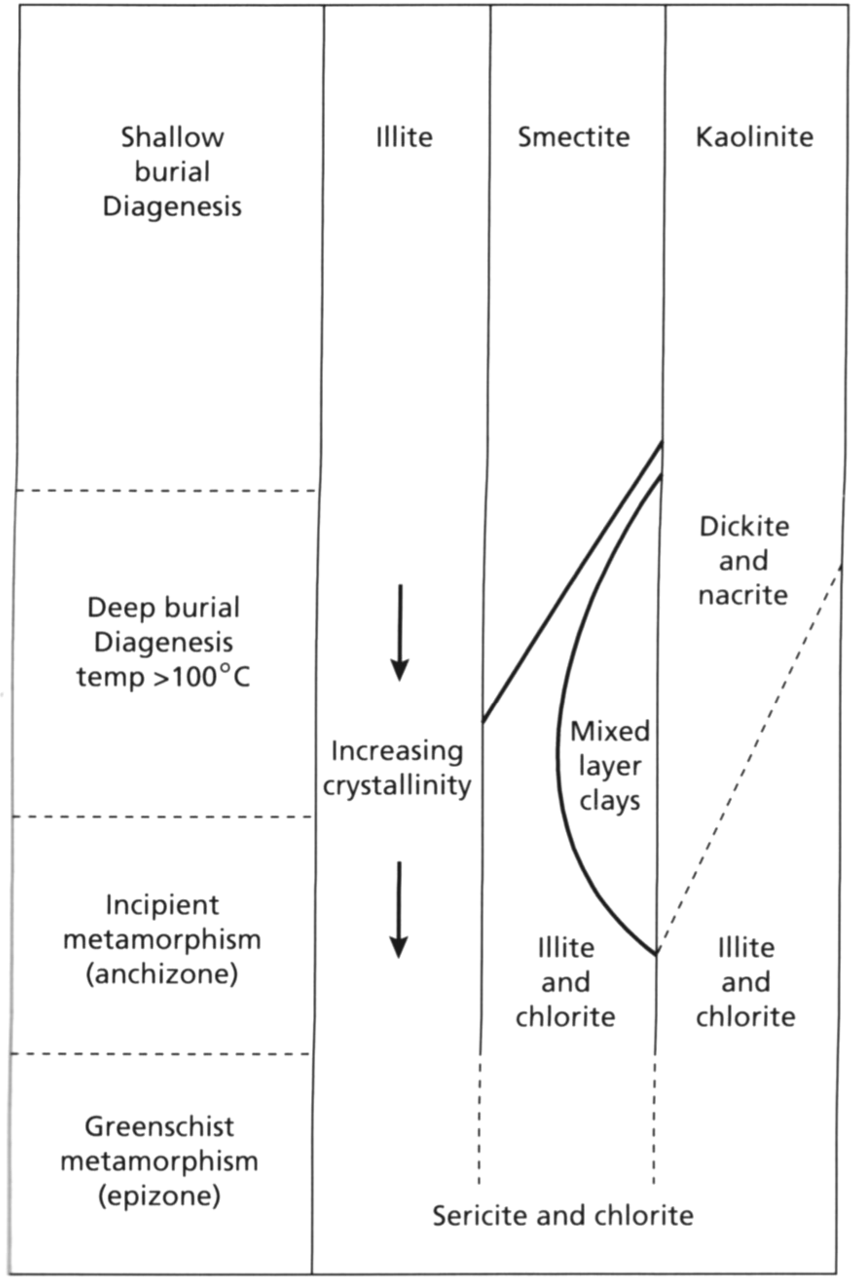

Fig. 3.9 Diagram illustrating the changes of clay minerals with increasing depth of burial and into metamorphism.

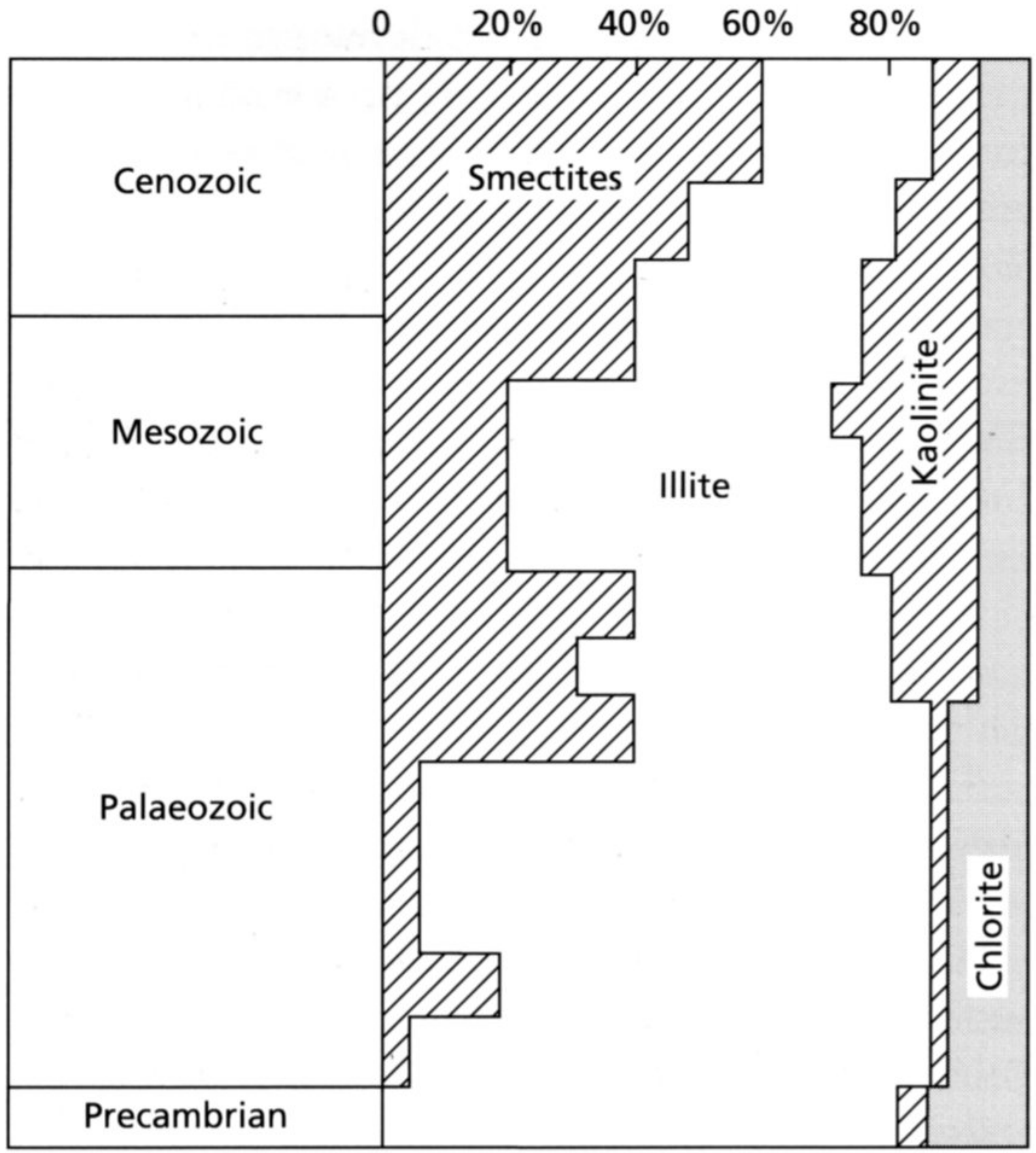

Fig. 3.10 The distribution of clay minerals through time.

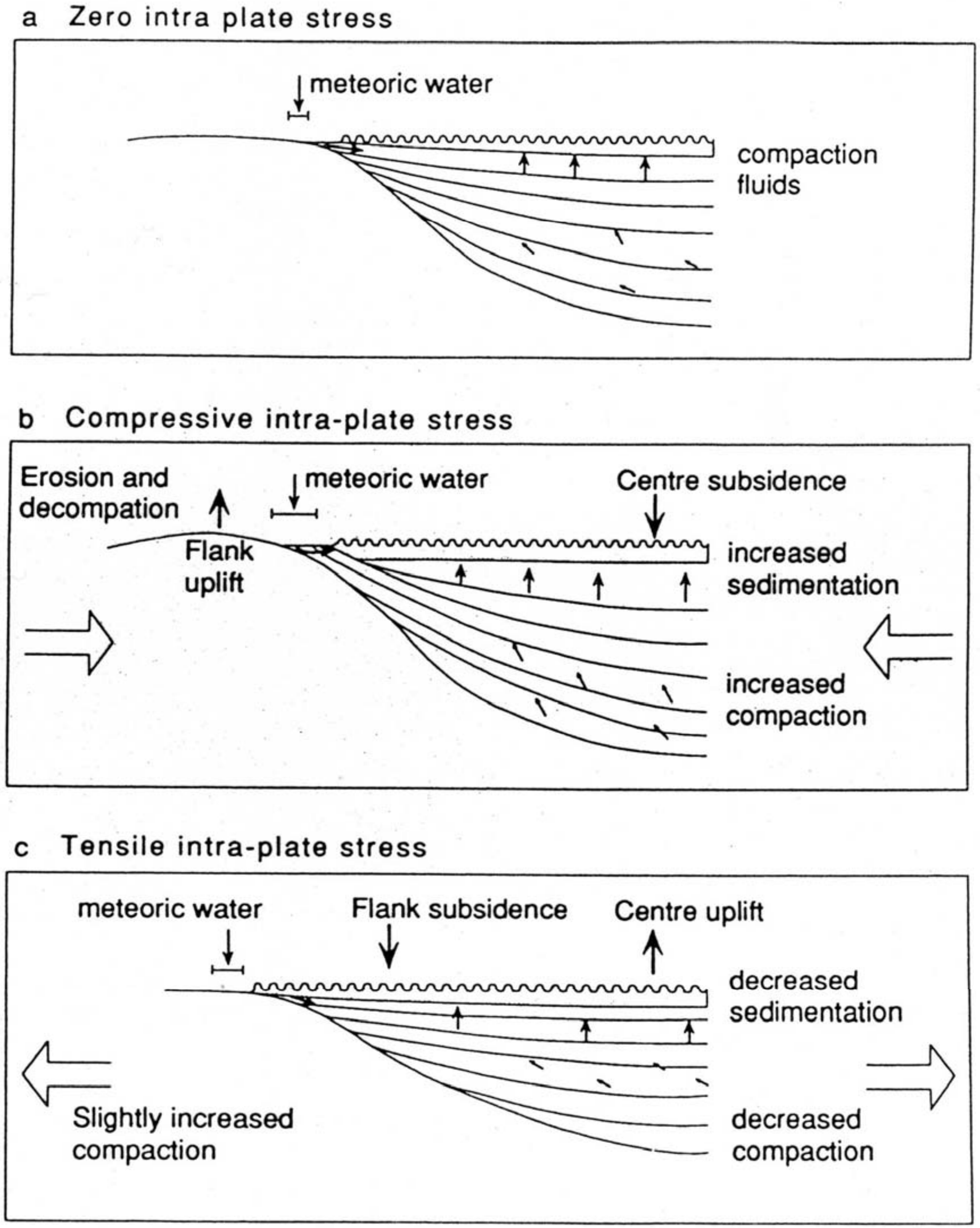

the effect of intra-plate stresses onfluid flow in sedimentary basins

van Baten&Cloeting 1994

Reading:

- **M.E.Tucker: Sedimentary petrology. 3rd ed. Blackwell, 2001, 2003.**
- Prothero: Interpreting stratigraphic record, 1990.
- Pettijohn F.J., Potter P.E. a Siever R. (1987): Sand and Sandstone. Springer-Verlag, New York, 553 pp.
- Chamley H. (1989): Clay Sedimentology. Springer-Verlag, Berlin, 623 pp.
- Potter P.E., Maynard J.B. a Pryor W.A. (1980): Sedimentology of Shale. Springer-Verlag, Berlin, 270 pp.